

THEORETICAL STUDIES OF MOLECULAR
DYNAMICAL PROCESSES IN
RARE-GAS MATRICES AND
IN THE GAS PHASE

By

RAN PAN

Bachelor of Science
Xinyang Teacher's College
Xinyang, P. R. China
1983

Master of Science
Jilin University
Changchun, P. R. China
1989

Submitted to the Faculty of the
Graduate College of the
Oklahoma State University
in partial fulfillment of
the requirements for
the degree of
DOCTOR OF PHILOSOPHY
July, 1996

THEORETICAL STUDIES OF MOLECULAR
DYNAMICAL PROCESSES IN
RARE-GAS MATRICES AND
IN THE GAS PHASE

Thesis Approved:

David M. Ray

Thesis Adviser

Donald L. Thompson

J. Paul Newton

W. S. Salt

Thomas C. Collins

Dean of the Graduate College

PREFACE

The studies were conducted to make a contribution to the understanding of some fundamental problems involved in the molecular dynamics of intramolecular vibrational relaxation of vinyl bromide and the diffusion dynamics of hydrogen in an imperfect rare gas matrix. The basic idea is to apply molecular dynamics theories and some computational techniques to the investigation of chemical dynamical processes. Our primary purpose is to predict certain physical quantities and to give a clear explanation to some phenomena which occurred both theoretically and experimentally for the chosen systems.

I wish to express my sincere appreciation to my research advisor, Dr. Lionel M. Raff for his guidance, patience, inspiration and understanding during my research work. His brilliant ideas and his ability to explain the most complex scientific subject for teaching and research will never escape from my memory. I am grateful to have had the opportunity to study under him.

I would also like to sincerely thank Drs. Donald Thompson, Paul Devlin, Larry Scott, and Xincheng Xie for serving on my committee, taking the time to read this thesis, and for their invaluable guidance, assistance and encouragement.

More over, I wish to express my sincere gratitude to those who provided friendship, discussions and suggestions for this work: Dr. Dan C. Sorescu, Dr. Yin Guo , Dr. Paras Agrawal and Dr. Ron Kay.

I would also like to give my special appreciation to my wife, Hongyun Liu and my lovely son, Jason Y. Pan for their love, support, encouragement at times of difficulty, understanding in every day life during this whole process.

Finally, I am pleased to acknowledge financial support from Department of Chemistry and National Science Foundation.

TABLE OF CONTENTS

Chapter	Page
I. INTRODUCTION.....	1
Format of The Thesis.....	2
References.....	3
II. BASIC CONCEPTS AND THEORETICAL METHODS IN MOLECULAR DYNAMICS.....	4
Potential-Energy Surface.....	4
Classical Dynamics.....	5
Monte Carlo Methods.....	7
Power Spectra Method.....	10
Non-statistical Effects and Intramolecular Energy Transfer.....	13
Variational Phase-Space Theory Methods.....	16
References.....	17
III. INTRAMOLECULAR ENERGY TRANSFER RATES PATHWAYS FOR VINYL BROMIDE.....	21
Introduction.....	21
Computational Methods and Potential Surface.....	25
Computational Methods.....	25
Potential-energy Surface.....	29
Numerical Procedures.....	30
Results and Discussions.....	32
Energy Transfer Rates and Pathways.....	32
First-order Relaxation Model.....	36
IVR in the Transition-State Regions for Three-Center Elimination.....	38
Summary.....	41
References.....	43
IV. POWER SPECTRA OF VINYL BROMIDE UNDERGOING CONTINUOUS FREQUENCY MODULATION AND INTRAMOLECULAR ENERGY TRANSFER.....	66

Introduction.....	66
Methods and Calculations.....	69
Potential Energy Surfaces.....	69
Continuous Frequency Modulation (CFM) Effect.....	70
Intramolecular Energy-Transfer Dynamics.....	74
Trajectory Procedures.....	75
Results and Discussion.....	76
Fundamental Frequency and Power Spectra.....	76
Isotope Effect to the Power Spectra.....	77
Line Spacing and Energy Transfer Rate Coefficients.....	78
Variation of Rate Coefficients with Internal Energy.....	80
Summary.....	81
References.....	83

V. THEORETICAL STUDIES OF HYDROGEN ATOM DIFFUSION RATES IN IMPERFECT RARE-GAS MATRICES..... 105

Introduction.....	105
Matrix Model.....	107
Potential Energy Surfaces.....	108
Computational Methods.....	110
Results and Discussion.....	118
Summary.....	124
References.....	125

LIST OF TABLES

Table	Page
I. Notation and frequencies for the vibrational modes of vinyl bromide.....	46
II. Primary and secondary relaxation pathways in vinyl bromide.....	47
III. Total IVR rates computed by least-squares fitting of Eq. (III.10). In each case, 3.0 eV of excitation energy in excess of zero point energy is initially partitioned into the indicated vibrational mode.....	48
IV. Notation and frequencies for the stretch modes of vinyl bromide.....	85
V. Parameters employed for the definition of local bond mode potentials.....	86
VI. Frequencies of local stretch modes obtained from power spectra lines.....	87
VII. Frequencies of C=C, C ₂ -Br and C ₂ -H ₃ stretch modes with Deuterium replacing of H ₄ and H ₅	88
VIII. Frequencies of C=C, C ₂ -Br and C ₁ -H ₄ stretch modes with Deuterium replacing of H ₃ and H ₅	89
IX. Frequencies of C=C, C ₂ -Br and C ₁ -H ₅ stretch modes with Deuterium replacing of H ₃ and H ₄	90

Table	Page
X. Intaramolecular energy transfer rate out of a given local mode by CFM method.....	91
XI. Non-linear fitting results for each local stretch mode.....	92
XII. Hydrogen/Lattice Pairwise Potential Parameters.....	127
XIII. Classical diffusion rates for hydrogen atoms in perfect fcc xenon matrix and in imperfect fcc xenon matrix with vacancy number = 5.....	128
XIV. Classical diffusion rates for hydrogen atoms in imperfect fcc xenon matrix with vacancy number =15.....	129

LIST OF FIGURES

Figure	Page
1. Simple illustration of statistical transition state theory.....	20
2(a).Temporal variation of the mode kinetic energy for ν_1 , ν_2 , and ν_3 computed using Eq. (III. 8) for the case in which 3.0 eV of excitation energy in excess of zero-point energy is initially partitioned into the C-H stretching mode ν_{10}	49
2(b).Temporal variation of the mode kinetic energy for ν_4 , ν_5 , and ν_6 computed using Eq. (III. 8) for the case in which 3.0 eV of excitation energy in excess of zero-point energy is initially partitioned into the C-H stretching mode ν_{10}	50
2(c).Temporal variation of the mode kinetic energy for ν_7 , ν_8 , and ν_9 computed using Eq. (III. 8) for the case in which 3.0 eV of excitation energy in excess of zero-point energy is initially partitioned into the C-H stretching mode ν_{10}	51
2(d).Temporal variation of the mode kinetic energy for ν_{10} , ν_{11} , and ν_{12} computed using Eq. (III. 8) for the case in which 3.0 eV of excitation energy in excess of zero-point energy is initially partitioned into the C-H stretching mode ν_{10}	52
3. Decay curves for the average mode energies for initial excitation of modes ν_6 and ν_{11} with 3.0 eV above zero-point energy.....	53

Figure	Page
4. Decay curve for the average mode energy for initial excitation of mode ν_9 with 3.0 eV in excess of zero-point energy.....	54
5. Decay curves for the average mode energy for initial excitation of mode ν_{10} with 3.0 eV in excess of zero-point energy.....	55
6 Decay curves for the average mode energy for initial excitation of modes ν_5 and ν_{11} with 3.0 eV in excess of zero-point energy.....	56
7. Temporal variation of two C-H distances and the H-H distance for a trajectory in which vinyl bromide is initially in the minimum-energy configuration on a dividing surface near the optimum critical surface for three-center H_2 elimination.....	57
8(a).Temporal variation of the mode kinetic energies of ν_1 , ν_2 , and ν_3 for the trajectory illustrated in Fig. 7.....	58
8(b).Temporal variation of the mode kinetic energies of ν_4 , ν_5 , and ν_6 for the trajectory illustrated in Fig. 7.....	59
8(c).Temporal variation of the mode kinetic energies of ν_7 , ν_8 , and ν_9 for the trajectory illustrated in Fig. 7.....	60
8(d).Temporal variation of the mode kinetic energies of ν_{10} , ν_{11} , and ν_{12} for the trajectory illustrated in Fig. 7.....	61
9(a).Temporal variation of the mode kinetic energies of ν_1 , ν_2 , and ν_3 with vinyl bromide initially in the minimum-energy configuration on the optimum dividing surface for three-center HBr elimination.....	62

Figure	Page
9(b).Temporal variation of the mode kinetic energies of ν_4 , ν_5 , and ν_6 with vinyl bromide initially in the minimum-energy configuration on the optimum dividing surface for three-center HBr elimination.....	63
9(c).Temporal variation of the mode kinetic energies of ν_7 , ν_8 , and ν_9 with vinyl bromide initially in the minimum-energy configuration on the optimum dividing surface for three-center HBr elimination.....	64
9(d).Temporal variation of the mode kinetic energies of ν_{10} , ν_{11} , and ν_{12} with vinyl bromide initially in the minimum-energy configuration on the optimum dividing surface for three-center HBr elimination.....	65
10(a).Power spectrum showing the fundamental frequency peaks for C ₁ -C ₂ when 1/10 ZPE is used.....	93
10(b).Power spectrum showing the fundamental frequency peaks for C ₂ -Br when 1/10 ZPE is used.....	94
10(c).Power spectrum showing the fundamental frequency peaks for C ₁ -H ₄ when 1/10 ZPE is used.....	95
10(d).Power spectrum showing the fundamental frequency peaks for C ₁ -H ₅ when 1/10 ZPE is used.....	96
10(e).Power spectrum showing the fundamental frequency peaks for C ₂ -H ₃ when 1/10 ZPE is used.....	97
11. (A) Power spectrum of C ₁ -H ₄ with no isotope effects, (B) Power spectrum of C ₁ -H ₄ with deuterium replacement of H ₂ and H ₃	98
12. Power spectrum of C-Br bond with initial excitation of 1.0 eV.....	99
13. Power spectrum of C ₁ -H ₅ bond with initial excitation of 1.0 eV and deuterium replacement of H ₃ and H ₄	100

Figure		Page
14.	(A) Total mode energy variation of C-Br with time, (B) Local mode kinetic energy variation of C-Br with time. In both cases, C-Br bond is excited with 1.0 eV.....	101
15.	Non-linear fitting of envelope function of total mode energy decay of C-Br bond initially excited with 1.0 eV.....	102
16.	Fine spectra structure spacing variation of C-Br bond with initial excitation energy.....	103
17.	CFM rate coefficient variation of C-Br bond with initial excitation energy.....	104
18.	Variation of the Hydrogen-Lattice interaction potential with vacancy number in the crystal.....	130
19.	Variation of system potential energy for hydrogen atom movement along a straight line connecting the two adsorption sites in a frozen lattice atoms.....	131
20.	Minimum-energy profile for hydrogen-atom diffusion in a xenon matrix with 5 vacancies.....	132
21.	Minimum-energy profile for hydrogen-atom diffusion in a xenon matrix with 15 vacancies.....	133
22.	Typical lattice atom motion occurring during the first 200,000 Markov steps in the Monte Carlo calculation.....	134
23.	Minimum-energy profile for hydrogen-atom diffusion in a xenon matrix with 5 vacancies.....	135
24.	Minimum-energy profile for hydrogen-atom diffusion in a xenon matrix with 15 vacancies.....	136
25.	Variation of the computed hydrogen-atom diffusion coefficient with percentage of vacant xenon lattice sites at 40 K.....	137

CHAPTER I

INTRODUCTION

Chemistry is concerned with the properties of molecules and their reactions. Most chemical processes occur in gas phases or condensed phases. Molecular dynamics simulation methods have proved to be an effective tool for the investigation of such processes.^{1,2} Simply, molecular dynamics is the study of the motion or movement of any kind of molecular species over time. This can be achieved by numerical integration of the classical equations of motion for the chosen system. The form of these equations depends upon the system potential energy and upon the choice of coordinate system. The quantities of interest and characteristics of the system can be determined from the results of the molecular dynamics simulations. The development of modern computer technology expands the possibilities of molecular dynamics simulations and allows the molecular dynamists to address larger and more difficult problems of chemical interest.

Classical molecular simulations involve three main steps. First, a model molecular system is created. Based on this model, a potential energy surface which contains the information related to inter- and intramolecular interaction is developed. Most potential energy surfaces are usually parametrized with the parameters being fitted to experimental data and the results of semiempirical or *ab initio* calculations. Second, classical trajectories on this

potential-energy surface are performed by integration of the classical equations of motion for the system of interacting particles over a given period of time. In stochastic cases, the classical trajectory is replaced by Monte Carlo simulations³ where the set of molecular coordinates at a given moment depends only on the molecular configuration at the previous moment. The final step of molecular dynamics methodology is the analysis of the trajectories. The macroscopic properties of the system are extracted from the dynamic behavior of the system at the molecular level. The calculations of diffusion rates, intramolecular and intermolecular energy transfer rates, or distribution of energy over the available degrees of freedom are typical examples of quantities determined from trajectory analysis.

Our studies presented in this thesis consist of three parts. The first part is concerned with the dynamics of intramolecular vibrational relaxation. The second part involves the investigation of intramolecular energy transfer and the power spectrum for vinyl bromide which exhibits a continuous frequency modulation (CFM) effect.⁴ The third part is directed toward the understanding of diffusion dynamics of chemical species isolated in an imperfect rare-gas matrix.

Format of the Thesis

Following this brief Introduction, we present some basic concepts and theoretical methods in Chapter II that are used in the molecular dynamics simulations. Statistical and nonstatistical dynamics, Monte Carlo methods and classical variational transition-state theory, the calculation of mode energies and the CFM power spectra method are discussed.

Chapter III reports studies of intramolecular energy transfer rates and pathways for vinyl bromide. Following an introduction in this field, the projection method is described. Next, the results of IVR dynamics studies are discussed. Chapter IV describes the investigation of CFM effects and intramolecular energy transfer dynamics in the vinyl bromide system. In Chapter V, we present studies of molecular dynamics in matrices. The diffusion of hydrogen atoms in rare gas matrices at cryogenic temperatures are investigated.

REFERENCE

1. L. M. Raff and D. L. Thompson, *Theory of Chemical Reaction Dynamics*, (edited by M. Bare, Chemical Rubber, Boca Raton, 1985), vol. III., p. 1.
2. R. N. Porter and L. M. Raff, in *Dynamics of Molecular Collisions*, (edited by W. H. Miller, Plenum Press, New York, 1976), vol. II, p.1.
3. J. P. Valleau and S. G. Whittington,, in *Modern Theoretical Chemistry*, (edited by B. J. Berne, Plenum Press, New York, 1977), vol. 5, p.137.
4. P. M. Agrawal, D. C. Sorescu, R. D. Kay, D. L. Thompson, L. M. Raff, J. B. Conrey, and A. K. Jameson, *J. Chem. Phys.* (in Press).

CHAPTER II

BASIC CONCEPTS AND THEORETICAL METHODS IN MOLECULAR DYNAMICS

Potential-Energy Surfaces

Using on Born-Oppenheimer approximation,¹⁻⁴ the motion of the electrons can be decoupled from that of the nuclei. Therefore, the Schrodinger equation for a molecule gives two separate equations representing electron and nuclei motion, respectively. In molecular dynamics simulations, the effort is concentrated on the motion of nuclei without explicit examination of the electrons. The equation describing the electronic motion depends only parametrically on the positions of the nuclei. The energy is a function of the coordinates of the nuclei alone and this energy is usually called the potential energy surface. The primary objective of molecular dynamics is the investigation of the motion of nuclei on the appropriate potential energy surface.

Potential energy surfaces are essential to our understanding of molecular stability, vibrational spectroscopy, conformational changes, and reaction dynamics. The potential energy surface gives the interaction energy as a function of system configuration space. The construction of specific potential energy surfaces for individual molecular systems involves the fitting

of parameters to the available experimental data and some semiempirical or *ab initio* computational results.

Classical Dynamics

The method of calculating classical trajectories is conceptually simple. The initial conditions for every atom in the system of interest are set and Hamilton's equations of motion are integrated until some predetermined condition, such as a reaction occurs or a predetermined time limit is reached. The final coordinates of each atom of each trajectory can then be analyzed. These methods have been described in detail elsewhere.^{1, 2, 5}

The first step of classical trajectory calculations is related to the choice of initial conditions. In our IVR studies, we used the projection method developed by Raff.^{6, 7} The method is based on the determination of the time dependence of the normal mode velocities by projection of the instantaneous Cartesian velocities of the atoms onto the normal mode vectors. The basic idea is as follows:

$$\dot{q}(t) = \mathbf{L}\dot{Q}(t), \quad (\text{II. 1})$$

where \mathbf{L} is a $(3N \times 3N)$ square matrix whose columns are the normalized projection vectors. $\dot{q}(t)$ is a $(3N \times 1)$ column vector whose elements are the Cartesian velocities and $\dot{Q}(t)$ is a $(3N \times 1)$ column vector whose elements are the normal mode, center-of-mass, and rotation velocities. The normal mode velocities may therefore be obtained from

$$\dot{Q}(t) = L\dot{q}(t) \quad (\text{II. 2})$$

The corresponding total kinetic energy can be calculated from the normal mode velocities. For the purpose of trajectory calculations, zero-point energy is first inserted into the molecule. This determines the initial normal mode velocities from which the initial Cartesian velocities are computed from the equation (II.1). The trajectory is then integrated for a random period of time which is less than the period for the lowest frequency vibrational mode in the molecule. This integration serves to randomize the energy between potential and kinetic energies and thereby provides the required vibrational phase averaging.

The projection method has been previously applied to the study of intramolecular energy flow in gas-phase 1,2-difluoroethane ⁶ and disilane ⁸. Decay rates and pathways of energy flow for initial excitation of each of the 18 vibrational modes have been determined. The results obtained from the time variation of the normal-mode velocities were used to extract the entire first-order mode-to-mode energy transfer rate coefficient matrix. Essentially, this provides a complete description of intramolecular energy flow in the molecule. We have used similar methods for the study of intramolecular vibrational relaxation dynamics of vinyl bromide.

Based on a given potential-energy surface and the selection of initial conditions, the Hamiltonian equations of motion^{1,9} determine the trajectory dynamics. For a system of N atoms,

$$\frac{\partial H(p,q)}{\partial p_i} = \dot{q}_i \quad (i=1,2,\dots,3N), \quad (\text{II. 3})$$

$$\frac{\partial H(p,q)}{\partial q_i} = -\dot{p}_i \quad (i=1,2,\dots,3N) \quad (\text{II. 4})$$

where $H(p,q)$ is the Hamiltonian of the system, and p and q are the set of $6N$ generalized coordinates. There are totally $6N$ -coupled differential equations of motion to be integrated for a given period of time. Depending on the time period and increment, this can be a computationally intensive calculation. The integration can be performed using a variety of numerical methods.^{1, 2} In our studies, a fourth-order Runge-Kutta routine¹ was used.

In the study of diffusion of hydrogen isolated in a matrix system, a damped trajectory method was used in which the system is allowed to relax toward its minimum-energy configuration. In this procedure, the kinetic energy of each lattice atom is set to zero and the classical Hamiltonian equations of motion for the lattice atoms are integrated until the total potential energy attains a minimum. This procedure can effectively increase the convergence rate of the required integrations.

Monte Carlo Methods

The multidimensional integrals that give the average properties of trajectories can be solved approximately by using Monte Carlo techniques. In fact, such statistical procedures are often the only practical approach to this problem. This is the case when one is attempting to study very rare events or events occurring on significantly different time scales. In general, the average or expectation value of a dynamical property, F , is given by

$$\langle F \rangle = \frac{\int_{\Omega} F(q)P(q)dq}{\int_{\Omega} P(q)dq}, \quad (\text{II. 5})$$

where the q are the independent variables that define the state in phase space Ω , and $P(q)$ is the probability density of the state of the system defined by q . For a canonical system, $P(q)$ is the Boltzmann distribution,

$$P(q) = \exp(-H(q)/k_B T), \quad (\text{II.6})$$

where $H(q)$ is the system Hamiltonian and k_B is the Boltzmann constant.

The simplest Monte Carlo approximant of equation (II. 5) is

$$\langle F \rangle \approx \frac{\sum_n F(q_n)P(q_n)}{\sum_n P(q_n)}, \quad (\text{II. 7})$$

where n is the set of random points chosen from phase-space. If phase space is sampled using a Markov walk based on the normalized probability distribution $P(q)$, Eq.(II.7) becomes

$$\langle F \rangle \approx \frac{1}{M} \sum_{n=1}^M F(q_n), \quad (\text{II. 8})$$

However, this method has severe limitations due to the fact that a Markov walk based on $P(q)$ is usually confined to the low-energy regions of phase space. This results in low rate of convergence.

"Importance Sampling"^{1,10} has proven to be an effective way to increase the convergence rate in the Monte Carlo evaluation of the integral values in Eq.(II. 5). In this method, the sampling of phase space is altered so as to concentrate the configuration points in the regions which make the most important contribution to the integrals. Eq.(II. 5) can be rewritten as

$$\langle F \rangle \approx \frac{\int_{\Omega} \left\{ \frac{F(q)}{P'(q)} \right\} w(q) dq}{\int_{\Omega} \left\{ \frac{1}{P'(q)} \right\} w(q) dq} \quad (\text{II. 9})$$

where a new weight function $[w(q)]$ is defined by

$$w(q) = N_0 P(q) P'(q) \quad (\text{II. 10})$$

in which N_0 is the normalization constant and $P'(q)$ is the importance sampling distribution which depends on the system to be analyzed. If phase space is sampled using a Markov walk based on $w(q)$, we have

$$\langle F \rangle \approx \frac{\sum_n F(q_n) [P'(q_n)]^{-1}}{\sum_n [P'(q_n)]^{-1}} \quad (\text{II. 11})$$

By choosing $P'(q)$ so as to increase the frequency with which phase-space points in critical regions are sampled, the convergence rate obtained from (II. 11) can be significantly increased relative to that for Eq.(II. 5).

In Metropolis sampling, a sequence of phase -space configurations are randomly generated to give a Markov chain. The probability that a system is in

a given state at the (i+1) step in a Markov chain is explicitly dependent only on the state at the (ith) step. A random walk of the system through the whole phase space is accomplished by moving one(or more) of the atoms at each step. A trial step is accepted or rejected in accordance with the probability $w(q)$. It is commonly assumed, on the basis experience, that the most rapid convergence rate is obtained if approximately 50% of the attempted moves are accepted.¹¹

Power Spectrum Method

Power spectra provide a convenient way to compute the vibrational frequencies of a given molecule in a realistic manner. Because power spectra yield vibrational frequencies characteristic of the system energy, in contrast to normal-mode analysis which provides a correct description only at low energies, the method is a powerful tool in dynamical studies.

It is known that the auto spectral density function can provide useful information on the intramolecular dynamics of polyatomic molecules. Whenever quasi periodic dynamics exist, sharp peaks corresponding to fundamentals, overtones and combination bands will be present in the auto spectral density function.¹² In contrast, ergodic dynamics leads to broadened spectra containing many smaller peaks. Smith and Shirts¹³ computed averaged power spectra for state-specific excitation of HCN. Their results show that the ensemble-averaged spectra do not exhibit the expected broadening and grassiness with increasing internal energy but that the spectra of individual trajectories do. Swell, Thompson, and Levine¹⁴ have explored the power spectra obtained from classical trajectory computations to

study the polyatomic molecules C₂H₄, CH₃ONO, and SiF₄ at the energies both below and above the dissociation threshold. It was observed that spectral mode identity is essentially retained even well above the threshold for dissociation and that no fully ergodic phenomena were observed. Chang *et al.*¹⁵ have used power spectra as a diagnostic tool to identify the presence of statistical dynamics. This characteristic is attributed to a very high level of mode-mode coupling and large intramolecular vibrational redistribution rates. Most recently, power spectrum line shapes for oscillators undergoing a continuous modulation of the vibrational frequency have been investigated by Agrawal *et al.*¹⁶ The results suggest that line shape analysis can be used effectively as a probe of energy transfer rates.

A power spectrum for a given coordinate, q , may be computed by taking the Fourier transform of either an autocorrelation function, $C_q(\tau)$, or by transforming the coordinate itself.¹² The procedure to evaluate the Fourier transform of the coordinate $q(t)$ is given by

$$I_q(\omega) = \lim_{T \rightarrow \infty} (2\pi)^{-1} \left[\int_{-T}^T q(t) \exp(-i\omega t) dt \right]^2, \quad (\text{II. 12})$$

The other procedure is to evaluate the Fourier transform of the autocorrelation function. The autocorrelation function is given by

$$C_q(\tau) = \lim_{T \rightarrow \infty} \left[(T)^{-1} \int_0^T q(t) q(t + \tau) dt \right], \quad (\text{II. 13})$$

The power spectrum of $C_q(\tau)$ is obtained from

$$I_c(\omega) = \lim_{T \rightarrow \infty} (2\pi)^{-1} \left[\int_{-T}^T C_q(\tau) \exp(-i\omega\tau) d\tau \right]^2, \quad (\text{II. 14})$$

Both $I_c(\omega)$ and $I_q(\omega)$ are easily obtained from the results of classical trajectory calculations.¹²

$I_c(\omega)$ and $I_q(\omega)$ are directly related in that $I_c(\omega)$ is the square of $I_q(\omega)$. This difference means that the two quantities emphasize the features of the dynamics in very different ways. Specific algorithms to evaluate either (II. 12) or (II. 14) can be found in Ref. (17). We have used this methodology in the present study to gain insight into the intramolecular energy transfer dynamics of vinyl bromide.

Agrawal *et al.*¹⁶ have shown that whenever an oscillator undergoes a continuous modulation of the vibrational frequency, the single, sharp line normally characteristic of such systems broadens and exhibits a wealth of fine structure components. The characteristic fine structure pattern is one of decreasing amplitude and spacing. By examination of a series of model oscillators that included harmonic systems with linear and exponential variation of the frequency without amplitude damping, a harmonic system with exponential damping of both the resonant frequency and the amplitude, and a Morse oscillator whose kinetic energy is being exponentially damped, it was shown that the position of the fine structure extrema depends linearly upon the initial oscillator frequency and the square root of the absolute value of the modulation rate. Since energy transfer in an anharmonic system produces a variation of the resonant frequency, a continuous frequency modulation (CFM) splitting of the power spectrum results. By assuming that the analytic result for a harmonic oscillator with a linear modulation is transferable to the

anharmonic case, Agrawal *et al.*¹⁶ have obtained an expression relating the peak-to-peak fine structure spacing to the Morse potential parameters, the initial oscillator energy and the IVR rate coefficient. The resulting equation is

$$\Delta x_{\max}^1 = -K \left\{ (kE\beta/4\pi) [2/\{\mu(D-E)\}]^{1/2} \right\}^{1/2}, \quad (\text{II. 15})$$

where Δx_{\max}^1 is the maximum peak-to-peak CFM splitting, D and β are the Morse well depth and curvature parameters, respectively, E is the initial oscillator energy, μ is the oscillator reduced mass, k is the IVR first-order rate coefficient and K is a proportionality constant which Agrawal *et al.*¹⁶ have found to be 0.667.

Non-Statistical Effects and Intramolecular Energy Transfer

The unimolecular decomposition of energized molecules is commonly treated using some form of statistical rate theory. The statistical assumptions of RRKM theory and classical variational transition-state theory imply that the molecular internal energy is randomly distributed over all the vibrational modes. That is, the energetically accessible phase space of the system must be fully explored on a time scale that is short relative to the reaction time. It has generally been assumed that this requirement will be fulfilled if the intramolecular energy transfer rate out of a given excited mode is large relative to the unimolecular reaction rate. If so, mode-specific chemical effects will not be observed. However, pronounced nonstatistical effects have been observed.¹⁸ Therefore, the finding that there may exist numerous systems for

which such an assumption is invalid calls into serious question the use of statistical theoretical methods.

Generally speaking, a statistical reaction rate is any rate computed using the assumption that the internal energy is randomly distributed throughout the molecule. k_{stat} can be obtained by full minimization of the flux of system crossing a dividing surface per unit time. The microcanonical rate coefficient $k(E)$ obtained from statistical transition state theory (EMS-TST) is one kind of statistical rate.

$k(E)$ can be expressed as an average over the microcanonical ensemble¹⁹⁻²⁰

$$k(E) = \frac{\frac{1}{2} \int d\Gamma \delta[H(\Gamma) - E] \times \delta(q_{\text{RC}} - q_c) \left| \dot{q}_{\text{RC}} \right|}{\int d\Gamma \delta[H(\Gamma) - E]}, \quad (\text{II. 16})$$

where Γ is the complete set of position and momentum coordinates $[p, q]$, $H(\Gamma)$ is the system Hamiltonian excluding the center-of-mass motion, $q_{\text{RC}} = q_{\text{RC}}(q)$ is the reaction coordinate, which may be a function of some or all of the coordinates q , and q_c is the critical value required for reaction. The integrals in Eq. (II. 16) are understood to be over the reactant part of phase space.

Since the dividing surfaces employed in the EMS-TST calculations completely separate the reactant and product configuration space, it is impossible for reactants to undergo reaction without traversing the dividing surface. Due to trajectories that recross the dividing surface, the numerator of Eq. (II. 16) will therefore always tend to yield upper bounds for the corresponding trajectory rates. Figure 1 gives a simple illustration of this

point. Clearly the number of dividing surface crossings and the flux through the dividing surface will tend to be an upper limit to the true reaction rate.

However, detailed comparisons of $k(E)$ computed using EMS-TST^{18,20} and trajectory methods²¹ on the same potential-energy surface shows that in some cases $k_{\text{traj}} > k_{\text{ems-test}}$. The only way such a result can occur is for the denominator of Eq.(II. 16), which sums the total phase space available to the reactant system, to be larger than that which is actually available in the trajectory calculations. This would mean that the trajectories are not sampling the entire phase space that is energetically accessible. Significant nonstatistical effects are clearly present. This would suggest that intramolecular vibrational relaxation(IVR) is not complete over the entire phase space of the molecule on the time scale of the reaction.

It is important to point out that the existence of very fast energy-decay rates out of all modes relative to the unimolecular reaction rates is not a sufficient condition to guarantee that the statistical assumption will hold. That is for a particular molecular system, it might be found that the intramolecular vibrational rate out of a given set of modes is fast relative to the unimolecular reaction rates but that the energy remains confined within a small subset of modes rather than becoming completely randomized over all the internal vibrational modes. IVR will be "globally" fast if and only if the mode-to-mode IVR rates between all modes are fast relative to the unimolecular reaction rate under investigation. The finding that IVR is not globally fast is sufficient to demonstrate that the unimolecular decomposition reactions of the molecule may not behave statistically.

Variational Phase-Space Theory Methods

Variational Phase-Space Theory methods provide a way to estimate the reaction rates for statistical systems.²² Numerous detailed studies of diffusion and mobility on surfaces have been carried out by this methods.²³⁻²⁸ Whenever the diffusion energy barrier is low, these processes can be most conveniently studied using classical trajectories. For processes involving a high diffusion energy barrier or very low temperatures, it is more computationally feasible to employ variational phase-space method.^{23, 27} The central idea of these methods is that a reacting system can be described by the motion of a representative point in the phase space of the system. As illustrated in Fig.1, phase space is divided by a dividing surface into two regions corresponding to reactant and product space. Evaluation of the flux at which representative points pass through this surface in one direction will give an upper limit to the reaction rates provided the system behaves statistically. In this procedure, Monte Carlo methods are utilized to evaluate the flux across a dividing surface, $S(p,q)$, in phase space. This flux is given by

$$F(T) = Q^{-1} \int \dots \int \delta[s - s_0] |V_s| e^{-\beta H} \prod_i dq_i dp_i, \quad (\text{II. 17})$$

where $\delta[s - s_0]$ is the Dirac delta function and s_0 denotes the position of the dividing surface, V_s is the velocity perpendicular to the dividing surface, $\beta = 1/kT$ where k is the Boltzmann constant, H is the system Hamiltonian, and Q is the reactant-state partition function. In actual practice, a set of dividing surfaces dependent on a set of parameters is chosen. Since $F(T)$ is an upper

limit to $k(T)$, the minimum flux obtained from this set of surfaces represents the best approximation to the true reaction rate.

The integrations over the momentum coordinates in Eq.(II.17) are done analytically so that only the configuration space integrations need to be done by Monte Carlo techniques. Because of the fact that the necessary condition for a reaction to take place corresponds to crossing the dividing surface at least once, we must have $F(T) \leq k(T)$. Therefore, if $F(T)$ is minimized with respect to the location and shape of the dividing surface, $F(T)$ must approach $k(T)$. If the statistical assumption holds and if the dividing surface is sufficiently general, we expect $F(T)$ to be a tight upper bound to the true reaction rate coefficient. This is particularly true if a correction factor for surface recrossing is determined in the calculations.²³

REFERENCES

1. L. M. Raff and D. L. Thompson, *Theory of Chemical Reaction Dynamics*, (edited by M. Bae, Chemical Rubber, Boca Raton, 1985), vol. III., p. 1.
2. R. N. Porter and L. M. Raff, in *Dynamics of Molecular Collisions*, (edited by W. H. Miller, Plenum Press, New York, 1976), vol. II, p.1.
3. J. P. Valleau and S. G. Whittington,, in *Modern Theoretical Chemistry*, (edited by B. J. Berne, Plenum Press, New York, 1977), vol. 5, p.137.
4. M. Born and J. R. Oppenheimer, *Ann. Physik* **84**, 457 (1927).
5. J. I. Steinfeld, J. S. Francisco, and W. L. Hase, *Chemical Kinetics and Dynamics*(Prentice-Hall, New Jersey, 1989).
6. L. M. Raff, *J. Chem. Phys.* **89**, 5680(1988).
7. L. M. Raff, *J. Chem. Phys.* **90**, 6313(1989).

8. H. W. Schranz, L. M. Raff, and D. L. Thompson, *J. Chem. Phys.* **95**, 106 (1991)
9. H. Goldstein, *Classical Mechanics*, 2nd ed. (Addison-Wesley, Reading Massachusetts, 1980).
10. Sabol, I. M., *Methods of Statistical Testing: Monte Carlo Method*. (edited by Elsevier, N. Y., 1964) Chapter 11.
11. Baker, J. A., *Lattice Theories of the Liquid State*, Macmillan, N. Y. (1963)
12. D. W. Noid, M. L. Koszykowski, and R. A. Marcus, *J. Chem Phys.* **67**, 404(1977).
13. R. Scott Smith and R. B. Shirts, *J. Chem. Phys.* **89**, 2948 (1988).
14. T. D. Swell, D. L. Thompson, and R. D. Levine, *J. Phys. Chem.* **96**, 8006 (1992).
15. X. Y. Chang, T. D. Swell, L. M. Raff, and D. L. Thompson, *J. Chem. Phys.* **97**, 7354 (1992).
16. P. M. Agrawal, D. C. Sorescu, R. D. Kay, D. L. Thompson, L. M. Raff, J. B. Conrey, and A. K. Jameson, *J. Chem. Phys.* (in Press).
17. J. S. Bendat and A. G. Piersol, in *Random Analysis and Measurement Procedures*, (John Wiley & Sons, New York, 1986).
18. H. W. Schranz, L. M. Raff, and D. L. Thompson, *J. Chem. Phys.* **95**, 106 (1991).
19. J. D. Doll, *J. Chem. Phys.* **73**, 2760 (1980); **74**, 1074 (1984).
20. H. W. Schranz, L. M. Raff, and D. L. Thompson, *Chem. Phys. Lett.* **171**, 106 (1991).
21. P. M. Agrawal, D. L. Thompson, and L. M. Raff, *J. Chem. Phys.* **92**, 1069 (1990).
22. J. C. Keck, *Advances In Chemical Physics*, (edited by I. Prigogine, Interscience, New York, 1967) Vol. XII, P. 85.

23. P. M. Agrawal, D. L. Thompson, and L. M. Raff, *J. Chem. Phys.* **91**, 6463 (1989).
24. I. NoorBatcha, L. M. Raff, and D. L. Thompson, *J. Chem. Phys.* **83**, 6009 (1985).
25. I. NoorBatcha, L. M. Raff, and D. L. Thompson, *J. Chem. Phys.* **82**, 1543 (1985).
26. I. NoorBatcha, L. M. Raff, and D. L. Thompson, *J. Chem. Phys.* **81**, 3715 (1984).
27. B. M. Rice, L. M. Raff, and D. L. Thompson, *J. Chem. Phys.* **88**, 7221 (1988).
28. B. M. Rice, I. NoorBatcha, D. L. Thompson, and L. M. Raff, *J. Chem. Phys.* **86**, 1608 (1987).

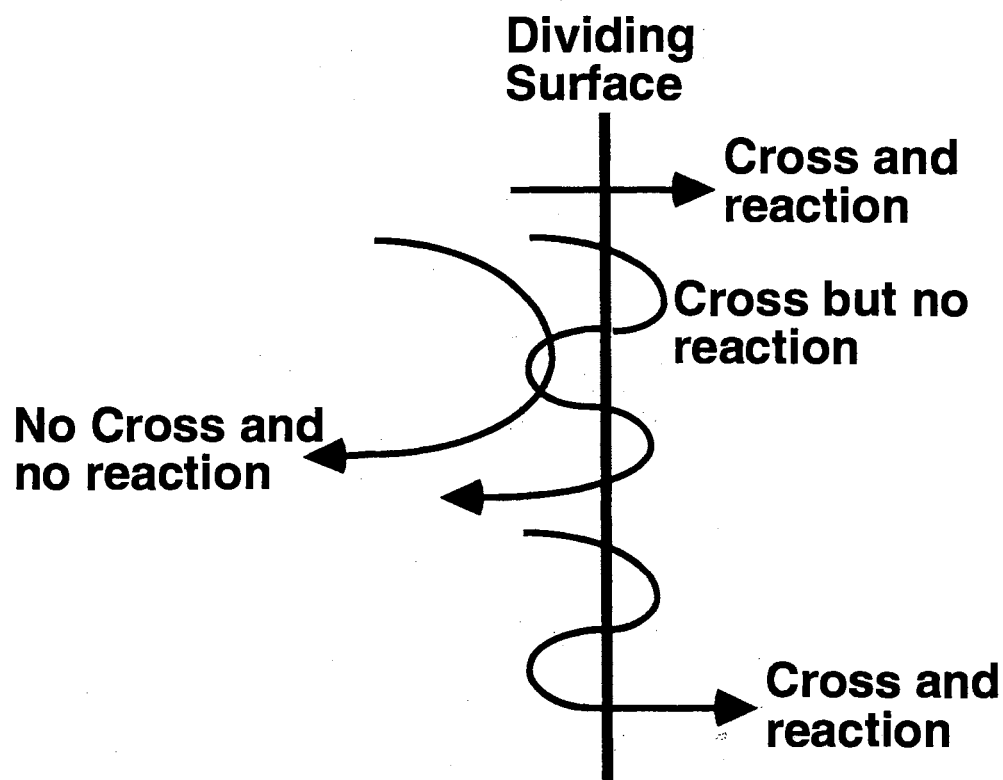


Figure 1. Simple illustration of statistical transition state theory. Phase space is divided by dividing surface into two regions corresponding to reactant configuration space and product configuration space. The space to the left of the dividing surface is the reactant configuration space and that to the right is product configuration space.

CHAPTER III

INTRAMOLECULAR ENERGY RATES AND PATHWAYS FOR VINYL BROMIDE

INTRODUCTION

It is well known that the dynamics of intramolecular vibrational relaxation (IVR) play an important role in unimolecular dissociation reactions. The statistical assumptions of unimolecular RRKM reaction rate theory and classical variational transition-state theory require that the molecular internal energy be randomly distributed over all the vibrational modes. This, in turn, requires that the IVR rate be large relative to the unimolecular reaction rate. It has previously been noted that this is a necessary, but not sufficient, condition to ensure a globally random distribution of internal energy¹. The observation of mode-specific effects implies that there exists an unimolecular reaction whose rate exceeds that needed for global intramolecular energy randomization. Since intramolecular energy transfer processes in most systems are fast², only a few cases of mode-specific rate enhancement have been reported.³

The computation of the rates and pathways of intramolecular energy flow for highly coupled, polyatomic systems has proven to be difficult. In general, classical studies of intramolecular energy transfer involve the

integration of the Hamiltonian equations of motion on a potential-energy surface. "Bond" or "mode energies" are then computed from the results. Intramolecular energy transfer pathways and rates are inferred from the calculated time variation of these quantities⁴. This procedure obviously involves an arbitrary definition of the "bond energy" which generally assumes a mode reparability that does not exist. Consequently, all potential and kinetic coupling terms involving the mode coordinates are omitted from the definition. As a result, one can never be certain whether a variation in "bond energy" is due to actual energy transfer to or from other modes or merely to changes in the magnitudes of the omitted coupling terms. Nor is it possible to be certain that the results themselves are not dependent upon the arbitrary definition adopted for "bond" or "mode energy". We have previously shown⁵ that these problems may be eliminated by analyzing the internal energy flow in a molecule from the envelope functions of the temporal variations of the mode kinetic energies computed using a coordinate system that diagonalizes the kinetic energy matrix.

It has generally been assumed that a molecular system will exhibit statistical behavior provided the intramolecular energy transfer rates are large relative to the unimolecular reaction rates of the system. Since this is usually the case, statistical behavior is the expected norm. However, in recent years, both theoretical and experimental results suggest that nonstatistical behavior may be much more prevalent than previously suspected. Schlag and Levine⁶ have noted that certain highly-excited, large molecules have been observed to dissociate much faster than RRK statistical theory⁷ would predict. Newman-Evans *et al.*^{8a} have reported experimental measurements of the thermal branching ratio of 1- and 2-phenylbicyclo[2.1.1]hex-2-enes-5-d to give

products differing only in the location of the deuterium atom. A 9:1 ratio of product isomers is observed rather than the 1:1 ratio predicted by statistical theories of reaction rates. Newman-Evans *et al.*^{8a} also found that optically active *trans*-2-methyl-1-(*trans*-2-phenylethenyl) cyclopropanes resulting from the unimolecular rearrangement of enantiomeric methyl phenyl cyclopentenes are formed in a 5.9:1 ratio. These results are obviously nonstatistical. In a study of bond inversion in aziridine, Borchardt and Bauer^{8b} also noted the deviations between the measured rates and RRKM predictions. The unimolecular dissociation reactions of 1,2-difluoroethane, disilane and the 2-chloroethyl radical have been investigated by Raff, Thompson, Sewell, and Schranz⁹⁻¹³ using both trajectory and classical variational transition-state theory (TST) with Efficient Microcanonical Sampling (EMS) methods. The calculations show the presence of significant nonstatistical effects on both the reaction rates and the product energy partitioning for 1,2-difluoroethane and disilane but not for the 2-chloroethyl radical¹³. Further investigations of these systems showed that the total IVR rate for the relaxation of a given mode is at least an order of magnitude greater than the reaction rates. Yet, nonstatistical dynamics still occurs. It was therefore suggested that the existence of a very fast IVR rate out of a given mode is not a sufficient condition to ensure statistical behavior^{1,9-12}.

Sorescu *et al.*¹⁴⁻¹⁶ have conducted detailed theoretical studies of statistical effects in the skeletal inversion of bicyclo(2.1.0) pentane¹⁴ and the decomposition of 2,3-diazabicyclo(2.2.1) hept-2-ene (DBH)^{15,16} using trajectory methods and EMS-TST statistical theory. The ring inversion is found to be statistical in all respects. The DBH reaction behaves statistically in that the distribution of energy is microcanonical and classical variational

transition-state theory calculations yield close upper bounds to the reaction rates. However, nonstatistical behavior is still found to be present because the system fails to explore all of the energetically accessible configuration space once it passes through the transition-state region.

Most recently, both trajectory and EMS-TST calculations on the unimolecular dissociation reactions of vinyl bromide have been carried out^{17,18}. The maximum reaction rate coefficient at the upper limit of internal energy considered (6.44 eV) is found to be 2.11 ps^{-1} . The trajectory results show that the ratio of HBr to Br products is greater than unity in spite of the fact that the threshold for C-Br bond rupture lies below that for HBr elimination. It is also found that three-center H₂ elimination is much more probable than four-center elimination even though the three-center threshold lies 0.33 eV above that for the four-center process. In view of these results, it was suggested¹⁷ that the decomposition of vinyl bromide may be nonstatistical. This possibility has been investigated by the computation of the reaction rates for C-Br bond scission, the three-center elimination of HBr and three-center H₂ elimination using statistical EMS-TST methods with the same potential hypersurface used in the trajectory calculations^{17,18}. The EMS-TST results for C-Br bond rupture and HBr three-center elimination are found to be upper bounds to the rate coefficients computed from the trajectory calculations. These data make it possible for C-Br bond scission and HBr elimination to be statistical processes. In contrast, the EMS-TST rates for three-center H₂ elimination are lower than the corresponding rates obtained from the trajectory studies. We have previously noted¹⁰⁻¹² that if $k(E)_{\text{EMS-TST}} < k(E)_{\text{trajectory}}$ on the same potential-energy surface, the system must behave nonstatistically. Thus, our previously drawn hypothesis¹⁷ that the

decomposition dynamics for vinyl bromide may be nonstatistical is at least partially correct.

In this chapter, the results of a detailed investigation of intramolecular energy transfer in vinyl bromide are reported. The primary objectives of the study are to determine the dynamics underlying the nonstatistical behavior of the three-center H₂ elimination process and to determine why C-Br bond scission and three-center HBr elimination appear to obey the assumptions of statistical theory. This chapter is organized into four parts. Following the Introduction, we review the basis of the computational method and provide a brief description of the potential-energy surface. Section III is devoted to the details of intramolecular energy transfer in vinyl bromide and their relationship to the statistical/nonstatistical behavior of the system. Section IV summarizes our principal findings.

Computational Methods and Potential Surface

A. Computational methods

The unimolecular dissociation dynamics of vinyl bromide have been investigated using standard classical trajectory and EMS-TST methods¹⁷⁻¹⁹. The results show that three-center H₂ elimination is a nonstatistical process whereas C-Br bond scission and three-center HBr elimination appear to behave statistically. In order to obtain quantitative information about the intramolecular energy transfer dynamics that lead to these results, we have employed a previously described projection method⁵. This method is based on the calculation of the temporal variation of a diagonal kinetic energy matrix.

The energy transfer rates and pathways are extracted from the envelope functions of this temporal variation. Since the potential energy is not involved in the analysis, all problems associated with potential coupling between the vibrational modes are eliminated. The basis of the method is reviewed below.

Let \mathbf{L}_i ($i = 1, 2, 3, \dots, 3N$) represent a set of normalized ($3N \times 1$) transformation vectors that project the normal mode vibrations, \mathbf{Q}_i ($1 \leq i \leq 3N - 6$), the center-of-mass translations, \mathbf{Q}_i ($3N - 5 \leq i \leq 3N - 3$), and the rotations about the molecular center-of-mass, \mathbf{Q}_i ($3N - 2 \leq i \leq 3N$) onto the Cartesian displacements, q_j ($j = 1, 2, 3, \dots, 3N$). At time t , the instantaneous Cartesian velocities may therefore be written as linear combinations of the elements of \mathbf{Q}_i :

$$\dot{q}_i(t) = \sum_{j=1}^{3N} \dot{Q}_j(t) L_{ij} \quad \text{for } i = 1, 2, 3, \dots, 3N. \quad (\text{III. 1})$$

Equation (III. 1) may be written in matrix form as

$$\dot{\mathbf{q}}(t) = \mathbf{L} \dot{\mathbf{Q}}(t), \quad (\text{III. 2})$$

where \mathbf{L} is a ($3N \times 3N$) square matrix whose columns are the normalized projection vectors \mathbf{L}_i . $\dot{\mathbf{q}}(t)$ is a ($3N \times 1$) column vector whose elements are the Cartesian velocities and $\dot{\mathbf{Q}}(t)$ is a ($3N \times 1$) column vector whose elements are the normal mode, center-of-mass, and rotation velocities. The normal mode velocities are therefore given by

$$\dot{\mathbf{Q}}(t) = \mathbf{L}^{-1} \dot{\mathbf{q}}(t). \quad (\text{III. 3})$$

The kinetic energy T at time t is:

$$T(t) = 0.5 \sum_{i=1}^{3N} m_i \dot{q}_i^2(t) . \quad (\text{III. 4})$$

Substitution of Eq.(III. 1) yields

$$\begin{aligned} T(t) &= 0.5 \sum_{i=1}^{3N} m_i \sum_{j=1}^{3N} \sum_{k=1}^{3N} \dot{Q}_j(t) \dot{Q}_k(t) L_{ij} L_{ik} \\ &= 0.5 \sum_{i=1}^{3N} m_i \sum_{j=1}^{3N} \dot{Q}_j^2(t) L_{ij}^2 , \end{aligned} \quad (\text{III. 5})$$

since the kinetic energy is diagonal when expressed in terms of the normal mode velocities . Consequently, the kinetic energy may be written as

$$T(t) = \sum_{j=1}^{3N} a_j \dot{Q}_j^2(t) , \quad (\text{III. 6})$$

provided the mode constant a_j is defined to be

$$a_j = 0.5 \sum_{i=1}^{3N} m_i L_{ij}^2 . \quad (\text{III. 7})$$

Equation (III. 6) shows that the total molecular kinetic energy is the uncoupled sum of the individual mode kinetic energies, $T_i(t)$, where

$$T_i(t) = a_i \dot{Q}_i^2(t) . \quad (\text{III. 8})$$

The total energy associated with a given mode alternates between potential and kinetic energy with a frequency characteristic of the mode fundamental. If there is no energy flow to or from the mode, the envelope of these oscillations will have a zero slope. A rapid energy transfer, however, will produce a large slope to the envelope function. Thus, the energy flow through the molecule may be determined directly from the temporal variation of the envelopes of the mode kinetic energies.

Using the virial theorem, we may compute an approximate average total energy associated with a given mode i from

$$\begin{aligned} \langle E_i(t) \rangle &= 2(\Delta t)^{-1} \int_{t_0}^{t_0+\Delta t} T_i(t) dt \\ &= 2(\Delta t)^{-1} \int_{t_0}^{t_0+\Delta t} a_i Q_i^2(t) dt, \end{aligned} \quad (\text{III. 9})$$

where t is a time in the interval $t_0 \leq t \leq t_0 + \Delta t$. The time interval Δt is chosen to average out most of the fluctuations in $T_i(t)$ due to beats and the interconversion of potential and kinetic energies within the same mode.

If the initial excitation energy is inserted into mode i , the temporal variation of $\langle E_i(t) \rangle$ is directly related to the rate of energy flow out of this mode. For the present study, we have assumed that this energy flow can be adequately described by a first-order rate law. While this assumption is not rigorously correct, it will be seen that it is sufficiently accurate to permit us to determine in a semiquantitative fashion the nature of IVR in vinyl bromide. Under these conditions, the intramolecular energy transfer rate coefficient k_i can be deduced by fitting the equation

$$\langle E_i(t) \rangle = E_i(0) \exp[-k_i t] + (1 - \exp[-a_i t]) \langle E_i(\infty) \rangle \quad (\text{III. 10})$$

to the data obtained from Eq.(III. 9). In Eq.(III. 10), k_i , a_i and $\langle E_i(\infty) \rangle$ are parameters representing the total relaxation rate coefficient of mode i , an average total rate coefficient for energy transfer into mode i and the statistical equilibrium value of $\langle E_i(t) \rangle$ at infinite time, respectively.

B. Potential-energy Surface

The potential surface used in the present studies is a global surface accurately fitted to all of the available structural, thermochemical, kinetic and spectroscopic experimental data and to the results of *ab initio* electronic structure calculations for the transition states for several decomposition channels¹⁷. The *ab initio* calculations were carried out using 6-31G(d,p) basis sets for carbon and hydrogen and Huzinaga's (4333/433/4) basis set augmented with split outer s and p orbitals and an f orbital for bromine. Electron correlation is incorporated using Möller-Plesset fourth-order perturbation theory with all single, double, triple, and quadruple excitations included. The average absolute difference between ΔE values for the various decomposition channels obtained from the global surface and experimental measurement is 1.76 kcal/mol. Predicted equilibrium geometries for reactants and products are in good to excellent accord with experiment. The average absolute difference between the fundamental vibrational frequencies predicted by the global surface and those obtained from Raman and IR spectra vary from 10.2 cm⁻¹ for H₂C=CHBr to 81.3 cm⁻¹ for H₂C=CH²⁰. The results for vinyl bromide are given in Table I. The potential barriers for seven

decomposition channels agree with the *ab initio* calculations to within an average difference of 1.4 kcal/mol.

C. Numerical Procedures

The initial states for the trajectories are prepared in the manner described in our previous investigation of the gas-phase, unimolecular decomposition of vinyl bromide¹⁷. Initially, vinyl bromide is placed in the equilibrium conformation predicted by the global surface¹⁷. Zero-point vibrational energy is inserted into each of the vinyl bromide normal modes using Eq.(III. 1) with the $\dot{\mathbf{Q}}_I(t)$ for rotation and translation set to zero. Hamilton's equations of motion are then integrated for a randomly chosen period t_p given by

$$t_p = \xi \tau, \quad (\text{III. 11})$$

where ξ is a random number selected from a distribution that is uniform on the interval $[0,1]$ and τ is the characteristic period of the lowest frequency vibrational mode in vinyl bromide. The numerical integrations are effected using a fourth-order Runge-Kutta procedure with a fixed step size of 0.01 t.u. (0.0001019 ps). Equation (III. 11) effectively averages over the vibrational phases of the lattice. Subsequent to the above integration, the desired excitation energy, E_{ex} , is inserted into the selected mode k . This is accomplished by first using Eq.(III. 3) to project out the instantaneous normal mode velocities, $\dot{\mathbf{Q}}_I(t_p)$. The velocity $\dot{\mathbf{Q}}_k(t_p)$ is then altered to $\dot{\mathbf{Q}}_k'(t_p)$ to reflect the insertion of the excitation energy E_{ex} . The required velocity is given by

$$\dot{\mathbf{Q}}_k'(t_p) = \pm \{ (a_k)^{-1} [a_k \dot{\mathbf{Q}}_k^2(t_p) + E_{ex}] \}^{1/2}, \quad (\text{III. 12})$$

where the sign is chosen randomly. The new Cartesian velocities are computed using Eq.(III. 1). In the present investigation, E_{ex} has been taken to be 3.0 eV.

The subsequent dynamical behavior of the system is followed for a period of 450 t.u. (4.586 ps) to determine the nature of the energy transfer. After every tenth integration step, Eq.(III. 3) is used to compute the instantaneous values of the $\dot{Q}_i(t)$ ($i=1,2,3,\dots,3N$). The mode kinetic energies are calculated using Eq.(III. 8). Approximate average mode energies at time t^* are obtained from Eq.(III. 9) using $\Delta t = 25$ t.u. (0.255 ps) and $t^* = t_0 + \Delta t/2$. Four significant digits of energy conservation is generally achieved.

The classical variational transition-state theory calculations (EMS-TST)¹⁸ are carried out by defining a series of dividing surfaces which completely separate the reactant and product configuration space. A Markov walk with importance sampling included is carried out using efficient microcanonical sampling methods^{11,12}. The flux across each of the dividing surfaces is computed from the results of the walk. If the system behaves statistically, the computed EMS-TST flux must be an upper bound to the rate calculated from the trajectory analysis since there are no corrections for recrossings of the dividing surface. Under these conditions, the dividing surface yielding the minimum flux is the best statistical approximation to the true trajectory rate. If we find $k_{EMS-TST}(E) < k_{Traj}(E)$, the system is not behaving statistically. Such a result has been obtained for three-center H_2 elimination from vinyl bromide, but not for three-center HBr elimination or for the C-Br bond scission¹⁸.

Intramolecular energy transfer near the transition states for three-center HBr and H₂ elimination is examined by placing the system in the minimum-energy configuration achieved during the Markov walk on one of the dividing surfaces. The excess energy, $E_{\text{total}} - E_{\text{potential}}$, is randomly partitioned among the internal coordinates using Eqs.(III. 1)-(III. 8). Energy transfer pathways from this initial configuration are then investigated using the procedures described above.

Results and Discussion

A. Energy Transfer Rates and Pathways

We have examined the pathways and rates of intramolecular energy flow out of each of the 12 vibrational modes in vinyl bromide. Figures 2a-2d show typical results. These figures report the temporal variation of the instantaneous mode kinetic energies computed from Eq.(III. 8) for the case in which 3.0 eV of initial excitation energy is partitioned into the C-H stretching mode ν_{10} . Some important qualitative features of the intramolecular energy transfer dynamics for vinyl bromide at or near its equilibrium configuration are immediately obvious upon inspection of Figs. 2a-2d. Figure 2a shows the kinetic energies in the low-frequency C-C-Br bending, CHBr wag and C-Br stretching modes while Fig. 2d shows the corresponding results for the high-frequency C-H stretching modes. The kinetic energies in the various bending, wags, torsion and C=C stretching modes are given in Figs. 2b and 2c. Inspection of the kinetic energy in ν_{10} reveals that the envelope function decreases to near equilibrium levels in 5-10 t.u. (0.051 - 0.102 ps). Obviously, the total energy transfer out of this mode is very fast.

The pathways of energy flow from mode ν_{10} are easily determined from the results given in Figs. 2a-2d. The primary transfer pathway from ν_{10} is clearly to ν_{12} since only ν_{12} has a kinetic energy amplitude that increases rapidly over the first 4 t.u. (0.0408 ps). Around 4 t.u., energy begins to flow into the third C-H stretching mode, ν_{11} . These results are not surprising in view of the near resonance between the C-H stretching modes. All other modes are at least 1400 cm^{-1} out of resonance with the C-H stretches.

The secondary pathways for energy flow from the C-H stretches may also be identified from Fig. 2. At 10 t.u. (0.102 ps), the kinetic energy in the CH_2 wag, ν_4 , begins to increase rapidly. At this point, only the C-H stretching modes are excited so we may safely draw the qualitative conclusion that for this trajectory, the CH_2 wag provides the major pathway for energy transfer from the C-H stretches to the other vinyl bromide modes.

Around 20 t.u. (0.204 ps), the C-Br stretch, ν_3 , and the ν_5 torsion begin to gain kinetic energy. Since the kinetic energy in these modes failed to increase significantly during the initial 20 t.u. (0.204 ps), it is reasonable to conclude that the energy flow is from the CH_2 wag, not the C-H stretches. All other modes are essentially inactive during the primary, secondary and tertiary phases of energy equilibration.

After 60 t.u. (0.601 ps) have elapsed, the C-C-Br bend (ν_1), CHBr wag (ν_2), C-C-H⁵ bend (ν_6), H-C-H bend (ν_8) and the C=C stretch (ν_9) begin to gain energy. These transfer processes probably involve primarily coupling of these modes to the C-Br stretch and torsional modes. Mode ν_7 , the C-C-H³ bend, is totally inactive throughout the entire process.

The above results demonstrate that although the total energy transfer rate out of ν_{10} is fast, it is not "globally" fast. IVR will be "globally" fast if and only if the mode-to-mode IVR rates between all modes are fast relative to the unimolecular reaction rate under investigation. If this condition exists, the internal energy will be distributed randomly over phase space on a time scale that is short relative to the characteristic lifetime of the reactant and the fundamental assumption of statistical theory will hold. This condition is not satisfied for vinyl bromide with 3.0 eV of excitation energy. Several of the modes remain nearly inactive for about 0.6 ps while ν_7 is inactive for over a full picosecond. This once again emphasizes the point we have previously made¹, a total energy transfer rate out of a given mode that is fast relative to a unimolecular reaction rate is a necessary condition for statistical behavior, but it is not a sufficient condition. If vinyl bromide were to undergo a unimolecular reaction at 3.0 eV excitation energy whose characteristic relaxation time were 0.5 ps, the assumption that the energy will be distributed microcanonically on this time scale would obviously not be valid.

The finding of a trajectory for which IVR is not globally fast is sufficient to demonstrate that the unimolecular decomposition reactions of vinyl bromide may not behave statistically. The internal energy will not be distributed microcanonically on a time scale that is short relative to the unimolecular reaction lifetime. Moreover, it may be inferred that the set of trajectories for which this is true must be very large otherwise the probability that such a trajectory would be found among the infinitude of possible trajectories would be vanishing small.

We have demonstrated the truth of the above statement by following the temporal variation of the mode kinetic energies in 10 additional trajectories

obtained by choosing differing values of t_p in Eq.(III. 11) prior to the 3.0 eV excitation of ν_{10} . In every case, the major energy transfer pathway is from ν_{10} to ν_{12} or to ν_{11} and ν_{12} . That is, the principal relaxation mechanism always involves transfer to the other C-H stretching modes. The secondary relaxation pathway for the trajectory leading to Fig. 2 is through the CH₂ wag (ν_4). Examination of all of the trajectories shows that the H-C-H bend (ν_8) also provides a secondary path in some cases. In all cases, modes ν_1 , ν_2 , ν_7 and ν_9 do not begin to exhibit significant excitation until about 50 t.u. (0.510 ps) have elapsed. IVR in vinyl bromide is not globally fast.

We have carried out similar calculations for all of the modes in vinyl bromide. That is, the temporal variations of the mode kinetic energies have been determined for 3.0 eV excitation of mode k for $k = 1, 2, 3, \dots, 12$. In each case, a single trajectory was examined. The results are qualitatively similar to those given in Fig. 2. IVR is never globally fast. There are always several modes present which are essentially inactive during the first 0.5 psec subsequent to excitation of mode k . As noted above, we do not expect this situation to be altered by examination of a large ensemble of trajectories. Table 2 summarizes the principal transfer pathways determined from these calculations. The results for initial excitation of ν_{10} suggest that the major pathways for energy transfer will be unaltered by the computation of an ensemble of trajectories. However, such extensive calculations would probably reveal the presence of other secondary pathways.

B. First-order Relaxation Model

By using Eq.(III. 9), an approximate average total energy associated with a given mode, $\langle E_j \rangle$, can be calculated. The data expressed in terms of the temporal variation of $\langle E_j \rangle$ are easier to visualize than the envelope of the mode kinetic energy. Figure 3 shows typical results for ν_{11} and ν_6 for the case in which 3.0 eV is initially partitioned into these modes. The calculated results are shown as points on the plot. These points are connected by straight lines for visual clarity. It can be seen that the decay rate for ν_{11} is about a factor of two slower than the corresponding rate for ν_6 . These energy transfer rates are much faster than those previously computed for the relaxation of various modes in 1,2-difluoroethane¹².

A more quantitative measure of the total relaxation rates may be obtained using Eq.(III. 10) to fit the data obtained from Eq.(III. 9). In Eq.(III. 10), k_i represents in an approximate fashion the total energy transfer rate coefficient from mode i. Thus,

$$k_i = \sum_{\substack{j=1 \\ (j \neq i)}}^{12} k_{ij} , \quad (\text{III. 13}) ,$$

where k_{ij} is the mode-to-mode energy transfer rate coefficient from mode i to mode j. Figure 4 shows a typical example of the degree of accuracy to be expected from Eq.(III. 10). In this case, 3.0 eV of excitation energy is initially partitioned into the C=C stretch (ν_9). Equation III.9 is used to compute the points shown in Fig. 4. The solid curve is the result of a least squares fitting of Eq.(III. 10) to these points. It is evident that the major features of the energy

transfer are sufficiently well described by the first-order model to make it a useful tool for the presentation of data in succinct form.

While it is possible to determine qualitatively the major energy transfer pathways and, to a lesser extent, the secondary pathways from the results of a few trajectories, this is generally not the case for rate coefficients. Accurate determination of these quantities requires averaging over a large ensemble sampled from appropriate distributions. Nevertheless, rate coefficients determined from limited subsets of trajectories generally give the correct order of magnitude and are often accurate to within a factor of two. This point is illustrated in Fig. 5 which shows the temporal variation of $\langle E(t) \rangle$ for the extremes of the rates obtained from the trajectories computed for 3.0 eV excitation of mode ν_{10} . The average result for all trajectories is shown as the solid curve. The values of k_{10} obtained by least-squares fitting of Eq.(III. 10) are $k_{10}^{\max} = 24.8 \text{ ps}^{-1}$, $k_{10}^{\min} = 6.5 \text{ ps}^{-1}$ and $k_{10}^{\text{ave}} = 13.3 \text{ ps}^{-1}$. The spread of the distribution gives a root-mean-square deviation from the mean of 1.7 ps^{-1} . We might therefore expect that the average deviation from the ensemble average of k_{10} computed from any single trajectory will be about 13% and the maximum deviation will be no more than a factor of two.

Table 3 presents a summary of the total relaxation rates for each of the 12 vibrational modes of vinyl bromide in the near vicinity of the equilibrium conformation. These rates were computed by fitting Eq.(III. 10) to the data obtained using Eq.(III. 9). The fastest relaxing modes are the torsion and the CH_2 wag modes, ν_5 and ν_4 , respectively. The slowest modes are the C-H stretch for the $-\text{CHBr}$ group, ν_{11} , and the C-C-Br bending mode, ν_1 . It is perhaps not unexpected that ν_{11} should relax slowly. The other modes associated with the $-\text{CHBr}$ moiety have very low frequencies. Hence, they

would be expected to be ineffective in relaxing the high-frequency C-H stretch. Figure 6 shows the data computed from Eq.(III. 9) and the first-order fits for the slowest and fastest relaxing modes in vinyl bromide. As noted above, we expect these rate coefficients to deviate from the ensemble average by an average of about $\pm 13\%$ and by no more than a factor of two. Consequently, they give a semiquantitative measure of the total relaxation rates of the vinyl bromide modes at 3.0 eV excitation energy.

Using classical trajectory methods²¹, the thermal gas-phase decomposition dynamics of vinyl bromide on the current ground-state potential surface have been investigated at several energies in the range 4.0 - 6.44 eV in excess of zero-point energy¹⁷. At each energy investigated, the total unimolecular reaction rate coefficient $k_T(E)$ was obtained by fitting the decay plot to a first-order expression. The maximum reaction rate coefficient at the upper limit of internal energy considered (6.44 eV) is 2.11 ps^{-1} . This value is a factor of 3.1 smaller than the total relaxation rate for the slowest of the 12 modes. It is a factor of 11.8 slower than the fastest relaxing mode, ν_5 . It is clear that the total energy transfer rates in vinyl bromide are fast relative to the unimolecular decomposition rates. It is therefore possible for the system to exhibit statistical behavior. However, because the energy transfer is not globally rapid, such statistical behavior is not guaranteed^{1,11,12}.

C. IVR in the Transition-State Regions for Three-Center Elimination

The fundamental assumption of all statistical theories of reaction rates is that all states or phase-space points with equal energy are sampled with equal probability. Thus, for a unimolecular reaction to be well-described by

statistical theory, the internal energy must be randomly distributed on a time scale that is fast relative to the reaction rate. This must be true not only for configurations at or near that for the reactant but also for all other nonequilibrium regions of configuration space such as those along the reaction coordinate and in the near vicinity of the transition state.

In all of the above calculations, vinyl bromide is near the equilibrium configuration. The results for this configuration show that the total energy decay rates for all vibrational modes are large relative to the unimolecular decomposition rates of vinyl bromide. However, it is also found that the intramolecular energy transfer is not globally rapid.

We have performed similar calculations with vinyl bromide initially in the minimum-energy configurations found in the EMS-TST calculations¹⁸ on the dividing surfaces for three-center H₂ and HBr elimination. In these calculations, the total energy is 6.44 eV plus zero-point energy. The excess energy, $E_{\text{total}} - V$ where V is the potential energy, is randomly distributed over the internal modes of the system using Eqs.(III. 1)-(III. 8). That is, the values of $T_i(0)$ in Eq.(III. 8) were chosen randomly subject to the constraint that

$$\sum_{i=1}^{12} T_i(0) = E_{\text{total}} - V \quad . \quad (\text{III. 14})$$

Using the procedures outlined in Section II, the intramolecular energy transfer dynamics for these configurations have been assessed.

Figure 7 shows the variation of the H-H and two of the C-H distances with time for a system that is initially in the minimum-energy configuration on a dividing surface near, but not quite at, the optimum surface for three-center H₂ elimination. As can be seen, this system fails to dissociate to H₂ and

bromovinylidene. The system samples configuration points along the reaction coordinate for about 50 t.u. (0.510 ps) after which it reenters the reactant configuration space. Figures 8a - 8d show the temporal variation of the mode kinetic energies during this process. The results are qualitatively similar to those seen in Fig. 2. Initially, the C-H stretching modes, the C-C-H⁵ bend (v₆), the CH₂ wag (v₄), the H-C-H bend (v₈), the C=C stretch (v₉) and the v₅ torsional mode gain a significant amount of kinetic energy as the system explores configurations along the reaction coordinate. The C-C-H³ bend (v₇) and the Br modes gain only small amounts of kinetic energy. This is not surprising since the transition state for three-center H₂ elimination found in the Markov walk¹⁸ is a nonplanar structure in which the H⁴----H⁵ moiety lies approximately perpendicular to the C=CHBr plane with its center below the C=C bond. Around 20 t.u. (0.204 ps), the energy in the C-H stretch (v₁₁) and the CH₂ wag (v₄) decrease to a near zero value. This energy is transferred primarily to v₅, v₆, v₈, v₉ and v₁₀. The C-C-Br bend (v₁), the CHBr wag (v₂) and the C-C-H³ bend (v₇) play very little role in the overall IVR dynamics. The kinetic energy profiles clearly show that IVR is not globally rapid.

Obviously, some of the mode-to-mode IVR rates in configurations along the reaction coordinate for three-center H₂ elimination are slow relative to the unimolecular reaction rate. This implies that some of the atom-atom coupling constants¹³ are very small in these configurations. When coupled with the fact that IVR is not globally rapid for the reactant configuration, these results suggest that three-center H₂ elimination from vinyl bromide may not be a statistical process. As mentioned earlier, recent EMS-TST studies¹⁸ confirm this expectation. These studies give the result $k_{\text{EMS-TST}}(E) < k_{\text{Traj}}(E)$ for all energies examined. This inequality shows the system to be nonstatistical.

Figures 9a - 9d report the temporal variation of the mode kinetic energies for a system that is initially in the minimum-energy configuration on the optimum dividing surface for three-center HBr elimination. This trajectory samples phase space points in the near vicinity of the transition state for about 25 t.u. (0.255 ps) after which HBr dissociation occurs. These data are significantly different than those seen in Figs. 2 and 8. Here, all modes except the C-C-Br bend (ν_1) participate fully in the IVR dynamics. There is a near globally random distribution of the energy on a time scale that is fast compared to the unimolecular reaction rate. The atom-atom coupling constants¹³ computed for the HBr dividing surface are, as the data in Fig. 9 suggest, much larger than the corresponding values obtained for the optimum three-center H₂ dividing surface¹⁸. Such data indicate that three-center HBr elimination from vinyl bromide may be well-described by statistical theory. The EMS-TST calculations¹⁸ support this prediction in that we find that for this reaction $k_{\text{EMS-TST}}(E) > k_{\text{Traj}}(E)$ for all energies investigated.

Summary

The dynamics of intramolecular energy transfer in vinyl bromide have been investigated using projection methods and results obtained from classical trajectories computed on a global potential-energy surface that has been fitted to thermochemical, structural, kinetic and spectroscopic data and the results of electronic structure calculations for the transition states¹⁷. The temporal variation of the average vibrational mode energies are computed

from the projected mode kinetic energy profiles using the virial theorem. Total energy decay rates and the pathways of energy flow for initial 3.0 eV excitation of each of the 12 vibrational modes in the equilibrium configuration have been determined. We have also investigated the energy transfer dynamics in systems for which the initial configurations correspond to the minimum-energy structure found in the EMS-TST calculations¹⁸ on one of the dividing surfaces for three-center H₂ and HBr elimination reactions.

The results for the equilibrium structure show that the total relaxation rate for each mode can be characterized with fair accuracy by a first-order rate law. Least-squares fitting of such a rate law to the computed data shows that the minimum decay rate among the 12 modes is at least 3.1 times larger than the decomposition rate for vinyl bromide at an internal energy of 6.44 eV¹⁷. Such an inequality is a necessary condition to satisfy the basic assumption of statistical theories. However, we also find that energy transfer is not globally rapid. Some modes are essentially inactive for over one picosecond. Consequently, it is possible that statistical theory will not adequately describe the decomposition processes occurring upon excitation of vinyl bromide.

In configurations along the reaction coordinate for three-center H₂ elimination, some mode-to-mode IVR rates are slow relative to the H₂ elimination rate. This fact, coupled with the absence of an IVR rate in configurations near equilibrium that is globally fast, indicates that three-center H₂ elimination from vinyl bromide may not be accurately described by statistical theory.

In configurations near the minimum-energy structure on the optimum dividing surface for three-center HBr elimination, all mode-to-mode IVR rates,

except those involving the C-C-Br bend, are fast relative to the HBr elimination rate. This suggests that statistical theory is more likely to accurately predict the three-center HBr elimination rate than the rate for three-center H₂ elimination.

REFERENCES

1. L. M. Raff, *J. Chem. Phys.*, **90**, 6313 (1989).
2. (a) F.F. Crim, *Annu. Rev. Phys. Chem.*, **35**, 657 (1984). (b) V.E. Bondybey, *ibid.* **35**, 591 (1984).
3. (a) L.L. Sibert; W.P. Reinhardt; J. T. Hynes, *J. Chem. Phys.*, **81**, 1115 (1984). (b) E.L. Sibert; J.S. Hutchinson; J.T. Hynes; W.P. Reinhardt, *Ultrafast Phenomena IV*, Eds. Auston, D. H.; Eisinger, K. B. (Springer, New York, 1984), p. 336. (c) P.J. Nagy; W.L. Hase, *Chem. Phys. Lett.*, **54**, 73 (1978); *ibid.*, **58**, 482 (1978). (d) K.L. Bintz; D.L. Thompson, *J. Chem. Phys.*, **86**, 4411 (1987). (e) K.L. Bintz; D.L. Thompson; J.W. Brady, *J. Chem. Phys.*, **85**, 1848 (1986).
4. (a) K.L. Bintz; D.L. Thompson; J.W. Brady, *Chem. Phys. Lett.*, **131**, 398 (1986). (b) Y. Guan; D.L. Thompson, *J. Chem. Phys.* **88**, (1988). (c) J.T. H. Uzer; W.P. Reinhardt, *Chem. Phys. Lett.* **117**, 600 (1985). *J. Chem. Phys.* **85**, 5791 (1986). (d) B.G. Sumpter; D.L. Thompson, *J. Chem Phys.* **86**, 2805 (1987); *ibid.* **86**, 3301 (1987). (e) P.R. Stannard; W.M. Gelbart, *J. Phys. Chem.* **85**, 3592 (1981).

5. L.M. Raff, *J. Chem. Phys.* **89**, 5680(1988).
6. E.W. Schlag; R.R. Levine, *Chem. Phys. Lett.* **163**, 523(1989).
7. P.J. Robinson; K.A. Holbrook, *Unimolecular Reactions* (Wiley, New York, 1972).
8. (a) R.H. Newman-Evans; R.J. Simon; B.K. Carpenter *J. Org. Chem.* **55**, 695(1990); also see J. Baggot, *New Scientist*, January 6, 33 (1990)
(b) D.R. Borchardt; S.H. Bauer, *J. Chem. Phys.* **85**, 4980(1983).
9. L.M. Raff; R.W. Graham, *J. Phys. Chem.* **92**, 5111(1988).
10. H.W. Schranz; L.M. Raff; D.L. Thompson, *Chem. Phys. Lett.* **171**, 68(1990).
11. H.W. Schranz; L.M. Raff; D.L. Thompson, *J. Chem. Phys.* **94**, 4219(1991); *ibid*, **95**, 106(1991).
12. H.W. Schranz; L.M. Raff; D.L. Thompson, *Chem. Phys. Lett.* **182**, 455(1991).
13. T.D. Sewell; H.W. Schranz; D.L. Thompson; L.M. Raff, *J. Chem. Phys.* **95**, 8089(1991).
14. D.C. Sorescu; D.L. Thompson; L.M. Raff, *J. Chem. Phys.* **101**, 3729(1994).
15. D.C. Sorescu; D.L. Thompson; L.M. Raff, *J. Chem. Phys.* **102**, 7910(1995).
16. D.C. Sorescu; D.L. Thompson; L.M. Raff, *J. Chem. Phys.* **103**, 0000(1995).
17. S.A. Abrash; R.W. Zehner; G.L. Mains; L.M. Raff, *J. Phys. Chem.* **99**, 2959(1995).
18. Kay, R.; Raff, L. M. in preparation.
19. G.J. Mains; L.M. Raff; S.A. Abrash, *J. Phys. Chem.* **99**, 3532(1995).
20. (a) H. Okabe, *J. Chem. Phys.* **62**, 2782(1975).
(b) *J. Phys. Chem. Ref. Data* **11**, 2-101(1982).
(c) L.M. Sverdlov; M.A. Kovner; E.P. Krainov, *Vibrational Spectra of Polyatomic Molecules*; 414-426 (Wiley, New York, 1974).

21.L.M. Raff; D.L. Thompson, "The Classical Trajectory Approach to Reactive Scattering." in *Theory of Chemical Reaction Dynamics*; Ed. Baer, M.Vol. III, p 1 (CRC press, Boca Raton, FL, 1985).

Table I

**Notation and frequencies for the
vibrational modes of vinyl bromide.
The atom numbering is given in the figure.**

Mode No.	Description of mode	ν^a (cm ⁻¹)	Expt. ^b (cm ⁻¹)
ν_1	C-C-Br bending	345	344
ν_2	CHBr wag	576	583
ν_3	C-Br stretch	623	613
ν_4	CH ₂ wag	889	902
ν_5	CH ₂ -CHBr torsion	963	942
ν_6	C-C-H ⁵ bending	1004	1006
ν_7	C-C-H ³ bending	1214	1256
ν_8	H-C-H bending	1377	1373
ν_9	C=C stretch	1606	1604
ν_{10}	C-H stretch	3004	3027
ν_{11}	C-H stretch	3086	3086
ν_{12}	C-H stretch	3121	3113

(a) Calculated by normal mode analysis on the global ground-state potential given in Ref. 17.

(b) Reference 20

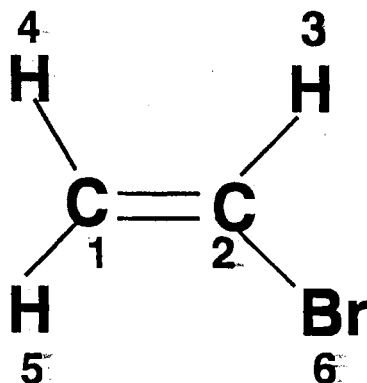


Table II

**Primary and secondary relaxation
pathways in vinyl bromide**

Major pathway	Major relaxation modes	Secondary relaxation modes
v1→v2	CHBr wag	C-C-H,H-C-H bending
v2→v1	C-C-Br bending	C-C-H bending
v3→v2,v5	CHBr wag,CH ₂ -CHBr torsion	C-C-Br bending
v4→v9	C=C stretch	C-C-H ⁵ bending
v5→v4 ,v3	CH ₂ wag, C-Br stretch	C=C, C-H stretch
v6→v4 ,v9,v11	CH ₂ wag, C=C stretch, C-H stretch	C-C-Br bending
v7→v8, v11	H-C-H bend, C-H stretch	C-H stretch
v8→v2, v10	CHBr wag, C-H stretch	CH ₂ wag
v9→v5,v2,v8	CH ₂ -CHBr torsion, CHBr wag, H-C-H bend	C-H stretch
v10→v11,v12	C-H stretch	CH ₂ wag
v11→v10,v12	C-H stretch	C=C stretch
v12→v10,v11	C-H stretch	CH ₂ wag, H-C-H bending

Table III

Total IVR rates computed by least-squares fitting of Eq.(III.10) to the results obtained using Eq.(III. 9). In each case, 3.0 eV of excitation energy in excess of zero point energy is initially partitioned into the indicated vibrational mode.

Mode i	k_i (ps ⁻¹)	α_i (ps ⁻¹)	$\langle E_i(0) \rangle$ (eV)	$\langle E_i(\infty) \rangle$ (eV)
v ₁	8.7	8.7	3.02025	0.289
v ₂	15.9	15.9	3.03394	0.267
v ₃	17.0	1.5	3.03571	0.317
v ₄	18.6	2.9	3.05512	0.315
v ₅	24.8	24.8	3.05968	0.284
v ₆	14.2	14.4	3.06219	0.328
v ₇	14.2	1.6	3.07520	0.309
v ₈	17.8	8.5	3.08383	0.328
v ₉	14.2	3.7	3.09923	0.317
v ₁₀ (a)	13.1	13.1	3.14621	0.330
v ₁₁	6.5	6.5	3.19093	0.301
v ₁₂	16.5	6.3	3.22701	0.352

(a) Average of 11 trajectories. All other entries are single trajectory results.

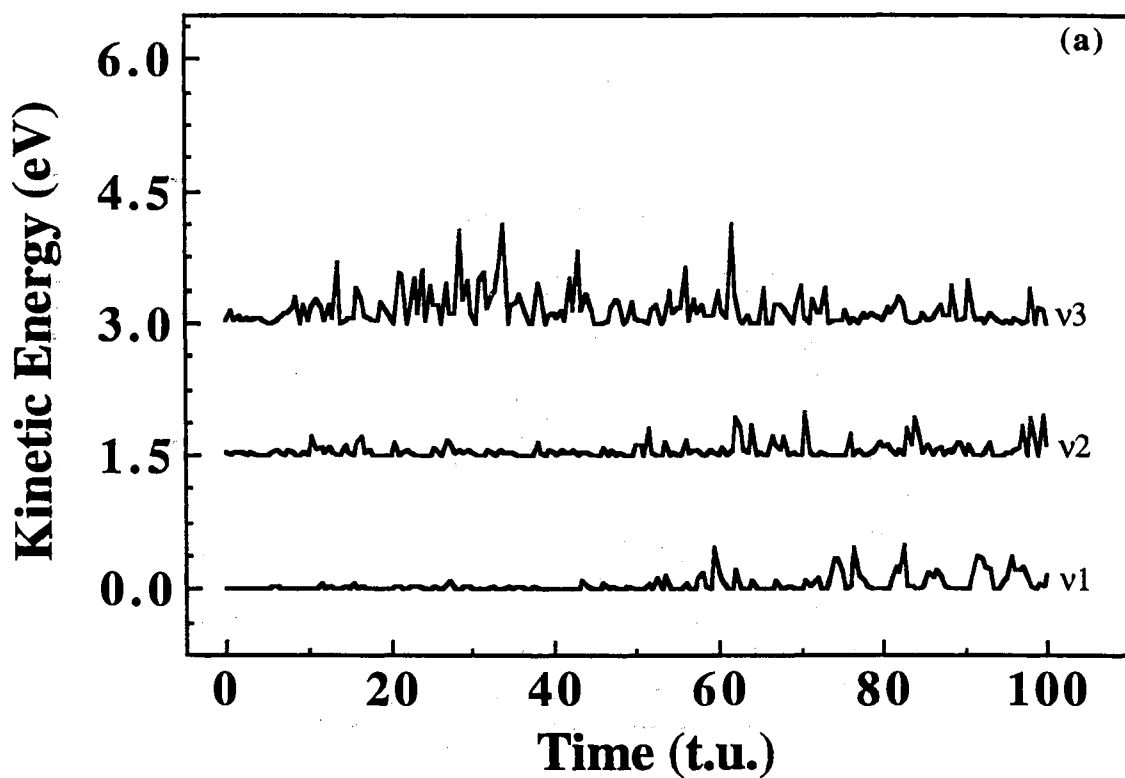


Figure 2(a): Temporal variation of the mode kinetic energy for v_1 , v_2 , and v_3 computed using Eq. (III. 8) for the case in which 3.0 eV of excitation energy in excess of zero-point energy is initially partitioned into the C-H stretching mode v_{10} . Each successive curve is displaced upward by 1.50 eV to provide visual clarity. The abscissa unit is 1 t.u. = 0.01019 ps. In this case, vinyl bromide is initially in its equilibrium conformation.

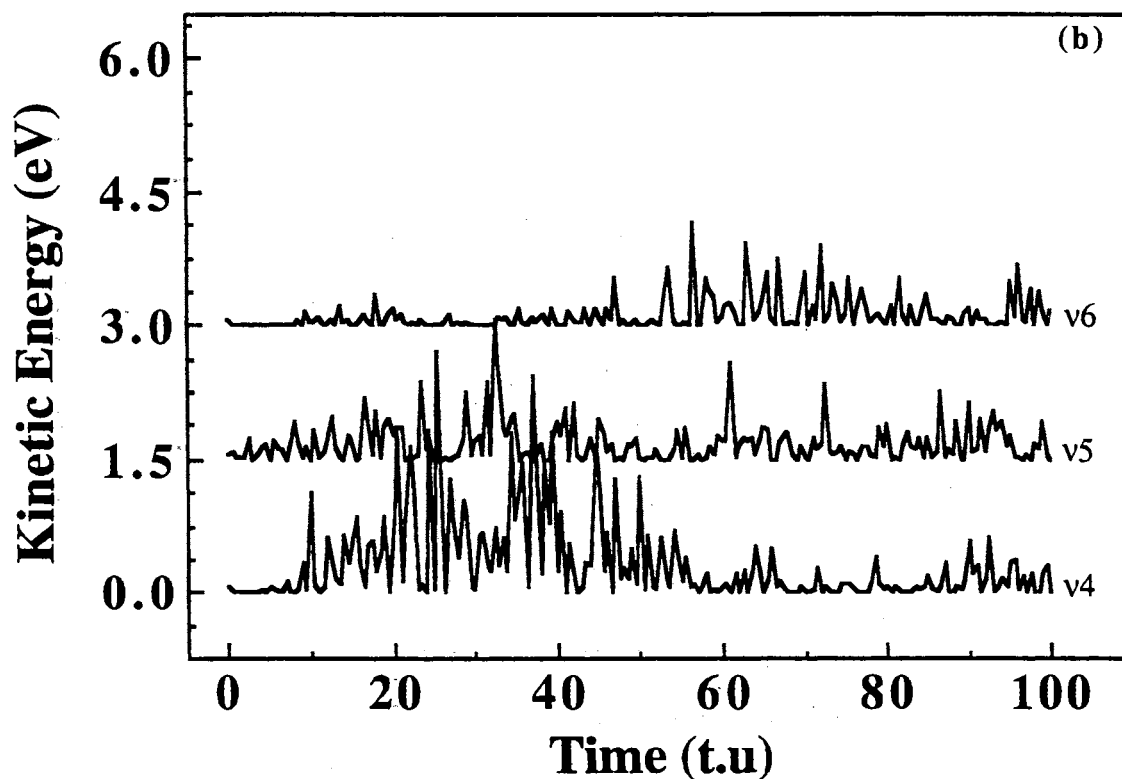


Figure 2(b): Temporal variation of the mode kinetic energy for v_4 , v_5 , and v_6 computed using Eq. (III. 8) for the case in which 3.0 eV of excitation energy in excess of zero-point energy is initially partitioned into the C-H stretching mode v_{10} . Each successive curve is displaced upward by 1.50 eV to provide visual clarity. The abscissa unit is 1 t.u. = 0.01019 ps. In this case, vinyl bromide is initially in its equilibrium conformation.

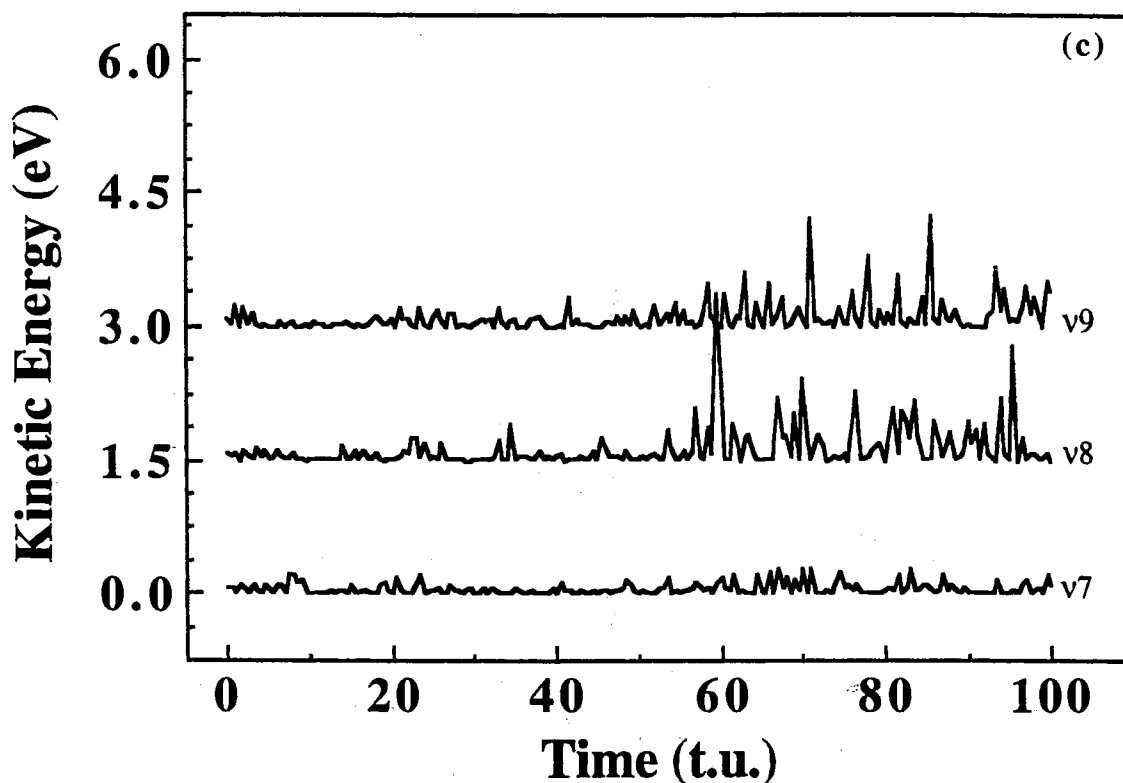


Figure 2(c): Temporal variation of the mode kinetic energy for v7, v8, and v9 computed using Eq. (III. 8) for the case in which 3.0 eV of excitation energy in excess of zero-point energy is initially partitioned into the C-H stretching mode v₁₀. Each successive curve is displaced upward by 1.50 eV to provide visual clarity. The abscissa unit is 1 t.u. = 0.01019 ps. In this case, vinyl bromide is initially in its equilibrium conformation.

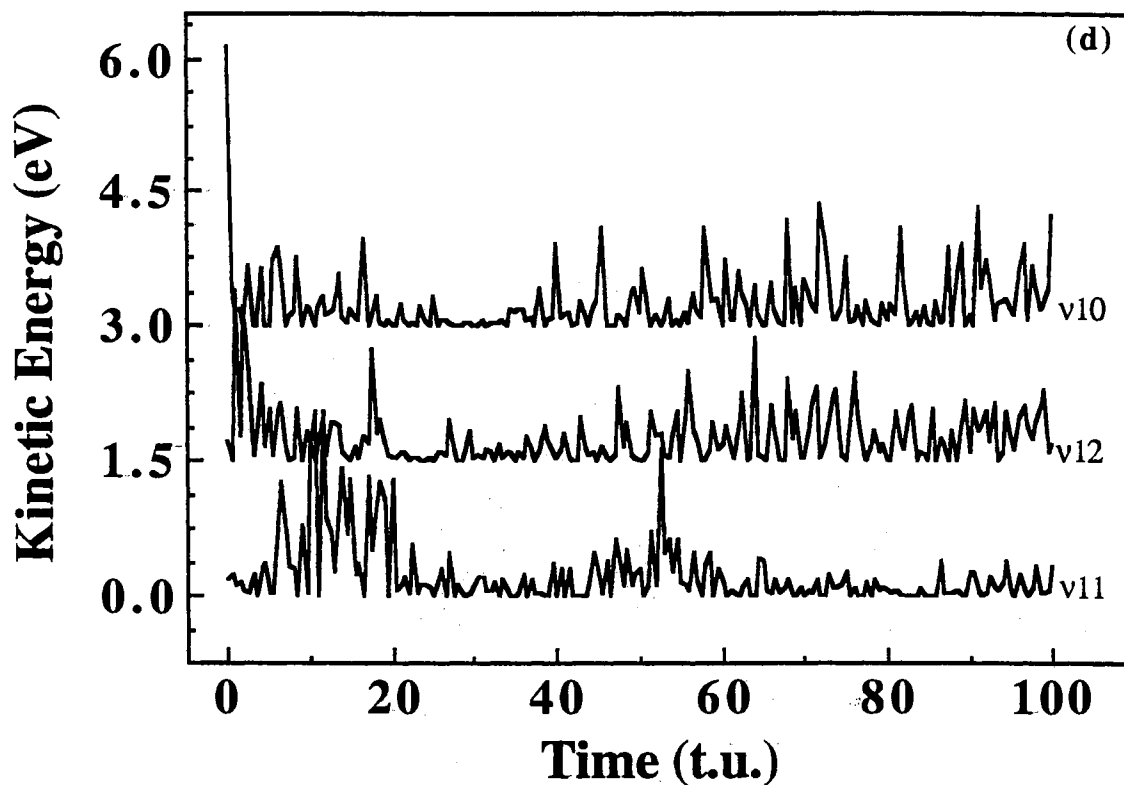


Figure 2(d): Temporal variation of the mode kinetic energy for ν_{10} , ν_{11} , and ν_{12} computed using Eq. (III. 8) for the case in which 3.0 eV of excitation energy in excess of zero-point energy is initially partitioned into the C-H stretching mode ν_{10} . Each successive curve is displaced upward by 1.50 eV to provide visual clarity. The abscissa unit is 1 t.u. = 0.01019 ps. In this case, vinyl bromide is initially in its equilibrium conformation.

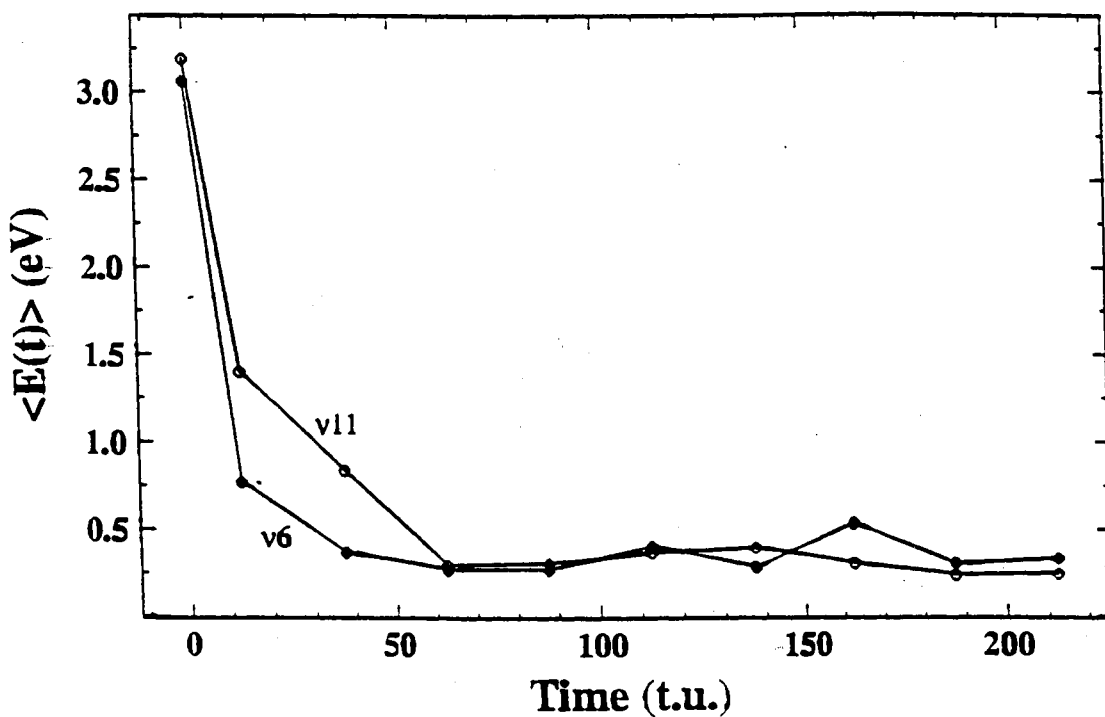


Figure 3: Decay curves for the average mode energies for initial excitation of modes v6 and v11 with 3.0 eV above zero-point energy. The points computed from the Eq.(III. 9) are connected with straight lines for visual clarity. The abscissa unit is 1 t.u. = 0.01019 ps.

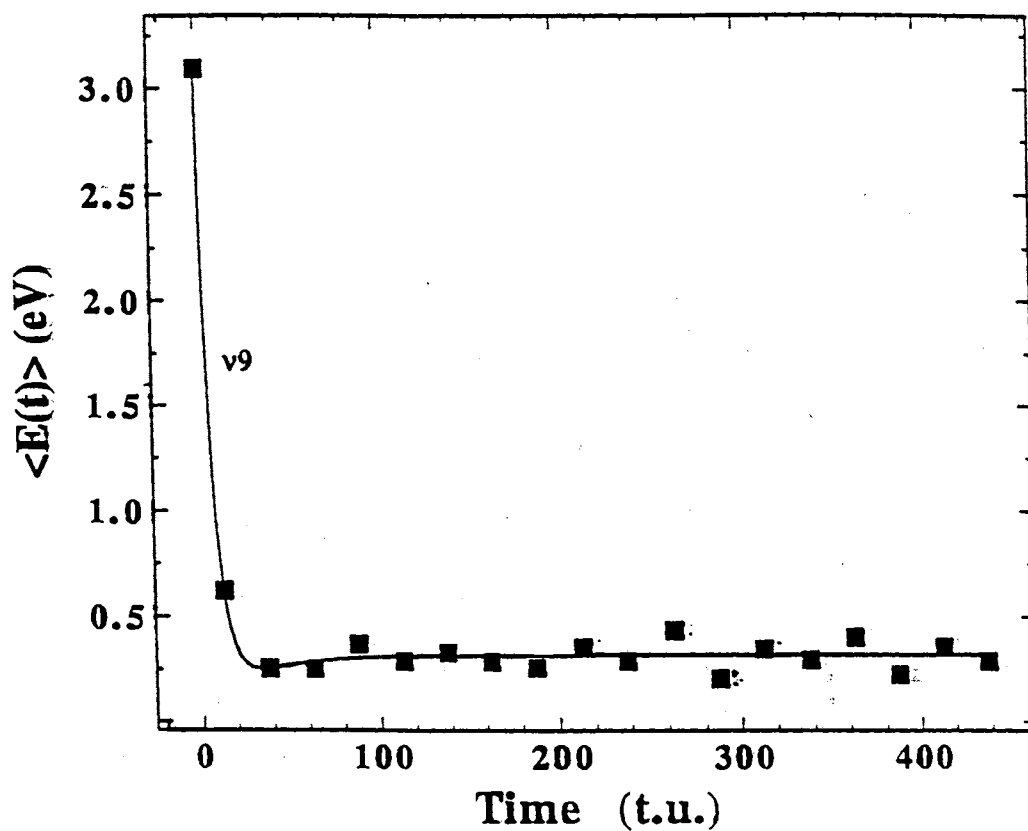


Figure 4: Decay curve for the average mode energy for initial excitation of mode ν_9 with 3.0 eV in excess of zero-point energy. The points are computed from the Eq. (III. 9). The solid line is the predicted first-order result obtained by least-squares fitting of Eq.(III. 10) to the points. The abscissa unit is 1 t.u. = 0.01019 ps.

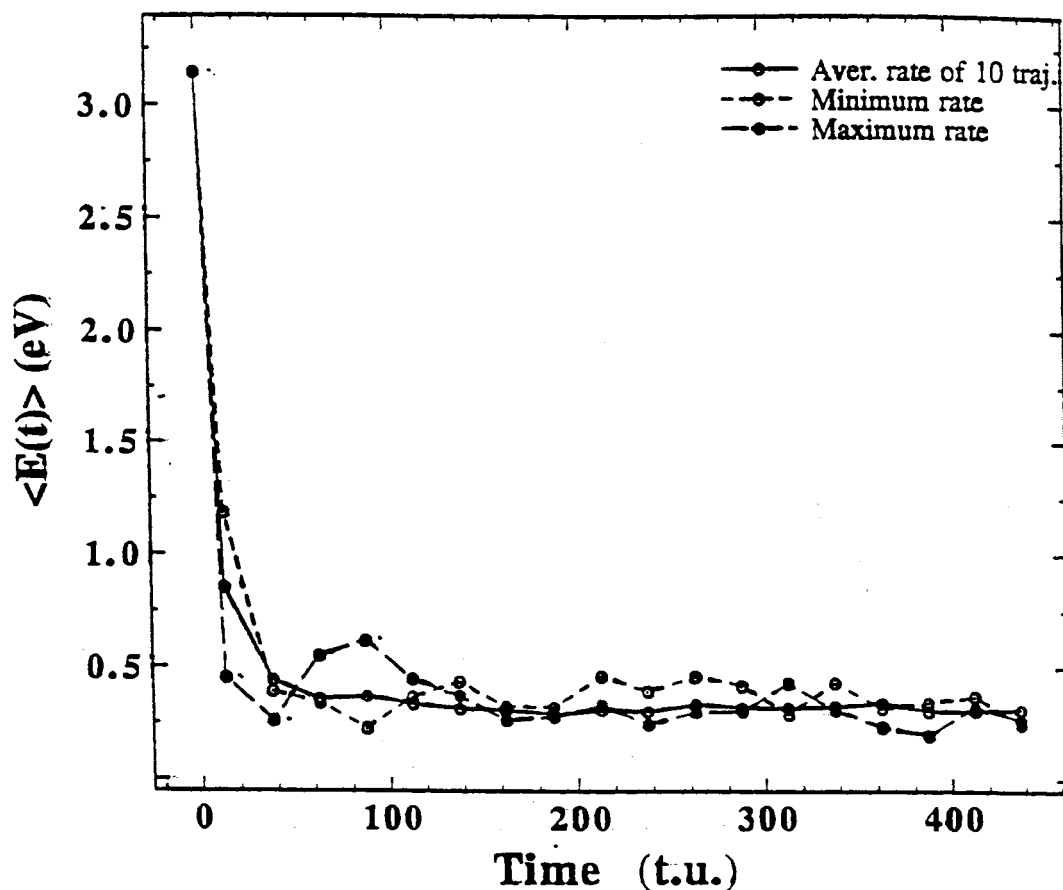


Figure 5: Decay curves for the average mode energy for initial excitation of mode ν_{10} with 3.0 eV in excess of zero-point energy. The points computed from Eq.(III. 9) are connected with line segments to enhance the visual clarity. The dashed results show the trajectories yielding the minimum and maximum decay rates obtained in the ensemble of 11 trajectories examined. The solid line shows the ensemble average. The abscissa unit is 1 t.u. = 0.01019 ps.

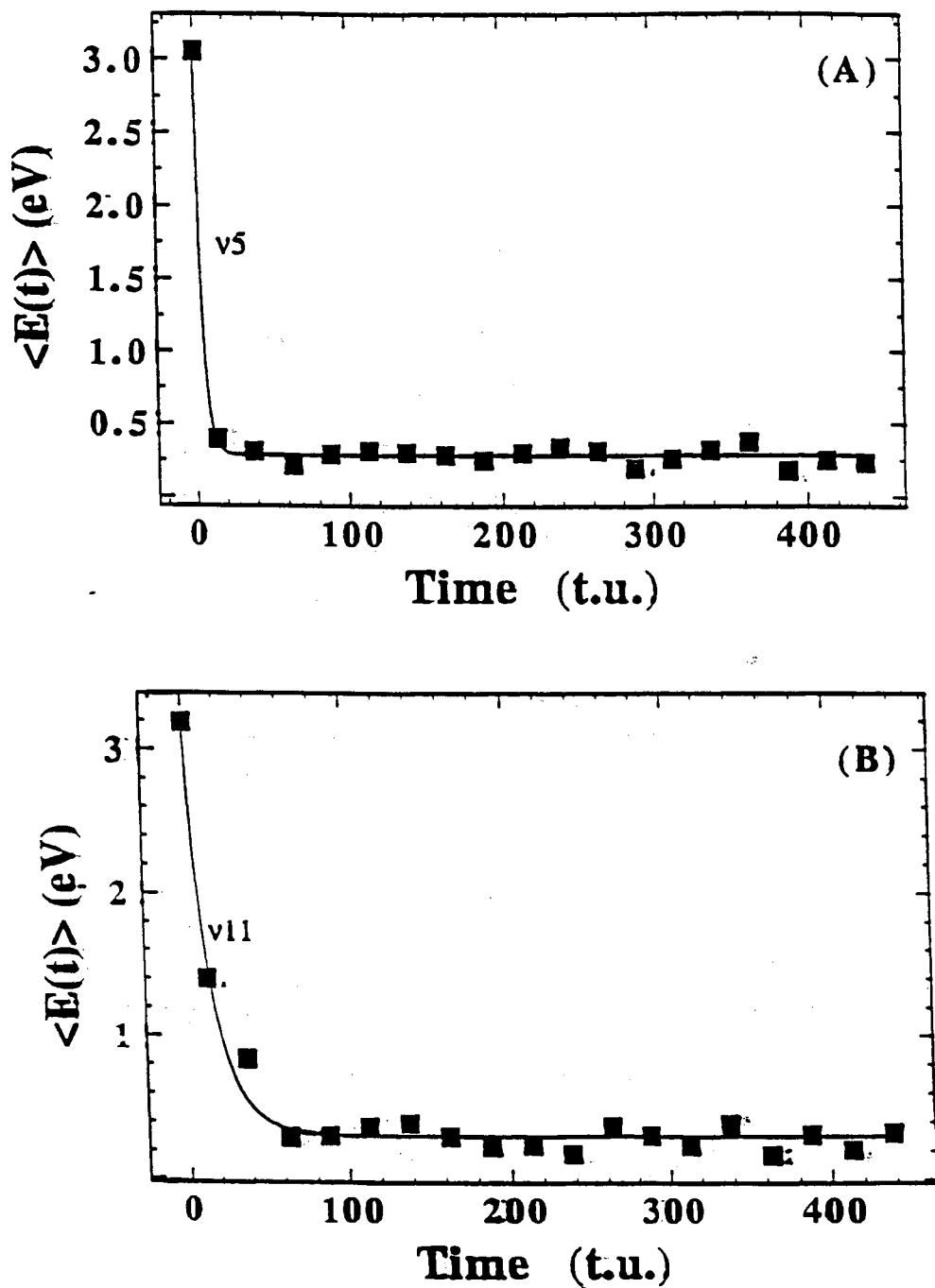


Figure 6: Decay curves for the average mode energy for initial excitation of modes v_5 and v_{11} with 3.0 eV in excess of zero-point energy. The points are computed from the Eq. (III. 9). The solid line is the predicted first-order result obtained by least-squares fitting of Eq.(10) to the points. (A) v_5 , (B) v_{11} . The abscissa unit is 1 t.u. = 0.01019 ps.

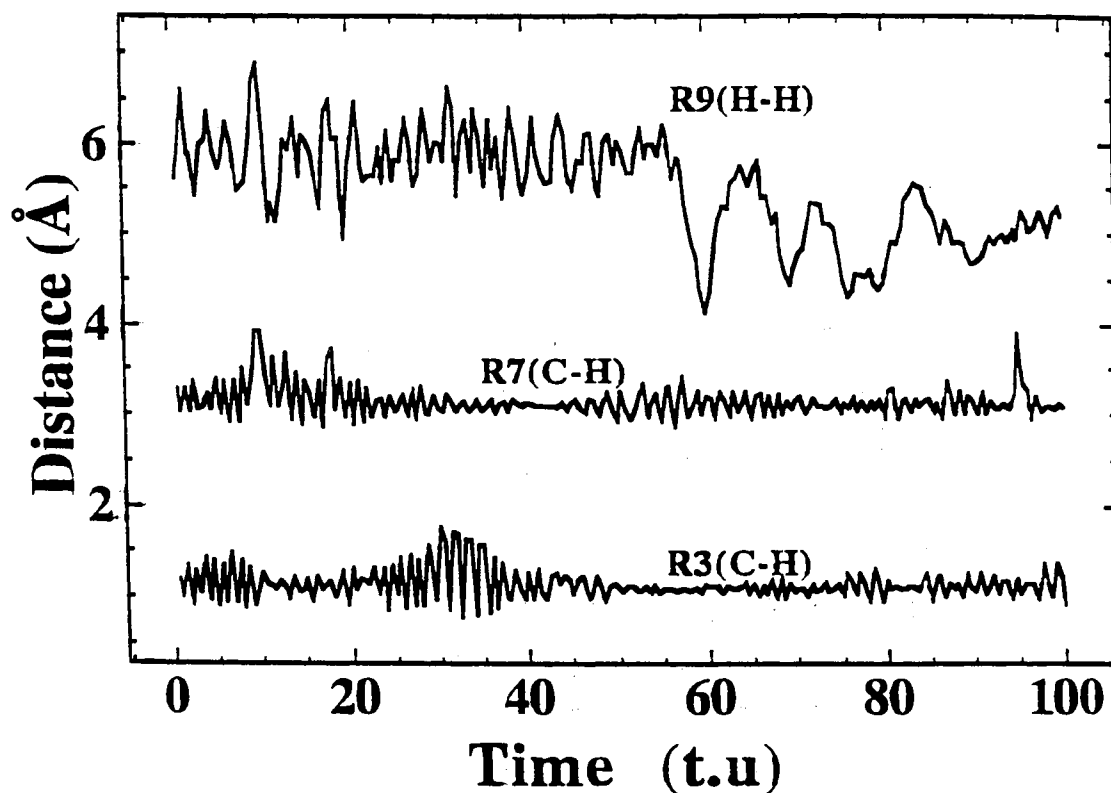


Figure 7: Temporal variation of two C-H distances and the H-H distance for a trajectory in which vinyl bromide is initially in the minimum-energy configuration on a dividing surface near the optimum critical surface for three-center H₂ elimination. The total energy is 6.44 eV plus the zero-point energy of vinyl bromide in the equilibrium configuration. Each successive curve is displaced upward by 2 Å to provide visual clarity. The abscissa unit is 1 t.u. = 0.01019 ps.

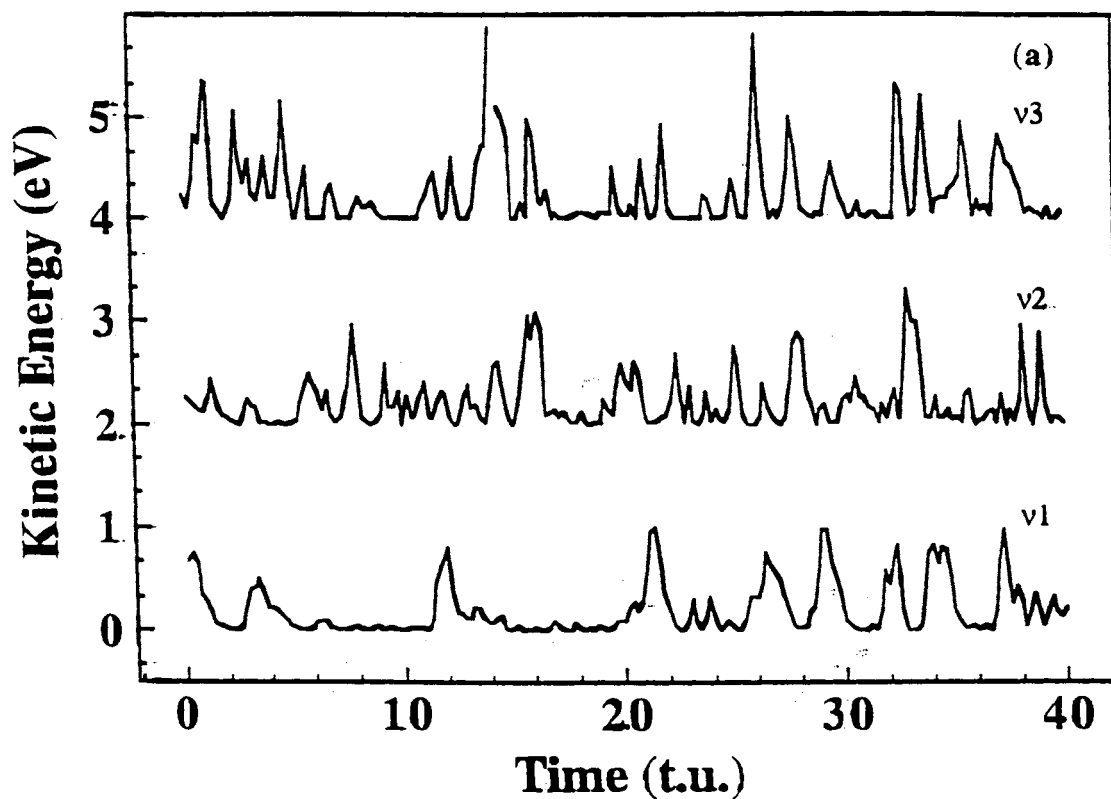


Figure 8(a): Temporal variation of the mode kinetic energies of modes v_1 , v_2 , and v_3 for the trajectory illustrated in Fig. 7. Each successive curve is displaced upward by 2.00 eV to provide clarity. The abscissa unit is 1 t.u. = 0.01019 ps.

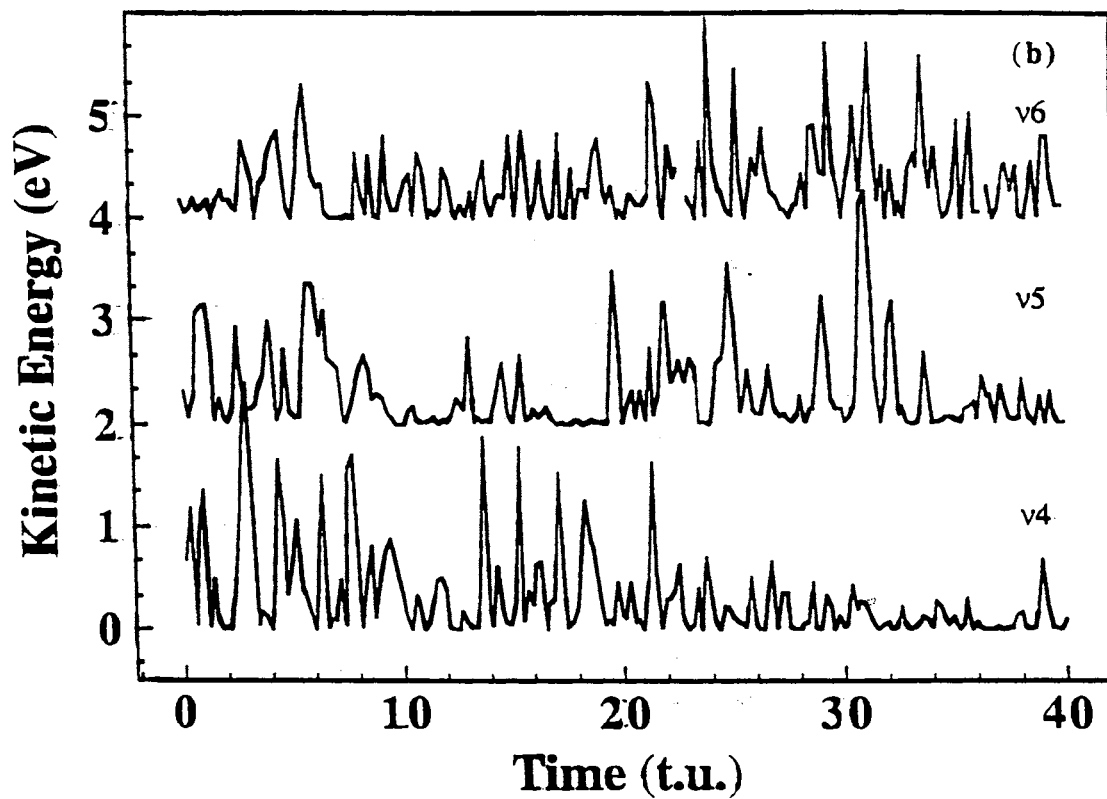


Figure 8(b): Temporal variation of the mode kinetic energies of modes v4, v5, and v6 for the trajectory illustrated in Fig. 7. Each successive curve is displaced upward by 2.00 eV to provide clarity. The abscissa unit is 1 t.u. = 0.01019 ps.

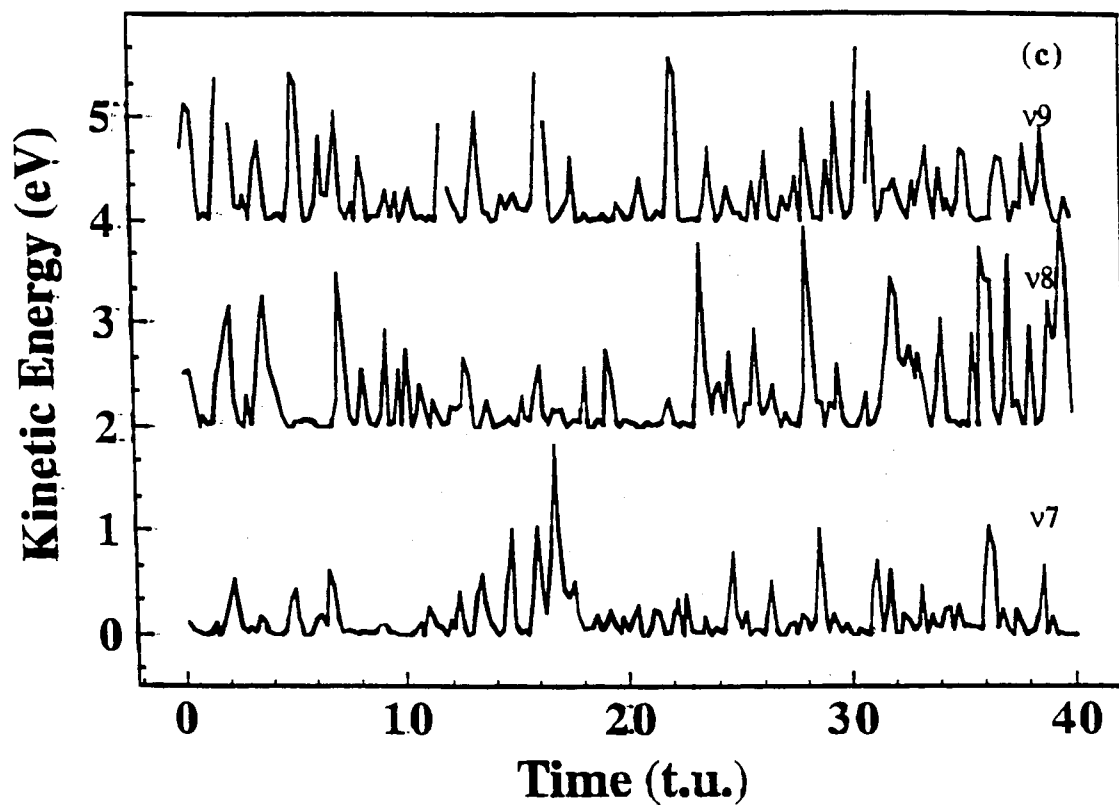


Figure 8(c): Temporal variation of the mode kinetic energies of modes v7, v8, and v9 for the trajectory illustrated in Fig. 7. Each successive curve is displaced upward by 2.00 eV to provide clarity. The abscissa unit is 1 t.u. = 0.01019 ps.

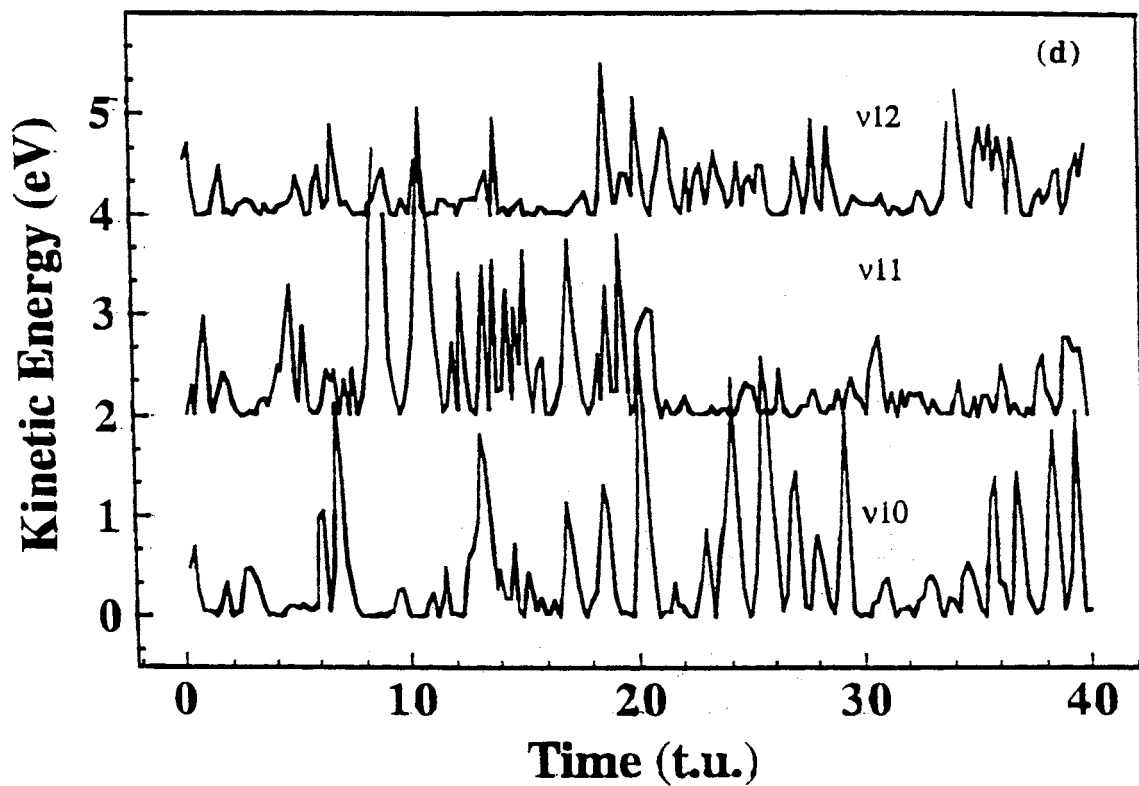


Figure 8(d): Temporal variation of the mode kinetic energies of modes v_{10} , v_{11} , and v_{12} for the trajectory illustrated in Fig. 7. Each successive curve is displaced upward by 2.00 eV to provide clarity. The abscissa unit is 1 t.u. = 0.01019 ps.

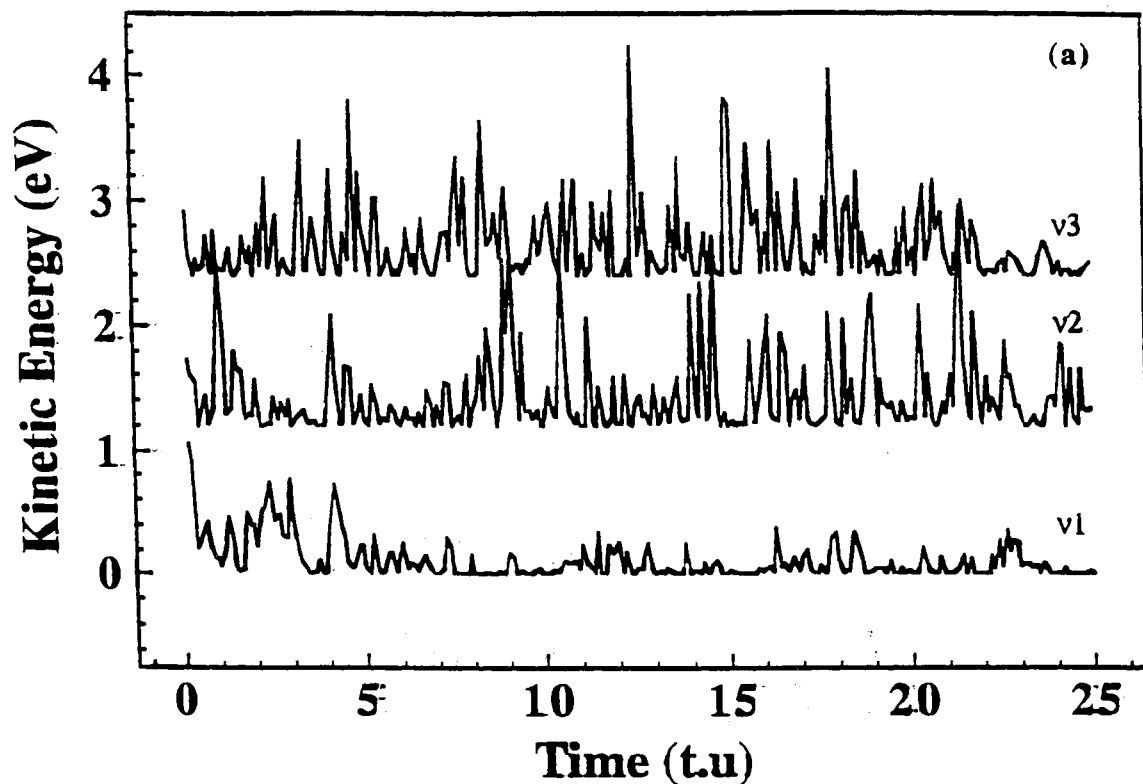


Figure 9(a): Temporal variation of the mode kinetic energies of modes v_1 , v_2 , and v_3 with vinyl bromide initially in the minimum-energy configuration on the optimum dividing surface for three-center HBr elimination. The total energy is 6.44 eV plus the zero-point energy of vinyl bromide in the equilibrium configuration. Each successive curve is displaced upward by 1.50 eV to provide clarity. The abscissa unit is 1 t.u. = 0.01019 ps.

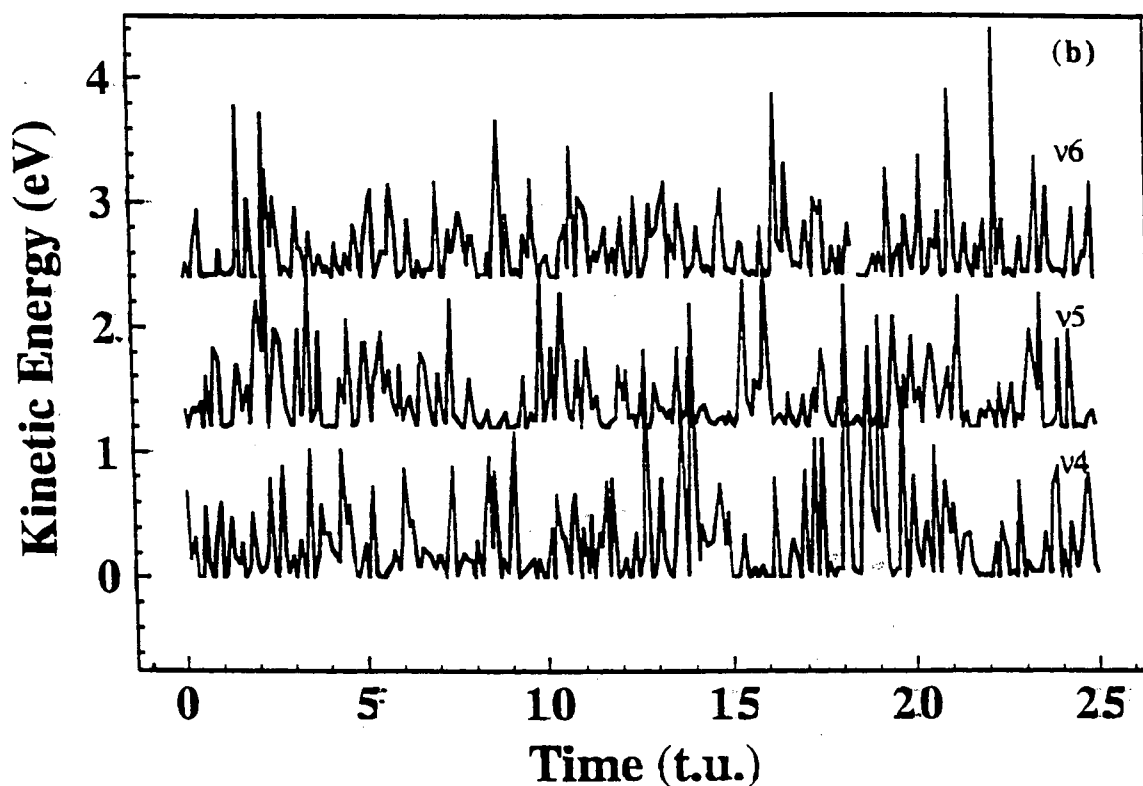


Figure 9(b): Temporal variation of the mode kinetic energies of modes v4, v5, and v6 with vinyl bromide initially in the minimum-energy configuration on the optimum dividing surface for three-center HBr elimination. The total energy is 6.44 eV plus the zero-point energy of vinyl bromide in the equilibrium configuration. Each successive curve is displaced upward by 1.50 eV to provide clarity. The abscissa unit is 1 t.u. = 0.01019 ps.

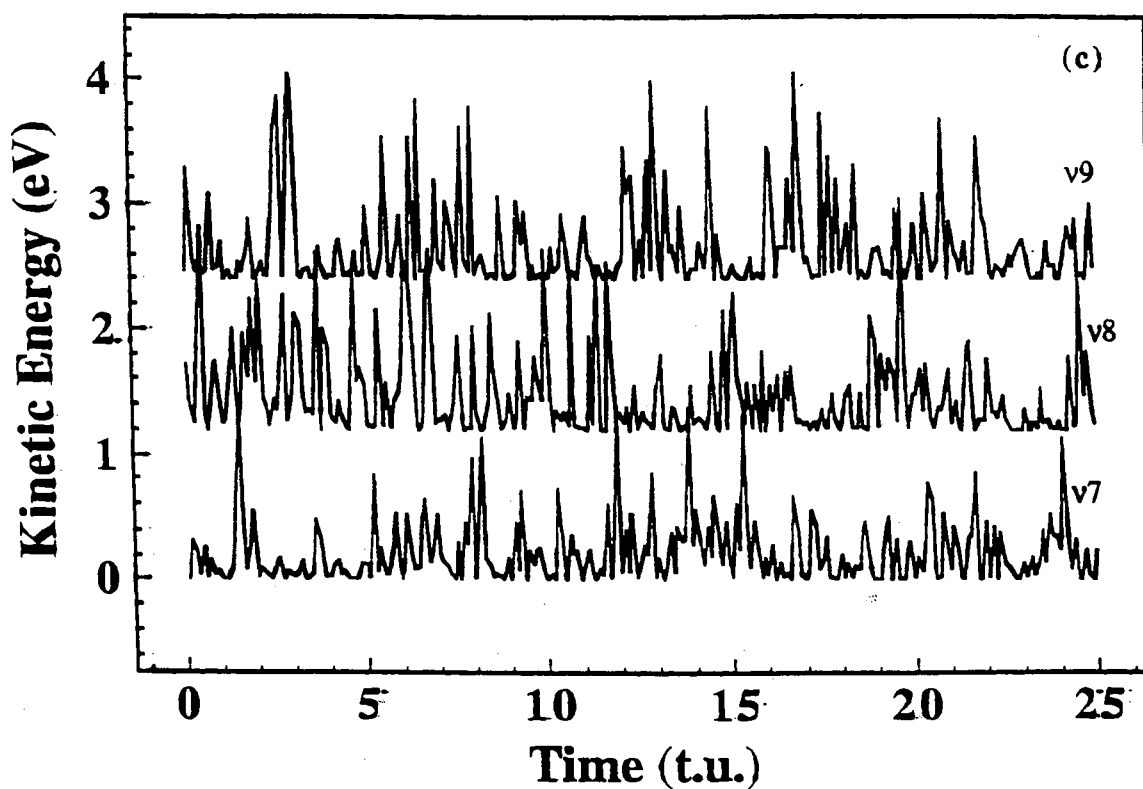


Figure 9(c): Temporal variation of the mode kinetic energies of modes v7, v8, and v9 with vinyl bromide initially in the minimum-energy configuration on the optimum dividing surface for three-center HBr elimination. The total energy is 6.44 eV plus the zero-point energy of vinyl bromide in the equilibrium configuration. Each successive curve is displaced upward by 1.50 eV to provide clarity. The abscissa unit is 1 t.u. = 0.01019 ps.

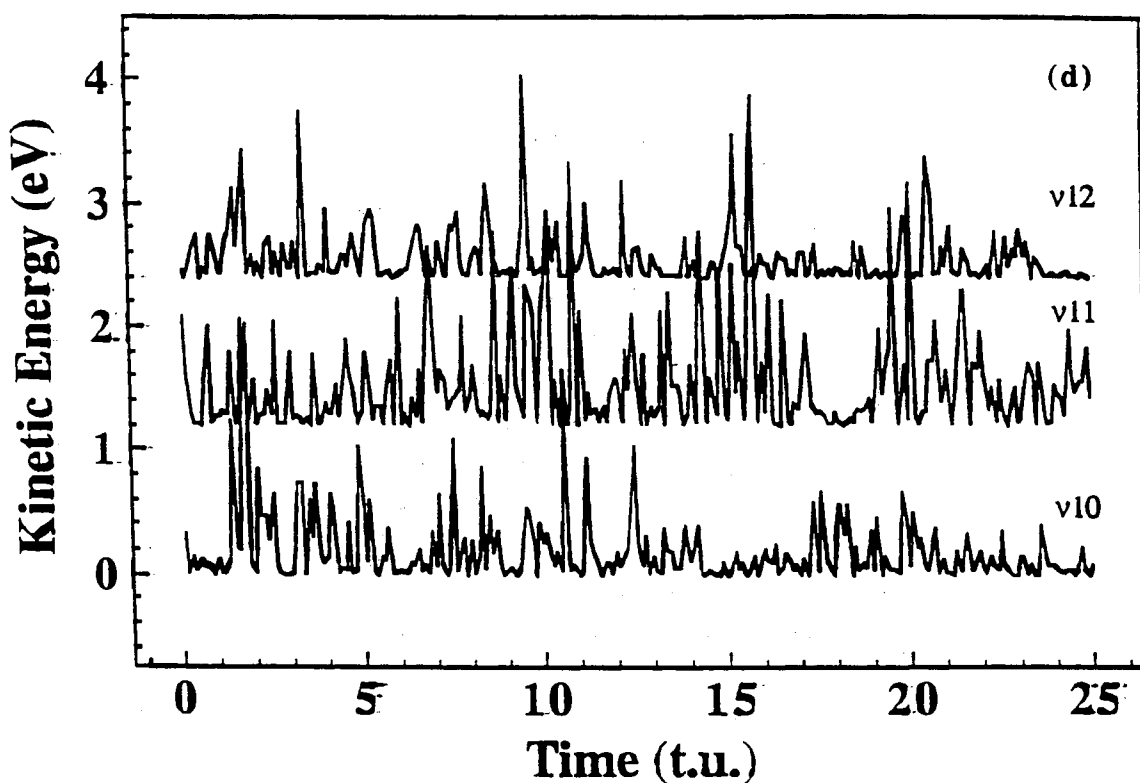


Figure 9(d): Temporal variation of the mode kinetic energies of modes v_{10} , v_{11} , and v_{12} with vinyl bromide initially in the minimum-energy configuration on the optimum dividing surface for three-center HBr elimination. The total energy is 6.44 eV plus the zero-point energy of vinyl bromide in the equilibrium configuration. Each successive curve is displaced upward by 1.50 eV to provide clarity. The abscissa unit is 1 t.u. = 0.01019 ps.

CHAPTER IV

POWER SPECTRA OF VINYL BROMIDE UNDERGOING
CONTINUOUS FREQUENCY MODULATION
AND INTRAMOLECULAR
ENERGY TRANSFER

Introduction

Trajectory and Molecular Dynamics (MD) are the most frequently used and powerful methods for investigation of the dynamical behavior of complex molecular systems. These techniques have been employed to calculate reaction rate coefficients, cross sections, diffusion rates, product energy partitioning, inter- and intramolecular energy rates and relaxation rates in both gas and condensed phases. Among them, energy transfer dynamics play a central role in unimolecular dissociation reactions. As described in Chapter III, we have investigated the dynamics of intramolecular energy transfer in vinyl bromide using projection methods and results obtained from classical trajectories ¹. This method is based on the calculation of the temporal variation of a diagonal kinetic energy matrix. Energy transfer rates and pathways are extracted from the envelope function of the temporal variations of the mode kinetic energies.

Power spectra are a valuable tool which can provide a wide variety of information about a molecule. ²⁻⁴ At low energies, a power spectrum contains

sharp peaks at the fundamental frequencies of vibration of the molecule. Overtones and combination bands may also be present. At higher energies, these peaks generally shift due to anharmonic potentials. Noid, Koszykowski, and Marcus⁵ used classical trajectories of anharmonic molecules to obtain the power spectrum of the dynamical variables. It was shown that in the vibrational quasiperiodic regime, the spectrum consists of sharp lines for fundamentals, overtones, and combination bands, while in the ergodic regime, the spectral lines are broad, with intensity spread over a wide band of frequencies. Based on these characteristics, power spectra can be used to qualitatively investigate the phase space structure of molecules. Smith and Shirts⁶ computed averaged power spectra for state-specific excitation of HCN. Their results show that the ensemble-averaged spectra do not exhibit the expected broadening and grassiness with increasing internal energy but that the spectra of individual trajectories do. Dumont and Brumer⁷ have pointed out that the observation of simple vs. complex power spectra do provide distinguishing characteristics. In particular, they have shown that for a simple Henon-Heiles model and for the three-body NaClK system, the statistical analysis of power spectra at fixed energy do provide an adequate method for making the distinction between chaotic and quasiperiodic motions. Chang, Swell, Thompson and Raff⁸ were able to demonstrate that the qualitative appearance of the power spectrum can be used as a diagnostic tool to assess the statistical character of a system. The presence of a diffusive spectrum exhibiting a nearly complete loss of isolated structures indicates that the dissociation dynamics of the molecule will be well described by statistical theories. If, however, the power spectrum maintains its discrete, isolated character, the opposite conclusion is suggested.

Molecular oscillators may undergo a continuous frequency modulation (CFM). Recent articles by Miller⁹ and by Wood and Strauss¹⁰ describe the connection between the adsorption line width, IVR rates and reaction rates. Following Kubo¹¹, both Wood and Strauss¹⁰ and Saven and Skinner¹² have discussed the modulation process in terms of a dimensionless parameter called the Kubo parameter. For the specific case of a Gaussian distribution of oscillator frequencies with a zero mean displacement, these reviews show that the form of the absorption function is well known for extreme values of this parameter. However, for intermediate values of Kubo parameter, these studies state that complicated line shape result.

Most recently, Agrawal *et al.*¹³ investigated the power spectrum line shapes for an oscillator undergoing a continuous linear or exponential modulation of the vibrational frequency. It is shown that, under these conditions, the single, sharp line normally characteristic of such systems broadens and exhibits a wealth of fine structure components. For the case of a simple harmonic model system undergoing a linear modulation of the frequency, it is possible to analytically compute the power spectra. The results demonstrate the nature of the power spectra expected for a continuous frequency modulated system. This CFM effect provides the explanation for the observations reported by Noid *et al.*⁵, Smith and Shirts⁶, Dumont and Brumer⁷ and Chang *et al.*⁸ Noid *et al.*⁵ found that ergodic dynamics leads to broadened spectra containing many smaller peaks. Since the IVR rate in an ergodic system is large, we expect the internal energy present in various modes to vary rapidly. Since the bond potentials are anharmonic, this will lead to a continuous frequency variation that will produce this type of broadening and fine structure. The diagnostic tests proposed by Chang *et al.*⁸ are also a direct consequence

of the CFM effect that produces very broad spectral bands each containing a wealth of fine structure.

Investigation of a Morse oscillator¹³ shows that energy transfer in an anharmonic system produces a CFM effect. By assuming that the analytic result for a harmonic oscillator with a linear modulation is transferable to the anharmonic case, Agrawal *et al.*¹³ were able to obtain an expression that relates the peak-to-peak fine structure spacing to the Morse potential parameters, the initial oscillator energy and the IVR rate coefficient. This relationship permits the calculated band splittings to be used as a probe of IVR rates. Agrawal *et al.*¹³ applied this method to extract energy transfer rate coefficients for a diatomic molecule isolated in an Ar matrix at 12 K and for total IVR rate coefficients for relaxation of HONO out of local stretch modes. The quality of the results suggested that line shapes analysis can be effectively used as new probe of energy transfer rates.¹³

The present work seeks to extend the CFM method to the study of IVR rates in six-atom molecules. We use vinyl bromide as our test system and investigate IVR rates out of local C-Br, C=C and C-H stretching modes.

Methods and Calculations

A. Potential energy surface

The potential energy surface used in present studies is a global surface accurately fitted to all of the available structural, thermochemical, kinetic and spectroscopic experimental data and to the results of *ab initio* electronic structure calculations for the transition state for several decomposition

channels.¹⁴ It has been previously employed in the study of intramolecular energy transfer dynamics¹ of vinyl bromide by projection methods as reported in Chapter III. The functional form of the surface and its strengths and weaknesses are discussed at length elsewhere.¹⁴ Fundamental frequencies for the local bond modes from theoretical and experimental results are listed in Table IV. The theoretical results are obtained by normal mode analysis based on the given global potential. Predicted fundamental frequencies by the global surface are in good to excellent accord with Raman and IR spectra.

B. Continuous Frequency Modulation (CFM) effect

In molecular dynamics simulations, bonding potentials are always anharmonic. Frequently, Morse functions are employed to represent such interactions.

$$V(r) = D[1 - \exp\{-\beta(r - r_e)\}]^2, \quad (\text{IV.1})$$

where D , β , and r_e are parameters which determine the potential well depth, curvature and potential minimum, respectively, and r is the bond length. The corresponding fundamental vibrational frequency for a Morse oscillator is given by¹⁵

$$\omega = \beta(2D / \mu)^{1/2}[1 - (E / D)]^{1/2}, \quad (\text{IV.2})$$

where μ is the reduced mass of oscillator and E is the oscillator energy. Consequently, if intra- or intermolecular vibrational energy transfer occurs, we see a continuous modulation of the frequency.

Agrawal *et al.*¹³ have considered several simple models of the type of line shapes to be expected in a power spectrum of an oscillator undergoing continuous frequency modulation. One such model is a modified "harmonic" oscillator for which the displacement, $f(t)$, is given by

$$\begin{aligned} f(t) &= r(t) - r_e = A \sin[\omega(t)t] \quad \text{for } 0 \leq t \leq T \\ &= 0 \quad \text{otherwise,} \end{aligned} \quad (\text{IV.3})$$

where A is a constant and $\omega(t)$ is defined by

$$\omega(t) = 2\pi\nu_0(1 - kt) = 2\pi\nu_0 - 2\pi\alpha t, \quad (\text{IV.4})$$

where ν_0 , k and T all positive. That is, the fundamental vibration frequency undergoes linear modulation with time. The power spectrum obtained from Eq.(IV.3) shows a broad band replete with fine structure components whose spacing first decreases and then increases as $\omega(t)$ decreases.¹³ An analytic expression for the power spectrum of this simple model can be obtained.¹³ The results show that the m th spacing between successive peak maxima is given by

$$\begin{aligned} \Delta\nu_{\max}^m &= -2\sqrt{\alpha} [s_{2m+1}^{1/2} - s_{2m-1}^{1/2}]. \\ &\approx -2\sqrt{\alpha} [(m+1-5/8)^{1/2} - (m-5/8)^{1/2}], \end{aligned} \quad (\text{IV.5})$$

where $\alpha = v_0 k = \left| \frac{dv}{dt} \right|$, $s_1=0.365...$, $s_2=0.878...$, $s_3=1.373...$ Eq. (V.5) shows that Δv_{\max}^m is independent of the total time for the process T and that it scales with $\sqrt{\alpha}$. The peak-to-peak spacing is therefore a direct measure of the rate of change of the vibrational frequency of the oscillator. The largest fine structure spacing will be the easiest to extract accurately. This corresponds to Δv_{\max}^1 . The results given above show that

$$\Delta x_{\max}^1 = -2\sqrt{\alpha}(s_{n=3}^{1/2} - s_{n=1}^{1/2}) = -1.13...\sqrt{\alpha}. \quad (\text{IV.6})$$

If it is assumed that we may generalize the analytic result obtained for the oscillator described by Eqs.(IV.3) and (IV.4), we can write

$$\Delta v_{\max}^m = -2[s_{2m+1}^{1/2} - s_{2m-1}^{1/2}] \left| \frac{dv}{dt} \right|^{1/2} = -K \left| \frac{dv}{dt} \right|^{1/2} \quad (\text{IV.7})$$

where K is a constant characteristic of the particular type of oscillator being considered.

For any anharmonic potential, the vibration frequency will be a function of the oscillator energy. As a result, energy transfer to or from the oscillator will produce a CFM effect and a complex power spectrum. To simulate internal energy transfer for an anharmonic potential, Agrawal *et al.*¹³ considered the case of a Morse oscillator whose kinetic energy decays exponentially with time. For such a systems, the Hamiltonian can be written as

$$H = T \exp(-2kt) + V(r), \quad (\text{V.8})$$

where k is the IVR first-order rate coefficient and $V(r)$ is given by Eq.(IV.1). Such an oscillator will exhibit both a CFM effect and an attenuation of amplitude. A useful expression for the fine structure spacing of a Morse oscillator can be obtained from Eq. (IV.7),

$$\Delta v_{\max}^m = -K \left| \frac{dv}{dt} \right|^{1/2} = -K \left| \left(\frac{dv}{dE} \right) \left(\frac{dE}{dt} \right) \right|^{1/2}. \quad (\text{IV.9})$$

From Eq.(IV.2), we obtain

$$\frac{dv}{dE} = -\left(\frac{\beta}{4\pi} \right) \left[\frac{2}{\mu} \right]^{1/2} [D - E]^{-1/2}. \quad (\text{IV.10})$$

Since many IVR processes in large molecules are first order, we may write

$$\frac{dE}{dt} = -kE. \quad (\text{IV.11})$$

Combination of Eqs.(IV.9)-(IV.11) gives

$$k = (4\pi/E\beta)(\Delta v_{\max}^1/K)^2 \{ [\mu(D - E)]/2 \}^{1/2}. \quad (\text{IV.12})$$

If we assume that the fine structure spacing is primarily determined by the maximum value of $\left| \frac{dv}{dt} \right|$, E may be replaced with E_0 , where E_0 is the initial energy of the oscillator. By examination of 125 cases, Agrawal *et al.*¹³ have found the best value of K to be 0.667.

C. Intramolecular Energy-transfer Dynamics

Our previous studies ¹ show that the vinyl bromide classical trajectories do not uniformly access all of the energetically available phase space of the system. Consequently, we may anticipate that while some mode-to-mode IVR rates may be very large, the intramolecular energy transfer cannot be globally rapid. As we know from the above section, investigation of a Morse oscillator shows that energy transfer in an anharmonic system produces a CFM effect. therefore, the CFM effect can be used to extract the rate coefficient for energy transfer from a local stretching mode.

An alternative approach that has frequently been employed to determine energy transfer rate out of a local stretching mode involves the computation of the time variation of the bond energy in a trajectory calculation. Such a local bond energy is usually defined by

$$E_b(t) = \frac{P_b(t)^2}{2\mu_b} + V_b[r_b(t)], \quad (\text{IV.13})$$

where μ_b is the reduced mass, $P_b(t)$ is the parallel momentum along the direction of the bond stretch, and $r_b(t)$ is the bond length. $V_b[r_b(t)]$ is taken to be a Morse function with parameters chosen so that it corresponds closely to the variation in potential energy on the global surface. The parameters employed for the definition of local bond mode energies are given in Table V. Most classical studies of intramolecular energy transfer have involved the calculation of some local bond energy such as that represented by

Eq. (IV.13).¹⁶⁻²⁰ The variation of $E_b(t)$ with time is then used to infer IVR rates.

D. Trajectory procedures

Hamilton's equations of motion were integrated using a fourth-order Runge-Kutta routine ²¹ with a fixed step size of 0.01 t.u. (0.0001019 ps). About four significant digits of energy conservation was generally achieved.

The unimolecular energy transfer and reaction dynamics of vinyl bromide were studied using a two step procedure. The first step is to use the projection method developed by Raff ²²⁻²³ to insert energy into specified or randomly chosen normal modes of the molecules. With the molecule in its equilibrium configuration, zero-point vibrational energy is placed in the normal modes, and the equations of motion are integrated for a random period of time t_p ,

$$t_p = \xi \tau_m, \quad (\text{IV.14})$$

where ξ is a random number chosen uniformly on the interval [0,1] and τ_m is the vibrational period for the lowest frequency mode in the molecule. Eq.(IV. 14) effectively averages over the vibrational phases of the molecule. Subsequent to the above integration, the desired excitation energy, E_{ex} , is inserted into the selected local stretching mode k . This is executed by replacing the momentum parallel to the k th bond axis, $P_b'(t)$, with $P_b(t)$ where

$$P_b(t) = [2\mu_b \{E_{ex} + E_k(t)\}]^{\frac{1}{2}}, \quad (\text{IV.15})$$

In Eq. (IV. 15), $E_k(t)$ is the instantaneous kinetic energy associated with motion parallel to the k th bond axis at time t and μ_b is the reduced mass of the bonded atoms. After preparation of the initial state, the trajectory is integrated for a time greater than 100 t.u. During the integration, instantaneous values of the stretching coordinate for k th mode, r_k , are stored for the computation of power spectrum.

A power spectrum of mode k is obtained from a direct transformation of r_k ,

$$I_q(\omega) = (2\pi)^{-1} \left| \int_0^{\infty} r_k(t) \exp(i\omega t) dt \right|^2 \quad (\text{IV.16})$$

The calculation of $I_q(\omega)$ is done using a Fast Fourier Transform(FFT) method.

Results and Discussion

A. Fundamental frequency and power spectra

Table IV lists the fundamental frequencies of the five local bond modes both from theoretical calculations and experimental measurement. The values in the parentheses are in units of t.u^{-1} , where $1 \text{ t.u.}^{-1} = 3278 \text{ cm}^{-1}$. These frequencies should also be reflected in the power spectra of the system at low internal energy. Figure 10 shows the power spectrum of $\text{C}_1=\text{C}_2$, $\text{C}_2\text{-Br}$, $\text{C}_1\text{-H}_4$, $\text{C}_1\text{-H}_5$, and $\text{C}_2\text{-H}_3$ stretching modes obtained at a total internal energy 10% of the zero-point energy. The reduction of zero-point energy to one tenth its normal value sharpens the spectral bands by reducing intramolecular energy transfer and by restricting molecular motion to regions of phase space near the potential minimum. Table VI lists all the frequencies

of local stretch modes obtained from power spectra. Obviously, the frequencies of the three C-H stretch modes are so close that they are not distinguishable in the power spectrum.

B. Isotope effect to the power spectra

As noted above, the very close frequency match of the three C-H stretches produces complex power spectra for the C-H stretch local modes and makes the spectra lines indistinguishable. Since the objective of the present study is to determine IVR rates by computation of power spectrum line splittings, we need to have the local mode frequencies separated from one another by an amount that is large relative to the line splittings. This condition is reasonably well satisfied by the local C-Br and C=C stretching modes, but not the C-H modes. The near superposition of these three modes makes it essentially impossible to accurately extract $\Delta\nu_{\max}^1$. Such band overlap places a fundamental limitation on the use of the CFM effect to extract IVR rates.

Although the CFM method cannot be used to determine IVR rates for the relaxation of the C-H stretching modes in vinyl bromide, it is ideally suited to the investigation of such rates for deuterium substituted vinyl bromide. If deuterium is substituted for two hydrogen atoms whose local mode relaxations are not being examined, the fundamental C-H and C-D band frequencies will be widely separated making it relatively easy to compute the CFM splittings. Tables VII, VIII, and IX give the computed fundamental frequencies for the three doubly-substituted vinyl bromides. In each case, the C-H stretch is seen to be widely separated from the two C-D local modes. Comparison of the C-Br and C=C stretching frequencies in Tables VI-IX

shows that these fundamentals are not significantly affected by deuterium substitution.

C. Line spacing and energy transfer rate coefficient

As described above, the intramolecular energy transfer rates can be extracted from the line spacing from the power spectra of the internal coordinates. The concept of a local bond mode is employed in present studies where a “local mode energy” is computed by integration of the Hamilton equations of motion and the use of Eq.(IV.13). The initial state corresponds to a 1.0 eV excitation of a given local mode. Typical power spectra are shown in Figures 11, 12, and 13. Figure 11(A) shows the computed C-H power spectrum for vinyl bromide. The complexity introduced by the three overlapping fundamentals is obvious. Figure 11(B) is the power spectra of the C₁-H₄ local mode with isotope replacement of H₃ and H₅. Compared with Figure 11(A), it is clear that the complexity of the power spectrum has been sharply reduced. As a result, the corresponding maximum line spacing can be easily extracted as 0.039 t.u.⁻¹. Figure 12 shows the power spectrum of C₂-Br when the initial state corresponds to a local excitation of the C-Br bond. In this case, the maximum line spacing is 0.046 t.u.⁻¹. Figure 13 shows a typical power spectrum for another CH stretch, C₁-H₅, with deuterium replacement of H₃ and H₄. The extracted line spacing for this mode is 0.035 t.u.⁻¹. Using Eq. (IV.12), the relaxation rates can be calculated. Five to ten trajectories were executed for each of the local modes with an excitation energy of 1.0 eV. Table X lists the average line spacing for each mode and the corresponding average rate coefficients.

The data given in Table X show that the C-H local mode is the slowest relaxation mode in the doubly-deuterium substituted vinyl bromides. Within the accuracy of the calculations, there is no difference between the relaxation of the C-H mode in the three substitute molecules. The slow C-H relaxation rate can be rationalized by noting that the C-H stretching frequency is isolated from the remaining eleven vibrational modes by about 780 cm^{-1} or more. None of the other modes are so isolated. This large frequency mismatch is expected to lead to extremely slow relaxation. This is in sharp contrast to the situation in unsubstituted vinyl bromide where we have previously found¹ the C-H normal modes to relax rapidly due to the near resonance that exists between the three C-H normal modes. The C-Br and C=C stretching modes relax about 7 and 4 times faster than the C-H modes, respectively. The C-Br stretch is in near resonance with the CHBr wag and the C=C stretch frequency is close to that for the H-C-H bend.¹⁴ These near frequency matches undoubtedly facilitate energy relaxation out of these modes.

Since Eq.(IV.13) omits all kinetic and potential coupling terms and assumes a mode reparability that does not exist, variations in the bond energy occur that are due to changes in the magnitude of the omitted coupling terms rather than to actual energy transfer between modes. The variations caused by the omitted coupling terms often appear as high-frequency oscillations in the bond energy decay curve. Figure 14(A) shows the temporal variation of the C-Br local mode energy when the mode is excited with 1.0 eV in excess of ZPE. Figure 14(B) shows the corresponding kinetic energy variation with time of the same mode. It can be seen that envelope functions of these two curves are nearly the same. We can express the envelope function of the local mode decay exponentially as follows

$$E_i(t) = E_i(0)\exp(-kt) + (1 - \exp(-\alpha_i t))E_i(\infty), \quad (\text{IV.17})$$

where $E_i(0)$ is the initial mode energy of mode i , k is the total IVR rate coefficient out of the local bond mode, α_i is an average total rate coefficient for energy transfer into mode i and $E_i(\infty)$ is, in principle, the statistical equilibrium value of $E_i(t)$ at infinite time. A least-squares fit of Eq.(IV.15) to the envelope function yields the total decay rate coefficient k . Figure 15 shows a typical fit for the C-Br local mode excited by 1.0 eV of energy. The average total decay rate obtained by least-square fitting of the C-Br decay envelope is 0.214 t.u^{-1} . Table XI gives the nonlinear fitting results for each of the 5 local bond modes. The ensemble average is based on 5 to 10 trajectories. A comparison between the rate coefficients obtained from CFM effects and local mode energy decay fitting shows that the rate coefficients from CFM effects are generally smaller than those obtained from least-square fitting of the envelope function data. However, the maximum deviation of CFM rate coefficients from energy decay fitting rates is 43% for the C₂-H₃ stretch. Other deviations are C-Br relaxation (19%), C=C stretch (15%), C₁-H₄ stretch (41%) and C₁-H₅ mode (32%). The average deviation is 30%. These results are in accord with the accuracy of Eq. (IV.12) ($\pm 25\%$) estimated by Agrawal *et al.*¹³. The deviation of the rate coefficients obtained from decay data and from CFM line splittings are the combined result of the approximations made to obtain Eq.(IV.12), and the statistical errors present in the decay plots.

D. Variation of rate coefficients with internal energy

At very low internal energy, intermode coupling and IVR rates are small. As a result, the normal modes are reasonably good action variables. As the

internal energy rises, the vibrational motion becomes increasingly anharmonic. This produces a larger intermode coupling and increased IVR rates. Equation (IV.12) suggests that increased CFM line splittings should also be observed.

The above point has been investigated by calculations of the power spectrum for the C-Br local stretch at local excitation energies between 0.2 eV and 1.2 eV. Averaged line spacings, $\langle \Delta \nu_{\max}^1 \rangle$, are obtained from the power spectrum of 5 different trajectories. Figure 16 shows the variation of $\langle \Delta \nu_{\max}^1 \rangle$ with local C-Br excitation energy. Figure 17 gives the corresponding IVR rate coefficients obtained from Eq.(IV.12). Below 0.8 eV, there is very little dependence of the IVR rate coefficient upon internal energy. This reflects the nearly constant curvature of the stretching potential in this energy range. Above 0.8 eV, however, the average line splitting, $\langle \Delta \nu_{\max}^1 \rangle$, and the IVR rate coefficient increase rapidly due to the increased intermode coupling that results from the anharmonic motion.

SUMMARY

We have used the CFM effect to calculate the energy transfer rate coefficients for the local C-Br, C=C, and C-H stretching modes of vinyl bromide. The global potential developed by Abrash *et al.*¹⁴ is used in all calculations. The local bond potential is a Morse function. Energy transfer rate coefficients for each trajectory are extracted from the fine structure spacing of the numerically computed power spectrum of $r(t)$. These individual rate coefficients are averaged over an ensemble of 5 to 10 trajectories for comparison with the local mode energy decay curves.

It has been shown that near overlapping resonances in the power spectrum make it very difficult to accurately extract CFM line splittings. This limitation effectively precludes the use of line splittings to investigate some IVR rates. For the specific case of vinyl bromide, we have demonstrated that the C-Br and C=C stretching modes have sufficiently isolated spectral bands that IVR rates out of these modes can be determined from the CFM line splittings. However, the near superposition of the three C-H stretching fundamentals makes it essentially impossible to accurately extract $\Delta\nu_{\text{max}}^1$ and the corresponding IVR rates. We have therefore investigated C-H relaxation in doubly-deuterium substituted vinyl bromides where the C-H fundamental is well isolated from the C-D stretching bands.

The IVR rate coefficients for C-Br and C=C relaxation in vinyl bromide and for C-H relaxation in deuterium-substituted vinyl bromide have been computed from CFM splittings and from the local mode energy decay curve envelope by least-square fitting. The difference between the two results varies from 15% for the C=C stretch to 43% for one of the C-H stretching modes. The average deviation is 30%, which is in accord with the accuracy of the method ($\pm 25\%$) previously estimated by Agrawal *et al.*¹³. The effect of initial local excitation energy on the line splittings and associated rate coefficients has also been investigated for the C-Br stretching mode. The results show that the line splitting and rate coefficients are nearly independent of excitation energy below 0.8 eV. Above this energy, the CFM line splittings and the IVR rate coefficients increase rapidly. This is interpreted as being due to increased intermode coupling at higher energies produced by the greater vibrational anharmonicity.

We conclude that line shape analysis can be effectively used as a probe of energy transfer rates in large molecules provided the modes under examination have reasonably isolated bands in the power spectrum.

REFERENCES

1. R. Pan and L. M. Raff, J. Phys. Chem. (in press)(1996)
2. S. C. Farantos and J. N. Murrell, Chem. Phys. **55**, 205(1981).
3. J. Tennyson and S. C. Farantos, Chem. Phys. **93**, 327 (1985).
4. X. Chang, D. L. Thompson, and L. M. Raff, Chem. Phys. Lett. **206**, 137(1993)
5. D. W. Noid; M. L. Koszykowski; and R. A. Marcus, J. Chem. Phys. **67**, 404(1944).
6. R. Scott Smith and R. B. Shirts, J. Chem. Phys. **89**, 2948(1988).
7. R. S. Dumont and P. Brumer, J. Chem. Phys. **88**, 1481(1988).
8. X. Y. Chang; T. D. Swell; L. M. Raff and D. L. Thompson J. Chem. Phys. **97**, 7354(1992).
9. W. H. Miller, Phys. Reports. **199**, 124(1991).
10. K. A. Wood and H. L. Strauss, J. Phys. Chem. **94**, 5677 (1990).
11. (a) R. Kubo, Adv. Chem. Phys. **15**, 101 (1969).
(b) R. Kubo, J. Math. Phys. **4**, 174 (1963).
12. J. G. Saven and J. L. Skinner, J. Chem. Phys. **99**, 4391(1993).
13. P. M. Agrawal; D. C. Sorescu; R. D. Kay; D. L. Thompson; L. M. Raff; J. B. Conrey; and A. K. Jameson J. Chem. Phys. (in press).
14. S. A. Abrash; R. W. Zehner; G. J. Mains and L. M. Raff J. Phys. Chem. **99**, 2959(1995).

15. R. N. Porter; L. M. Raff and W. H. Miller, J. Chem. Phys. **63**, 2214 (1975).
16. H. Gai and D. L. Thompson, Chem. Phys. Lett. **168**, 119(1990).
17. E. L. Sibert; J. S. Hutchinson; J. T. Hynes; and W. P. Reinhardt, in *Ultrafast Phenomena* IV, edited by D. H. Auston and K. B. Eisenthal (Springer, New York, 1984); G. S. Ezra, in *Intramolecular and Nonlinear Dynamics*, edited by W. L. Hase (JAI, 1990).
18. P. J. Nagy and W. L. Hase, Chem. Phys. Lett. **54**, 73(1978).
19. B. G. Sumpter and D. L. Thompson, J. Chem. Phys. **88**, 6889(1988); H. Gai; D. L. Thompson; and G. A. Fisk, *ibid.* **90**, 7055(1989); A. Preiskorn and D. L. Thompson, *ibid.* **91**, 2299(1989); J. Chem. Phys. **92**,313(1990).
20. B. G. Sumpter and D. L. Thompson, J. Chem. Phys. **87**, 5809(1987).
21. L. M. Raff and D. L. Thompson, in *Theory of Chemical Reaction Dynamics*, edited by M. Baer (Chemical Rubber, Boca Raton, 1985), Vol. III, p.1
22. L. M. Raff, J. Chem. Phys. **90**, 6313(1989).
23. L. M. Raff, J. Chem. Phys. **89**, 5680(1988).
24. H. W. Schranz, L. M. Raff and D. L. Thompson, J. Chem. Phys. **95**, 106(1991)

Table IV

**Notation and frequencies for the stretch
modes of vinyl bromide. Frequencies
are given in cm⁻¹**

Mode No.	Description of mode	ν^a	Expt. ^b
ν_1	C-Br stretch	623 (0.190)	613 (0.187)
ν_2	C=C stretch	1606 (0.490)	1604 (0.489)
ν_3	C-H stretch	3004 (0.941)	3027 (0.916)
ν_4	C-H stretch	3086 (0.923)	3086 (0.941)
ν_5	C-H stretch	3121 (0.949)	3113 (0.949)

- (a) Calculated by the normal mode analysis on the global ground potential of vinyl bromide. The decimal value in the parentheses is in the unit of t.u.⁻¹, 1 t.u.⁻¹=3278 cm⁻¹
- (b) Reference 13

Table V

Parameters^a employed for the definition of local bond mode potentials

Local Mode	D (eV)	R ⁰ (Å)	α (Å ⁻¹)
C ₂ -Br ₆ stretch	3.339	1.890	1.720
C ₁ =C ₂ stretch	4.959	1.330	2.120
C ₂ -H ₃ stretch	4.876	1.077	1.823
C ₁ -H ₄ stretch	4.876	1.083	1.809
C ₁ -H ₅ stretch	4.876	1.085	1.809

(a) Taken from Reference 1

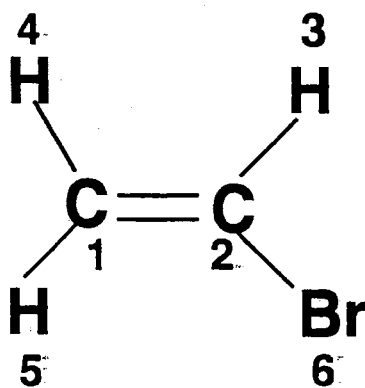


Table VI

**Frequencies of local stretch modes
obtained from power spectra lines**

Description of mode	$\nu(\text{t.u.}^{-1})$
C-Br stretch	0.188
C=C stretch	0.492
C ₂ -H ₃ stretch	0.977
C ₁ -H ₄ stretch	0.992
C ₁ -H ₅ stretch	0.992

Table VII

**Frequencies of C=C, C₂-Br and C₂-H₃ stretch modes
with Deuterium replacing of H₄ and H₅**

Description of mode	$\nu(\text{t.u.}^{-1})$
C-Br stretch	0.176
C=C stretch	0.461
C ₂ -H ₃ stretch	0.984
C ₁ -D ₄ stretch	0.746
C ₁ -D ₅ stretch	0.746

Table VIII

**Frequencies of C=C, C₂-Br and C₁-H₄ stretch modes
with Deuterium replacing of H₃ and H₅**

Description of mode	$\nu(\text{t.u.}^{-1})$
C-Br stretch	0.168
C=C stretch	0.465
C ₂ -D ₃ stretch	0.715
C ₁ -H ₄ stretch	0.973
C ₁ -D ₅ stretch	0.734

Table IX

**Frequencies of C=C, C₂-Br and C₁-H₅ stretch modes
with Deuterium replacing of H₃ and H₄**

Description of mode	$\nu(\text{t.u.}^{-1})$
C-Br stretch	0.168
C=C stretch	0.469
C ₂ -D ₃ stretch	0.719
C ₁ -D ₄ stretch	0.727
C ₁ -H ₅ stretch	0.973

Table X

**Intaramolecular energy transfer rate out of a
given local mode by CFM method**

Local mode	Line spacing(t.u. ⁻¹)	k(t.u. ⁻¹ .)
C-Br stretch	0.0560	0.180
C=C stretch	0.0468	0.101
C2-H3 stretch	0.0330	0.023
C1-H4 stretch	0.0390	0.029
C1-H5 stretch	0.0346	0.025

Table XI
Non-linear fitting results for each local stretch mode

Local mode	$k(\text{t.u.}^{-1})$	$\alpha(\text{t.u.}^{-1})$	$E_{\infty}(\text{eV})$	error(%)
C-Br stretch	0.214	0.212	-4.808	3.09
C=C stretch	0.116	0.115	-3.187	1.34
C2-H3 stretch	0.033	0.029	-4.614	3.47
C1-H4 stretch	0.041	0.039	-4.492	2.09
C1-H5 stretch	0.033	0.034	-4.321	5.45

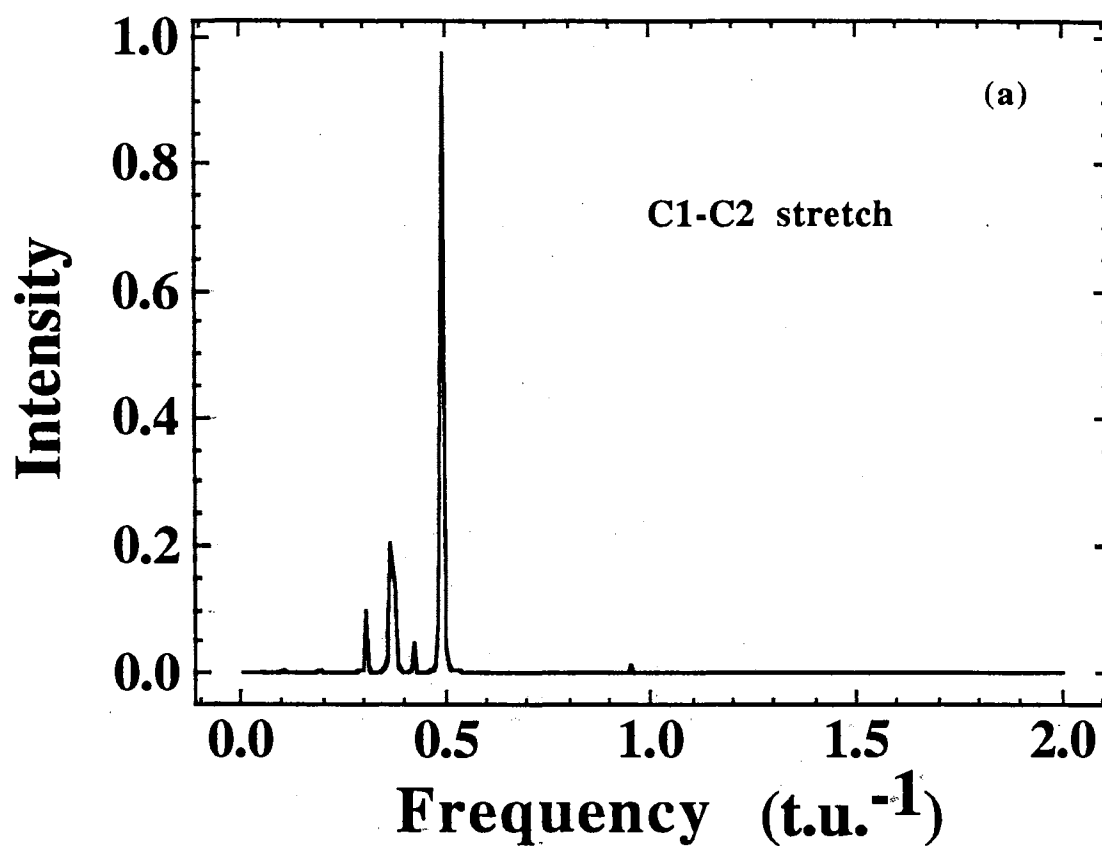


Figure 10(a): Power spectrum showing the fundamental frequency peak for C₁-C₂ when 1/10 ZPE is used

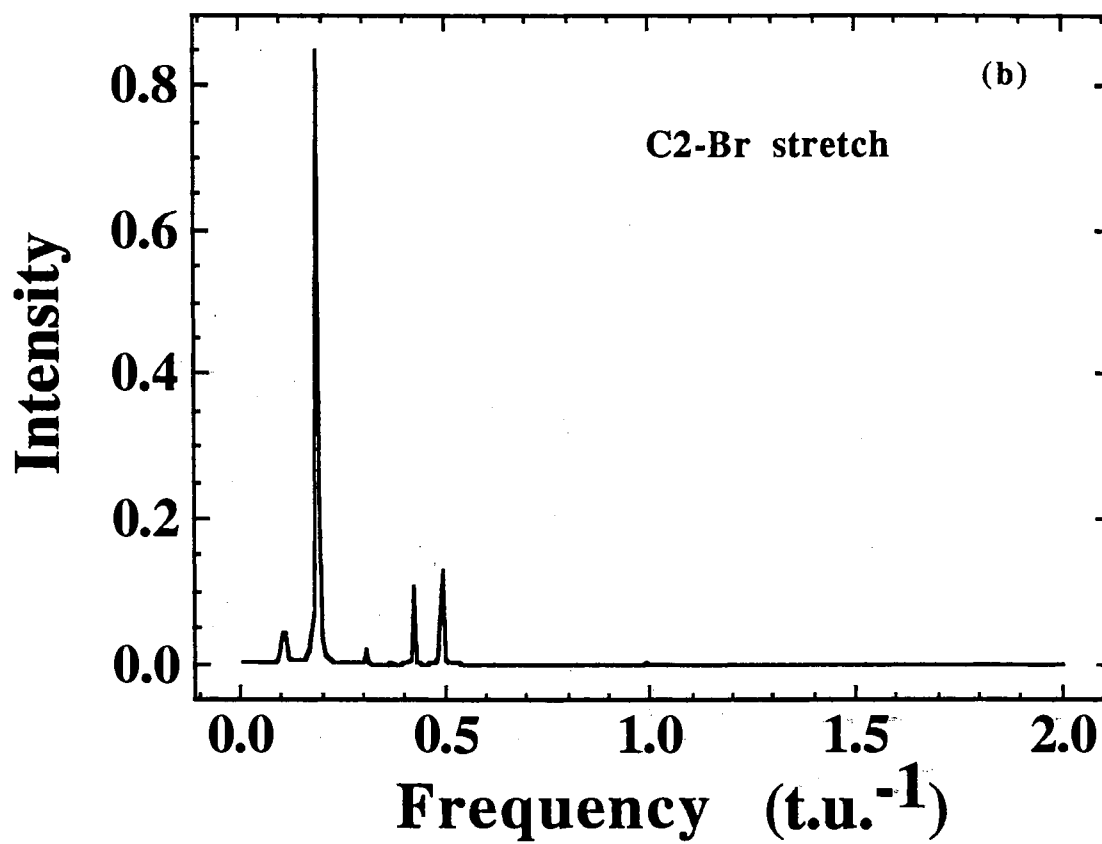


Figure 10(b): Power spectrum showing the fundamental frequency peak for C₂-Br when 1/10 ZPE is used

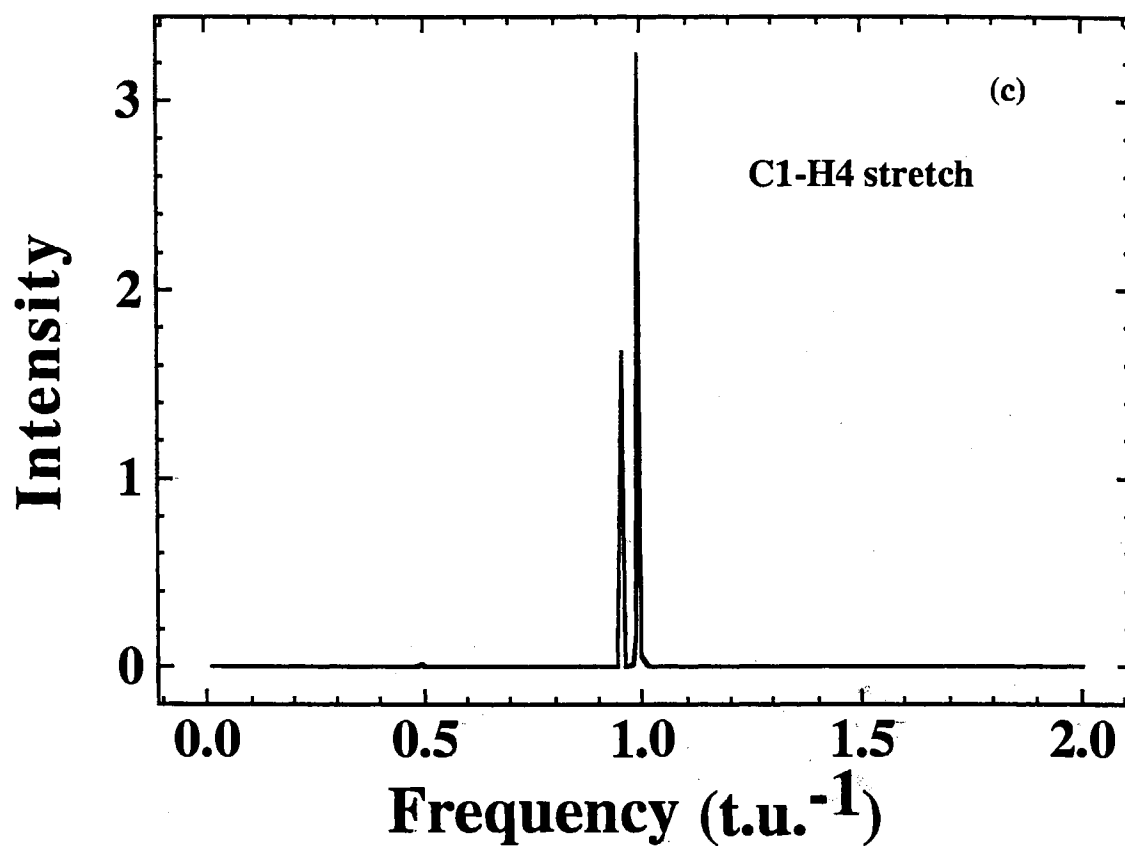


Figure 10(c): Power spectrum showing the fundamental frequency peak for C1-H4 when 1/10 ZPE is used

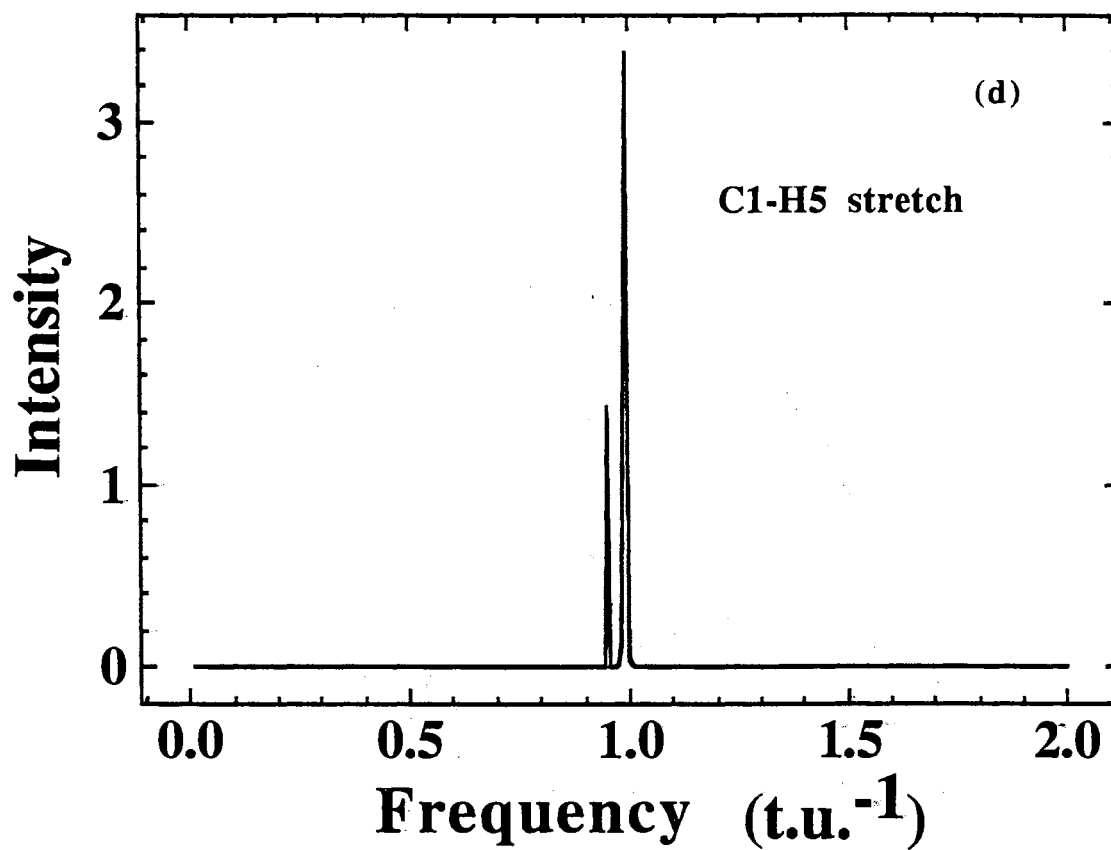


Figure 10(d): Power spectrum showing the fundamental frequency peak for C₁-H₅ when 1/10 ZPE is used

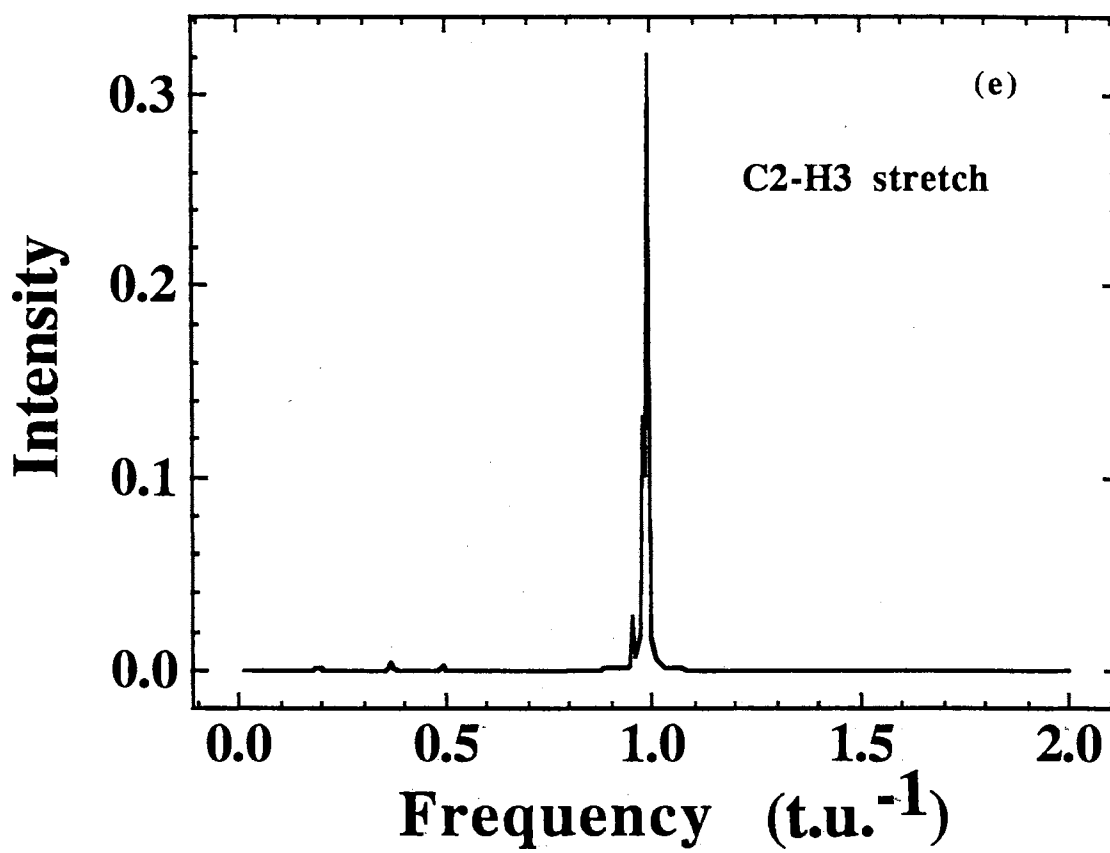


Figure 10(e): Power spectrum showing the fundamental frequency peak for C₂-H₃ when 1/10 ZPE is used

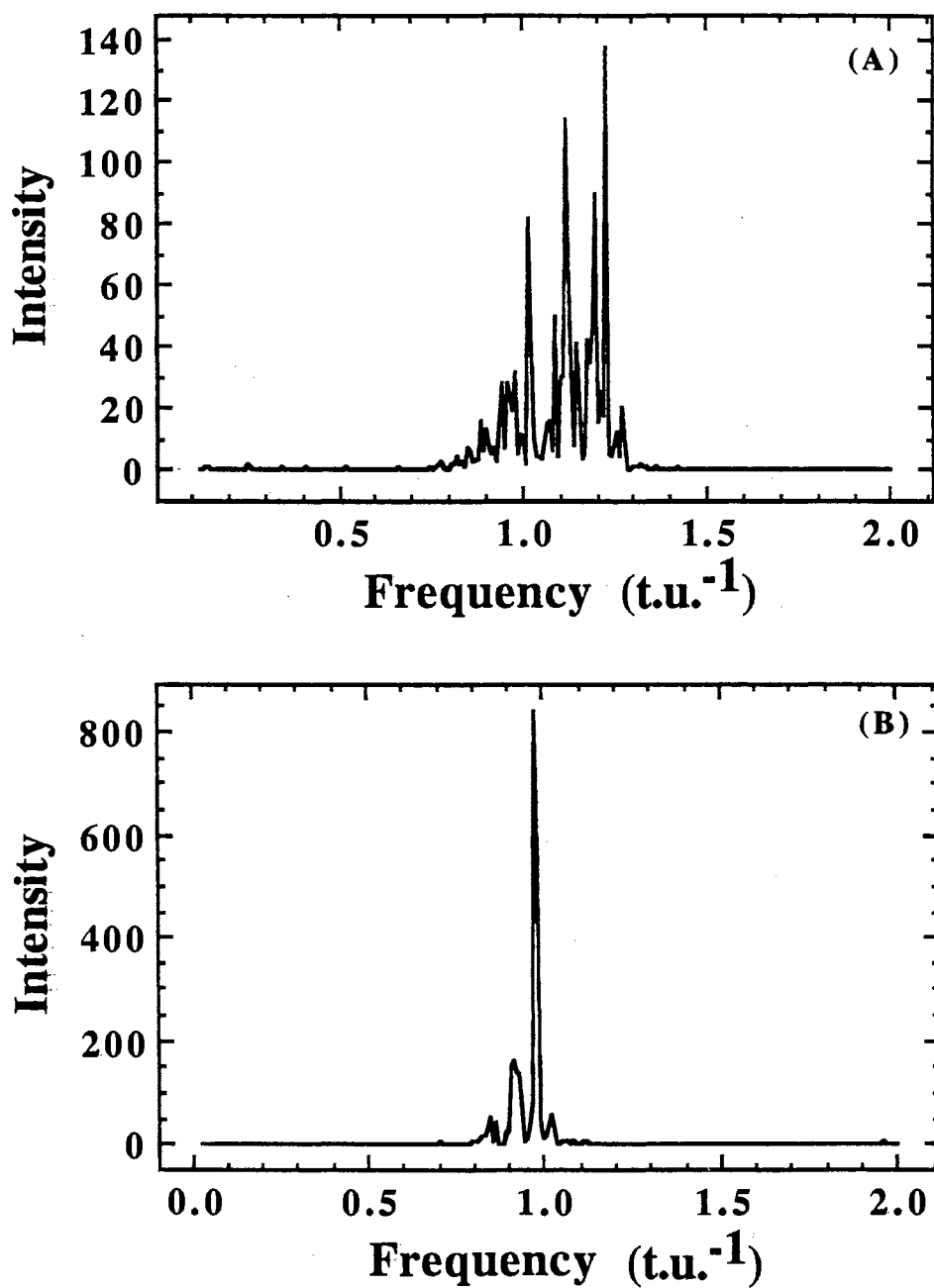


Figure 11. (A) Power spectrum of C₁-H₄ with no isotope effects, (B) Power spectrum of C₁-H₄ with deuterium replacement of H₂ and H₃. In both cases, the initial excitation of C₁-H₄ bond is 1.0 eV.

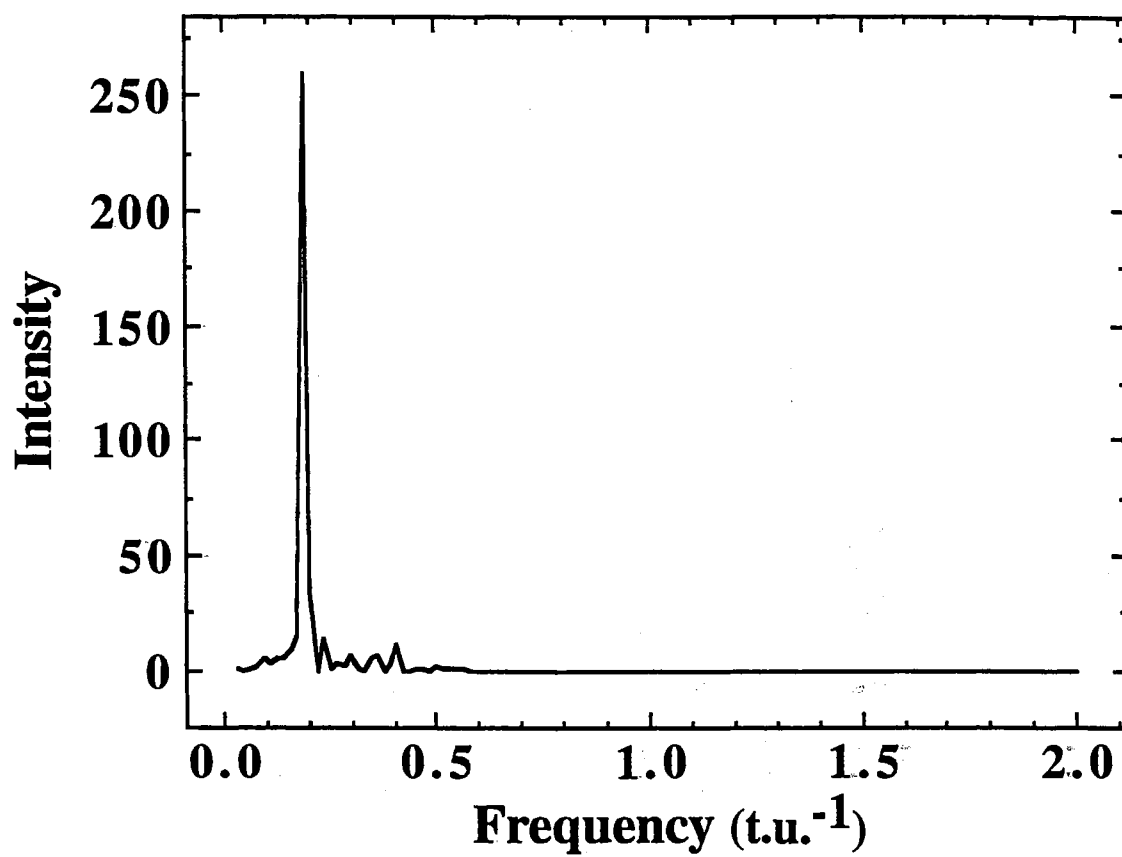


Figure 12. Power spectrum of C-Br bond with initial excitation of 1.0 eV.

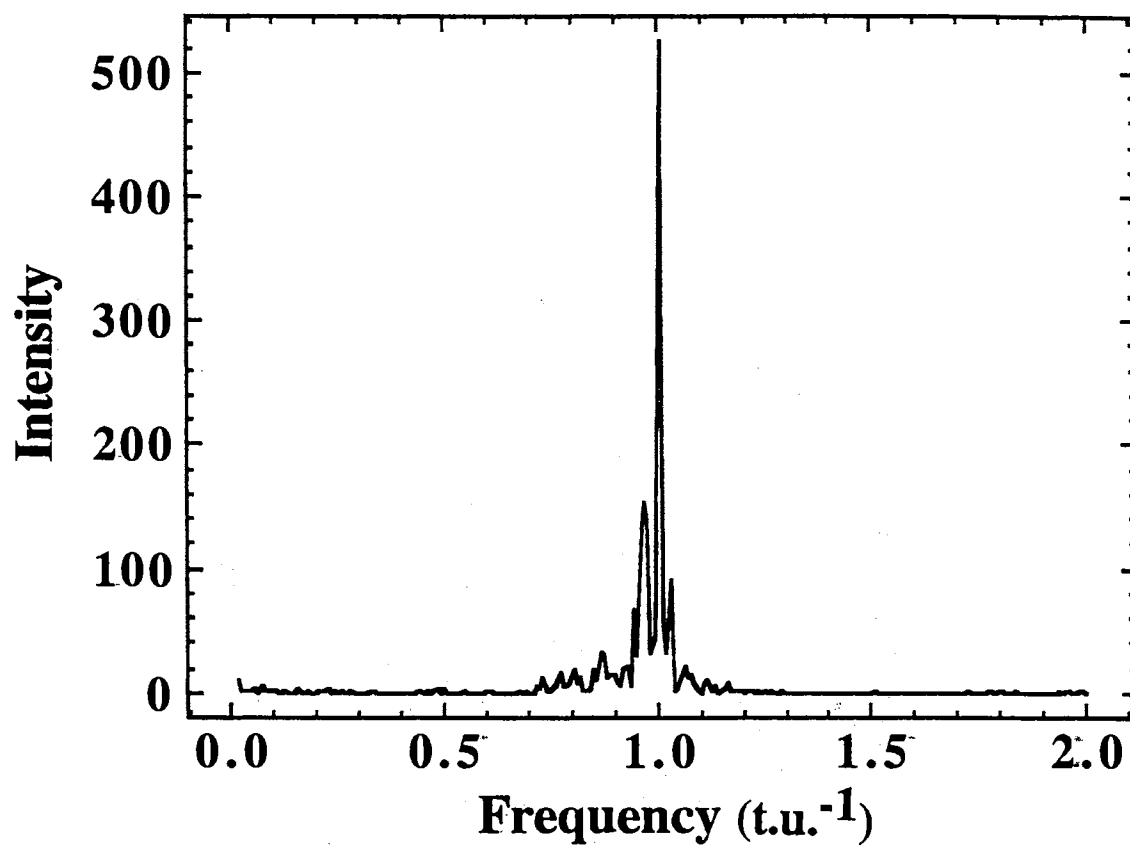


Figure 13. Power spectrum of C1-H₅ bond with initial excitation of 1.0 eV and deuterium replacement of H₃ and H₄.

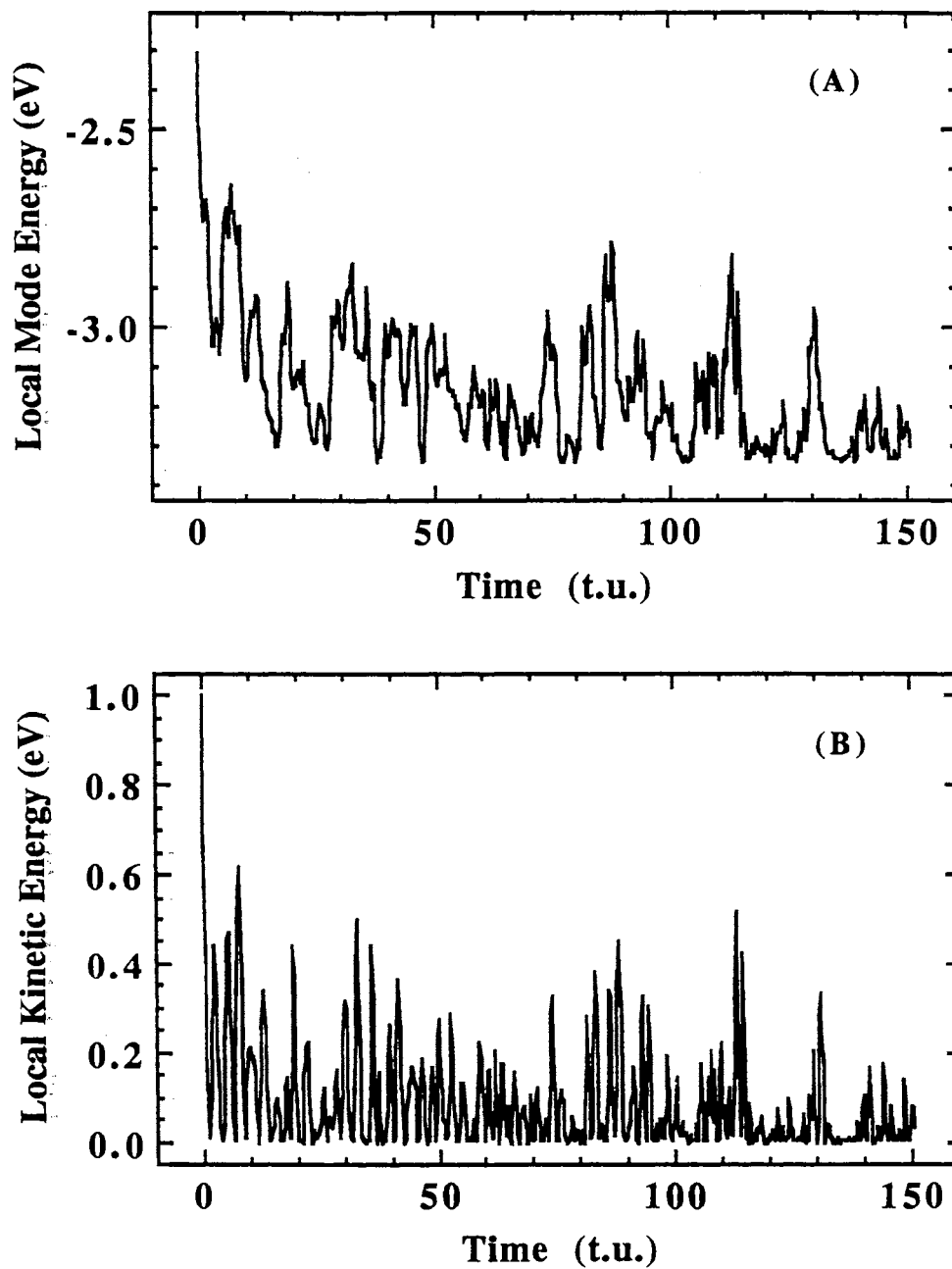


Figure 14. (A) Total mode energy variation of C-Br with time, (B) Local mode kinetic energy variation of C-Br with time. In both cases, the C-Br bond excitation is 1.0 eV.

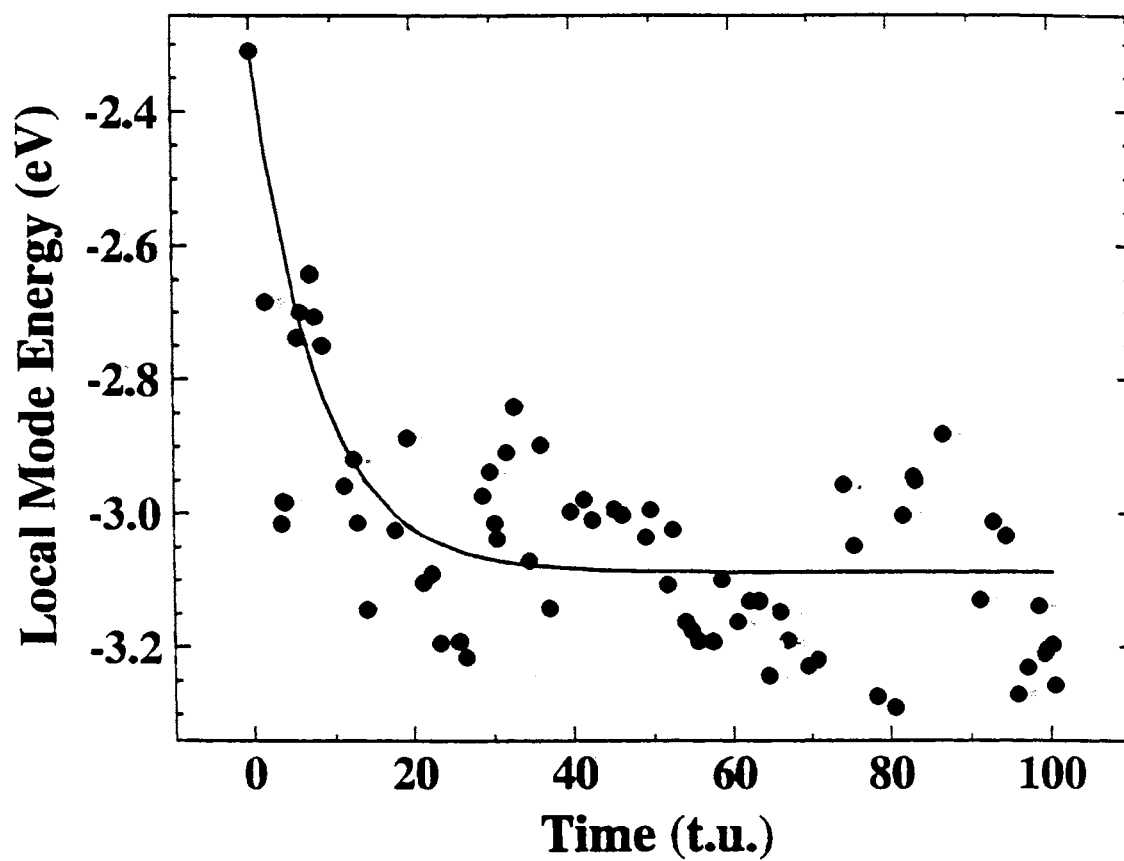


Figure 15. Non-linear fitting of envelope function of total mode energy decay of C-Br bond initially excited with 1.0 eV.

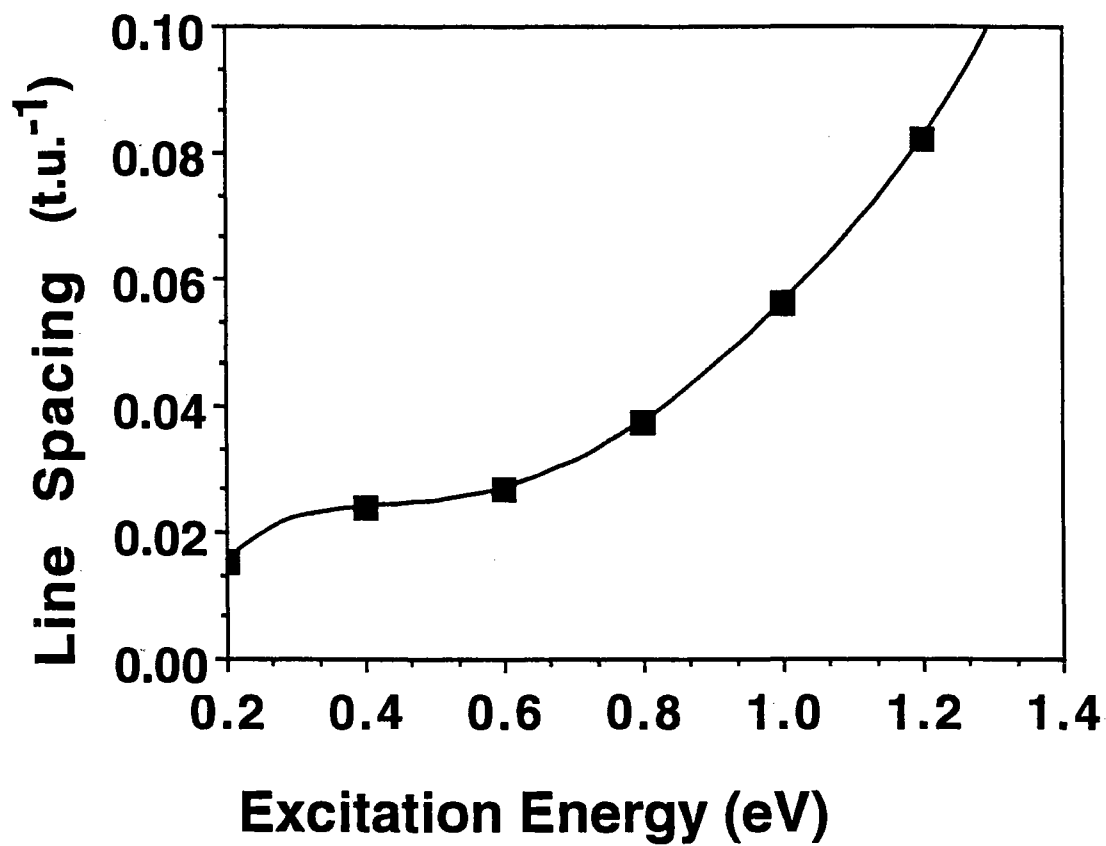


Figure 16. Fine spectra structure spacing variation of C-Br bond with initial excitation energy. Each point is ensemble-averaged with five individual trajectories.

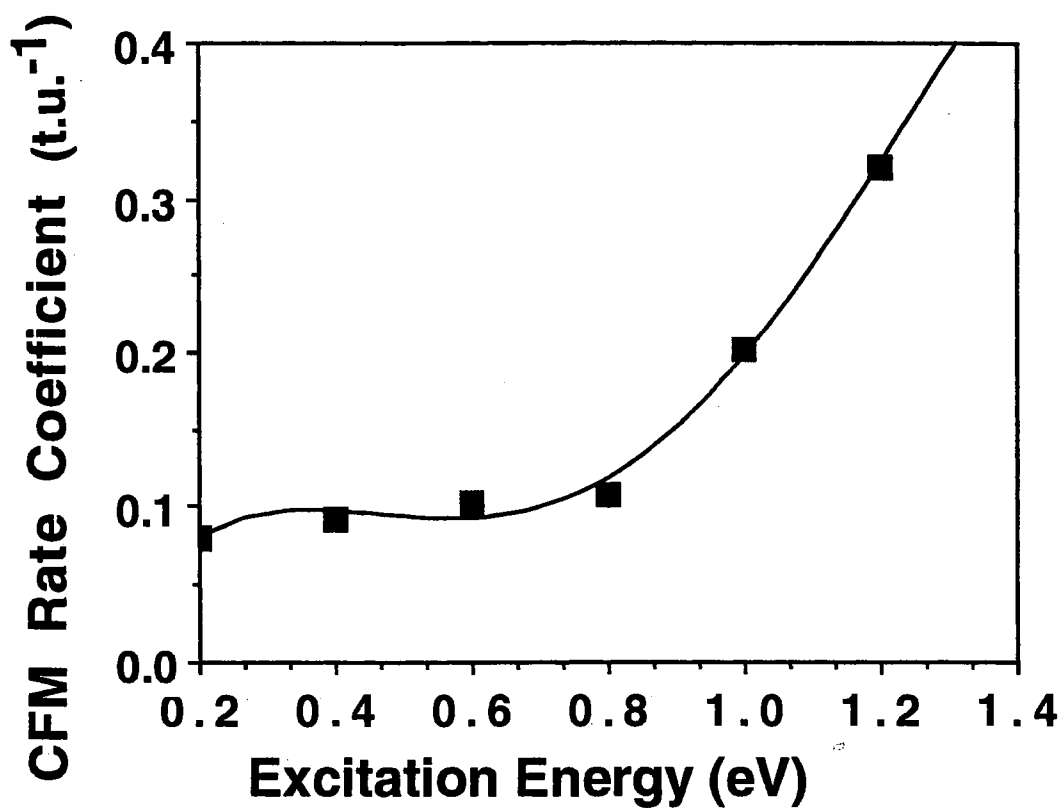


Figure 17. CFM rate coefficient variation of C-Br bond with initial excitation energy. Each point is ensemble-averaged with five individual trajectories.

CHAPTER V

THEORETICAL STUDIES OF HYDROGEN ATOM DIFFUSION RATES IN IMPERFECT RARE-GAS MATRICES

Introduction

The study of chemical systems under matrix isolation conditions at cryogenic temperatures has attracted much attention during the last decade because the use of such matrix-isolation techniques has led to a wealth of information related to structure, dynamics, and mechanism of many processes that would be difficult or impossible to investigate under the corresponding solution or gas-phase conditions. The low temperature, constrained environment of the matrix cage serves to moderate some fast reactions which are typically characterized by low activation energies, such as rotational isomerizations, radical recombination processes, and highly exothermic reactions, thereby increasing the half-life and permitting a variety of experimental measurements to be made. Mobility and diffusion often play critical roles in reactions occurring under matrix-isolation conditions. The importance of these effects becomes obvious when the matrix is used as a means for containing high-energy density materials. The bimolecular addition of F_2 to ethylene is a case in point.¹⁻⁵ The theoretical studies show that the

diffusion rates within the matrix cage directly affect the extent to which an atomic addition mechanism is involved in the reaction. ⁶

So far, there are very little experimental data related to diffusion and mobility in matrices and even fewer theoretical treatments. Feld, Kunttu, and Apkarian ⁷ have reported measurements of fluorine atom mobilities in an argon matrix subsequent to photodissociation. Lawrence and Apkarian ⁸ have measured the mobility of photoexcited oxygen atoms in Xe lattices. Theoretically, Ford *et al.* ⁹ have calculated diffusion rate coefficients for oxygen atoms diffusing in perfect face-centered cubic (fcc) xenon matrices. This work was stimulated by the experimental observations of Krueger and Weitz. ¹⁰ Comparison of the two treatments shows that the experimental diffusion coefficients are several orders of magnitude greater than the calculated values. More recently, LaBrake and Weiz have reported results for hydrogen atom diffusion in Xenon matrices at 40 K. ¹¹ Correspondingly, theoretical work was carried out by Perry *et al.* ¹² The results suggest that thermal diffusion rates of hydrogen atoms in fcc xenon crystals are very slow with activation energy between 2 and 3 kcal/mol. At temperatures below 12 K, hydrogen atom tunneling is the major diffusion process. At the higher temperatures, tunneling is negligible. Comparison of the results with measured diffusion coefficients¹² indicates that nearly all of the experimentally observed diffusion coefficients is occurring along lattice defects such as vacancies. In fact, the matrices produced experimentally are not perfect fcc lattices but rather have different kind of imperfections which allow for faster diffusion of the hydrogen atom through the matrix. The presence of such imperfections are also suggested by the experimental results reported by Krueger and Weitz. ⁹ The two diffusion coefficients reported by them for

the oxygen atom/Xe system are interpreted as representing average values over the low and high ends of a diffusion coefficient distribution that is characteristic of the number and nature of the lattice imperfections present in the experimental matrices.

In this chapter, we focus attention on the effects of imperfections on the diffusion rates of hydrogen atoms in xenon matrices.

Matrix Model

In the present study, mobility and diffusion in an imperfect face-centered-cubic rare-gas crystals are investigated. The matrix model used is the (5x5x5) fcc lattice of 125 unit cells containing 666 lattice atoms previously described by Raff.¹³ This model has been found to be sufficiently large to accurately represent the density and volume expansion upon trapping of 1,2-difluoroethane.¹³ In order to represent bulk effects upon energy transfer that would be present for an infinite lattice model, the velocity reset method developed by Riley *et al.*¹⁴ is employed. To do so, the 666 lattice atoms are first divided into three discrete zones. This division is determined once the size of the lattice model has been chosen using density, volume expansion, or other criteria. The boundary zone (B zone) comprises the atoms located on the boundary of the crystal. There are 302 such atoms in the present case. The positions of these lattice atoms are fixed. Their presence reduces edge effects and maintains the desired lattice symmetry. The secondary zone (Q zone) contains the 302 lattice sites within one unit cell distance of the outer boundary. The solution of Hamilton's equations for the motion of these atoms is modified by the reset functions associated with each atom in the Q zone.

This procedure maintains the temperature of the lattice as energy is removed or inserted by the chemical or physical processes that are occurring. The primary zone (P-zone) comprises the remaining atoms (62 in the present case) of the crystal. The motions of these atoms are affected only by the forces produced by the interaction potential. The above procedure is used for the perfect crystal model. The model for an imperfect lattice is constructed based on the model for the perfect lattice as described above. n lattice vacancies are created by randomly removing n lattice atoms in the P and Q zone.

Potential Energy Surfaces

The total potential, V_T , for the hydrogen atom/matrix system is assumed to be the separable sum

$$V_T = V_M + V_I, \quad (V.1)$$

where V_M is the interaction potential between lattice atoms, and V_I is the matrix-hydrogen interaction. The potential for the lattice interaction is assumed to have the form

$$V_I = \sum_{\substack{i < j \\ i, j \neq k}}^N V_{ij}(r_{ij}), \quad (V.2)$$

where r_{ij} is the distance between lattice atoms i and j , and N is the total number of the lattice atoms in the matrix model. k is the index number of vacancies in the crystal. V_{ij} is taken to be a Morse potential with a cutoff radius, $r_{ij} = R_C$, given by

$$V_{ij} = D \left[\exp \left\{ -2\alpha(r_{ij} - r_0) \right\} - 2 \exp \left\{ -\alpha(r_{ij} - r_0) \right\} \right] \quad \text{for } r_{ij} \leq R_c$$

$$V_{ij} = 0 \quad \text{for } r_{ij} > R_c \quad (V.3)$$

The parameters for the Morse potential are taken from the data reported by LeRoy ¹⁵ and Barker *et al.*¹⁶ The cutoff radius, R_c , is selected so that $V_{ij}(r_{ij}=R_c)$ is approximately 4% of the two-body well depth, D . Table XII gives the values of all matrix potential parameters along with the value of $V_{ij}(R_c)/D$.

The intermolecular potential for the hydrogen-lattice interaction is assumed to have the pairwise form

$$V_M = \sum_{\substack{i=1 \\ i \neq k}}^N V_{iH}(r_{iH}), \quad (V.4)$$

where r_{iH} is the distance between lattice atom i and the hydrogen atom. The V_{iH} term is taken to be a Lennard-Jones(12,6) potential given by

$$V_{iH} = \epsilon \left\{ \left(\sigma / r_{iH} \right)^{12} - 2 \left(\sigma / r_{iH} \right)^6 \right\}. \quad (V.5)$$

The potential parameters required in Eq. (V.5) are obtained by fitting the results of *ab initio* calculations.¹² In the first set of calculations a double- ζ (DZ) basis set combined with the pseudopotential for the xenon core developed by Wadt and Hay ¹⁷ was employed. The Xe-H equilibrium interatomic distance and the potential-well depth relative to the separated atoms were computed at the Hartree-Fock(HF), Möller-Plesset second-order perturbation theory (MP2) and MP4 levels of theory using GAUSSIAN 92 ¹².

The resulting parameters are given in Table XII. They show that the Xe-H doublet is unbound at the HF level of theory. At the MP2 level, it is very weakly bound with a well depth of 0.000272 eV at an equilibrium Xe-H separation of 4.5903 Å. At the equilibrium separation predicated by the MP2 calculations, MP4 calculations with all single, double, triple and quadruple excitations included predicted a well depth of 0.0001888 eV. These latter results are the ones employed for the Xe-H interactions in the present study.

Computational Methods

Initially, the rare-gas atoms are arranged in the (5x5x5) fcc lattice configuration. The hydrogen atom is placed at the most stable absorption site which is often the center of the innermost unit cell of the (5x5x5) matrix. Because of the creation of n vacancies in the crystal, the symmetry of the whole system is destroyed and the position of the most stable absorption site may be changed. The objective of the present study is to calculate the diffusion rate to an adjacent site, which, in a fixed fcc matrix, would be located at the midpoint of an edge of the center unit cell. Although the existence of vacancies introduces deviations from the expected symmetry, we shall assume that such deviations may be ignored in the computation of the jump frequency between adsorption sites.

The hydrogen-atom diffusion rate is calculated from the jump frequency or flux across a theoretical dividing surface separating the two adsorption sites. If the system behaves statistically, this flux must be an upper limit to the actual diffusion rate since all diffusion events involve crossing of the dividing surface but not all crossings result in diffusion. Consequently, we seek the

dividing surface that minimizes the flux. Several spherical and cubical surfaces have been examined to effect this minimization. It has previously been shown that cubical surfaces generally yield a higher flux.⁹

The total energy of the H/matrix system is given by

$$E = \sum_{\substack{i=1 \\ i \neq k}}^N [p_{xi}^2 + p_{yi}^2 + p_{zi}^2] / 2m_i + [p_{xH}^2 + p_{yH}^2 + p_{zH}^2] / 2m_H \quad (V.6)$$

where $p_{qi}(q=x,y,z)$ represents the momentum of the lattice atom i in the q direction. The subscript runs over all lattice atoms except the vacancy positions, k , and "H" denotes the hydrogen atom. It is assumed that the system behaves statistically with a canonical distribution of energies. Under these conditions, the jump frequency is proportional to the probability of the hydrogen atom being on the dividing surface and to the velocity of the atom perpendicular to that surface. Thus, the flux, $F(T)$, can be expressed by the sum of all such products averaged over the phase space of the system divided by the total available phase-space volume. This is,

$$F(T) = \frac{\int \int_{p,q} \exp(-E/k_b T) |V_{\pm}| \delta(q - q_c) \prod_{\substack{i=1 \\ i \neq k}}^{3N} dq_i dp_i}{\int \int_{p,q} \exp(-E/k_b T) \prod_{\substack{i=1 \\ i \neq k}}^N dq_i dp_i} \quad (V.7)$$

where the delta function, $\delta(q - q_c)$, is unity when on the dividing surface and zero otherwise. The configuration space integrals cover the space corresponding to reactant conformations. The integrations over momenta in

Eq. (V.7) can be done analytically for spherical or cubic dividing surfaces. Such integration yields

$$F(T) = \langle v \rangle_q \frac{\int_q \exp(-V_T / k_b T) \delta(q - q_c) \prod_{\substack{l=1 \\ l \neq k}}^{3N} dq_l}{\int_q \exp(-V_T / k_b T) \prod_{\substack{l=1 \\ l \neq k}}^N dq_l} \quad (V.8)$$

where $\langle v \rangle$ represents the average velocity of the hydrogen atom.

Since the potential being employed is separable into a lattice potential plus an hydrogen-lattice interaction, then, Eq.(V. 8) may be written in the form

$$F(T) = \langle v \rangle_q \frac{\int_q \exp(-V_M / k_b T) \exp(-V_l / k_b T) \delta(q - q_c) \prod_{\substack{l=1 \\ l \neq k}}^{3N} dq_l}{\int_q \exp(-V_M / k_b T) \exp(-V_l / k_b T) \prod_{\substack{l=1 \\ l \neq k}}^N dq_l} \quad (V.9)$$

The complexity of the potential precludes analytical evaluation of Eq.(V.9). We therefore utilize the Monte Carlo method as described in the Chapter II to execute the required integrations. A Metropolis sampling procedure is employed in which the dividing surface is replaced with a dividing "slab" of width Δw . If Δw is sufficiently small that the integrand of Eq.(V.9) is constant across the width, Eq. (V.9) becomes

$$F(T) = [\langle v \rangle / \Delta w] \frac{\int_q \exp(-V_M / k_b T) \exp(-V_I / k_b T) \delta(\Delta w) \prod_{\substack{l=1 \\ l \neq k}}^{3N} dq_l}{\int_q \exp(-V_M / k_b T) \exp(-V_I / k_b T) \prod_{\substack{l=1 \\ l \neq k}}^N dq_l} \quad (V.10)$$

where $\delta(\Delta w)$ is unity if a configuration point lies within the dividing slab and zero otherwise. In principle, Eq.(V.10) may be evaluated using a random set of M points in the multidimensional configuration space of the system. For such a randomly selected set of points, the Monte Carlo approximant for Eq. (V.10) is

$$F(T) \approx [\langle v \rangle / \Delta w] \frac{\sum_i^M [\exp(-V_M / k_b T) \exp(-V_I / k_b T) \delta(\Delta w)]_i}{\sum_i^M [\exp(-V_M / k_b T) \exp(-V_I / k_b T)]_i} \quad (V.11)$$

Although Eq.(V.11) yields the flux across the dividing slab, its convergence rate will be extremely slow if totally random points are selected for all atoms since virtually all points selected will correspond to highly improbable configurations. The situation may be improved by selecting the points from a Markov walk weighted by the canonical distribution function $\exp[-V_T/kT]$. In this case, the flux will be given by

$$F(T) \approx [\langle v \rangle / \Delta w] \sum_i^M [\delta(\Delta w)]_i \quad (V.12)$$

The convergence rate of Eq.(V.12) will be significantly greater than that of Eq.(V.11). However, convergence will still be very slow due to the infrequency

of sampling in the regions of high potential. A more satisfactory convergence rate may be obtained by using a Markov walk weighted by the canonical distribution function for the lattice alone, $\exp[-V_M/kT]$. For such a selection method,

$$F(T) \approx 0.5[\langle v \rangle / \Delta w] \frac{\sum_i^M [\exp(-V_i / k_b T) \delta(\Delta w)]_i}{\sum_i^M [\exp(-V_i / k_b T)]_i} \quad (V.13)$$

where a factor of 0.5 is included to correct for entries into the dividing volume from the wrong direction. Eq.(V.13) has previously been used to compute silicon and hydrogen atom diffusion rates on Si(111) and Si(111)-(7x7) surfaces.¹⁸

The convergence rate by Eq.(V.13) is still very slow although it can be used to obtain diffusion rates on surfaces and in matrices. Typically, millions of Markov steps are required for surface diffusion. For matrices at cryogenic temperatures, convergence is even slower. A new method was proposed by Ford *et al.*⁹ in recent calculations. The method is based on the assumption that the major contribution to $F(T)$ in Eq.(V.10) arises from configurations in the neighborhood of the minimum-energy pathway for the diffusion process. These configurations were conveniently located and sampled by using a combination of canonical Markov moves on the lattice atoms and totally random moves on the embedded hydrogen atom followed by a series of damped trajectory cycles in which the lattice is allowed to relax toward its minimum-energy configuration in the field of a stationary hydrogen atom.^{6,13} A Monte Carlo integration was observed to converge at a much greater rate since all of the sampling was done in statistically important regions of

configuration space near the minimum-energy path. For spherical dividing surfaces, it is convenient to write Eq.(V.10) in the form

$$F(T) \approx \left[\langle v \rangle / \Delta w \right]^q \frac{\int \exp(-V_M / k_b T) \exp(-V_I / k_b T) \delta(\Delta w) \prod_{l=1}^{3N} dq_l r_H^2 dr_H \sin \theta_H d\theta_H d\phi_H}{\int_q \exp(-V_M / k_b T) \exp(-V_I / k_b T) \prod_{l=1}^{3N} dq_l r_H^2 dr_H \sin \theta_H d\theta_H d\phi_H} \quad (V. 14)$$

where hydrogen atom coordinates are separated and expressed in a spherical system. The Monte Carlo approximant for Eq.(V.14) is similar in form to Eq.(V. 11). It is

$$F(T) \approx \left[1 / (2 \times 12 \times \Delta r) \right] (8k_b T / \pi M_H)^{1/2} \frac{\sum_i^M \left[\exp(-V_M / k_b T) \exp(-V_I / k_b T) r_H^2 \delta(\Delta w) \right]_i}{\sum_i^M \left[\exp(-V_M / k_b T) \exp(-V_I / k_b T) r_H^2 \right]_i} \quad (V.15)$$

where the terms under the summations are evaluated after every Markov step on the lattice and after every damped trajectory cycle. In Eq.(V 15), Δr is the width of the dividing spherical slab and M_H is the hydrogen-atom mass. The factor of 2 corrects for surface crossings in the wrong direction. The factor of 12 removes the degeneracy in the calculation which is present since a spherical dividing surface counts jumps to 12 equivalent diffusion sites.

In practice, the Markov walk is executed by moving m randomly selected lattice atoms ($7 \leq m \leq 20$) and the hydrogen atom in each step of the walk. The lattice atoms are moved according to

$$q_i^{\text{new}} = q_i^{\text{old}} + \xi_i \Delta q \quad (i=1,2,3,\dots,m) \quad (\text{V. 16})$$

where q_i^{new} and q_i^{old} are the new and old x, y, and z coordinates of the lattice atom i , respectively, and Δq is the Markov step size. The ξ_i are random numbers selected from a uniform distribution on the interval [0.1]. For the hydrogen atom,

$$\Delta x_H = \Delta Q \sin \theta_H \cos \phi_H \quad (\text{V.17})$$

$$\Delta y_H = \Delta Q \sin \theta_H \sin \phi_H \quad (\text{V.18})$$

$$\Delta z_H = \Delta Q \cos \phi_H \quad (\text{V.19})$$

where

$$\theta_H = \cos^{-1}[1 - 2\xi_{H1}] \quad (\text{V.20})$$

$$\phi_H = 2\pi\xi_{H2} \quad (\text{V.21})$$

$$\Delta Q = \Delta q \xi_{H3} \quad (\text{V.22})$$

The value of m and Δq are adjusted to produce a near-unit ratio between accepted and rejected moves. In most cases, $m=7$ and Δq is 0.0866Å for both the lattice atoms and hydrogen. The width of the dividing slab, Δr , is chosen

to be equal to the maximum step size to ensure that the hydrogen atom cannot traverse the dividing slab without entering its volume at least once.

To increase convergence speed, subsequent to the Markov step described above, K damped trajectory cycles are executed holding the hydrogen atom stationary.^{6,13} In this procedure, the kinetic energy of each lattice atom is set to zero and the classical Hamiltonian equations of the motion for the lattice atoms are integrated until the total potential energy attains a minimum. This is defined to be one trajectory cycle. Subsequent cycles are executed by repeating the above procedure starting with the lattice configuration achieved in the previous cycle. The use of this technique causes the Markov steps to be taken in the near vicinity of the minimum-energy pathway. This significantly reduces the computational time required to achieve convergence.

It is obvious that the system potential is independent of mass, therefore, the actual execution of the above procedure can be greatly facilitated by making use of this fact. Consequently, Hamilton's equations may be integrated with the mass of all atoms set to 1.0 amu. In addition, we may employ a very large integration step size since we need not be concerned with the conservation of energy. The use of these two techniques significantly reduces the computational time required for convergence.

A partial minimization of $F(T)$ is carried out by computing the flux through a set of spherical dividing slabs with radii of $(R=0.05jd)$ for $j=1,2,3,\dots,20$, where d is the total diffusion distance measured from the initial adsorption site. The hydrogen atom is initially placed near the most stable site, which is the geometric center of the innermost unit cell before the

vacancies are created, and the entire system is allowed to relax to the nearest potential minimum using a set of 100 damped trajectory cycles. The initial adsorption site is taken to be the point that leads to the lowest total potential.

Because the ratio of hydrogen atoms to the number of adsorption sites is small, the diffusion coefficient can be related to the jump frequency by

$$D(T) = \frac{[d^2k(T)f]}{\alpha} \quad (V.23)$$

where f is the fraction of vacant sites ($f=1$ here), α is the dimensionally factor, which is three in the present case since diffusion within the matrix is three-dimensional, and $K(T)$ is the jump frequency. The variational transition-state theory method assumes that $K(T)$ can be accurately replaced with $F_{\min}(T)$, where $F_{\min}(T)$ is the minimum flux obtained in the variational adjustment of the dividing slab.

Results and Discussion

Starting from a hydrogen atom in the innermost cell of the lattice, we consider the diffusion to other similar neighbor lattice sites. In previous studies¹² based on a perfect fcc lattice, the destination site for diffusion has almost exactly the same lattice environment as the starting site. However, for an imperfect crystal, the system symmetry is broken. Consequently, the diffusion destination site is similar but not identical to the starting site.

The Markov walk/damped trajectory procedure described in the above section is found to converge at a rate much faster^{9, 12} than normally seen in the calculation of diffusion rates using classical variational transition-state

theory methods.^{17, 19} Convergence of the diffusion rates for oxygen atoms in xenon matrices⁹ was achieved in 5×10^4 steps with the Markov/damped trajectory procedure. In contrast, it was not possible to obtain convergence with 10^6 Markov moves for employing classical variational transition-state methods alone. In the present study, the Markov walk/damped trajectory method is used to compute the hydrogen diffusion rates in an imperfect fcc xenon matrix at cryogenic temperatures. In all cases, convergence is obtained with $0.75 - 2.0 \times 10^5$ Markov steps.

As described in Section III, the hydrogen-lattice interaction is assumed to be a sum of Lennard Jones(12,6) pairwise potentials. The H-Lattice interaction energy changes as the vacancy number changes. Figure 18 shows the typical results. As the vacancy number increases, the system H-Lattice potential decreases. We may therefore expect that the existence of vacancies will favor the fast diffusion of hydrogen atom in the lattice relative to the perfect system.

The total potential of the system varies significantly as the hydrogen atoms moves within a cell. The variation in system potential for the straight-line diffusion of hydrogen from one adsorption site to another with frozen lattice atoms and no relaxation is shown in Figure 19. Although the system has 15 vacancies, the potential variation curve has the same shape as that for a perfect fcc system. As expected, the potential energy along such a path attains a maximum value when the hydrogen atom is located at a point midway between the two sites. The barrier for diffusion in this case is about 2.855 eV. For more attractive potentials with large values of ϵ , the potential barrier to diffusion in a fixed lattice becomes larger.

It seems impossible that thermal diffusion of hydrogen atoms at temperatures characteristic of matrix experiments could be observed with a diffusion barrier of 2.85 eV or higher. However, when the lattice is permitted to relax in the potential field of the hydrogen atom and the phonon modes of the lattice are permitted to contribute to the diffusion process, the diffusion barrier generally decreases by more than an order of magnitude. In our case, minimum-energy reaction paths have been determined for hydrogen-atom diffusion in a xenon lattice by recording the minimum system potential for each of the dividing slabs obtained from hydrogen-atom crossings observed during the Markov/damped trajectory walk. Typical results are shown in Figure 20 and Figure 21. Figure 20 shows the minimum energy reaction path for a system with 5 vacancies, and Figure 21 shows a case with 15 vacancies. Previous results¹² showed that the potential barrier maximum along the minimum-energy reaction path occurs in the neighborhood of the dividing slab located at $d/2$ as expected for a perfect fcc system. However, for the case of 5 vacancies and a LJ(12,6) potential with $\epsilon=0.000188$ eV, the relaxation of the lattice reduces the energy barrier from 2.855 eV to 0.1146 eV. The position along the diffusion path at which the maximum potential occurs shifts to larger distance. The energy barrier for 5 vacancies is lowered 0.0064 eV relative to the perfect system. For the case with 15 vacancies, the minimum-energy reaction path becomes more complicated. Relaxation of the system reduces the energy barrier from 2.885 eV to 0.093 eV while the position of the barrier crest shifts to about 1.2 Å. The maximum potential value is lowered 0.0216 eV relative to the case of 5 vacancies. Therefore, it can be concluded that the existence of vacancies lowers the energy barrier for the diffusion of hydrogen atoms and that the more the vacancies exist, the lower the energy barrier.

The calculated hydrogen atom diffusion rates in Xe matrices with 5 vacancies and 15 vacancies are given in Table XIII and Table XIV, respectively. With 5 vacancies, the diffusion rate of hydrogen at 40 K is obtained by averaging five different calculations, each calculation is executed with a different set of vacancy sites. The averaged diffusion rate is a factor of 26.56 faster than that for the perfect fcc crystal, while the corresponding diffusion barrier is 4.63% lower. The diffusion rate of hydrogen at 40 K is several orders of magnitude faster than that in the perfect crystal, and the corresponding diffusion barrier is lowered 0.028 eV relative to the perfect fcc lattice. Consequently, we conclude that the diffusion rates of hydrogen in xenon matrices increases as the number of vacancies increase. Table XIV also shows that the classical diffusion rates increase with temperature. It can be seen that the calculated diffusion rates are found to be sensitive to the potential barrier which is dependent on the potential parameters. In general, the diffusion rate decreases as the attractive interaction between the hydrogen atom and the lattice atom increases. Perry *et al.*¹² proposed three sets of hydrogen lattice interaction potentials, and pointed out that differences in the potential can cause large changes in the calculated diffusion rates. Because of the small mass of hydrogen, tunneling processes would be expected to make an important contribution to diffusion. This has been previously verified.¹²

It is important to note that the calculations show that the vacancy sites are mobile. A typical example is shown in Figure 22 for the case of xenon lattice at 40 K containing 5 vacancies. The figure illustrates the mobility of one of these vacancies during the initial 200,000 Markov steps. As can be seen, five translations of this vacancy occur during this period. These translations are

induced by the hydrogen-atom diffusion which causes the lattice to shift toward a thermodynamically stable configuration.

The translation of site vacancies can significantly affect the hydrogen-atom diffusion rate since the process alters the potential barrier to diffusion. Figure 23 and 24 illustrate this point. Figure 23 shows the variation of the system potential between the initial and final absorption sites after 200,000 Markov steps have been executed on a xenon lattice containing 5 vacant sites. Comparison of these results with those given in Fig. 20 shows that the barrier to diffusion has completely vanished. More detailed investigation demonstrates that this drastic alteration of diffusion barrier is the result of vacancy site mobility. Figure 24 shows a similar result after 100,000 Markov steps on a xenon lattice containing 15 vacant sites. Our studies show that the propensity for vacant site mobility increases as the total number of vacancies increases.

Qualitatively, it is clear that vacant site mobility will increase the hydrogen-atom diffusion rate through the lattice since the process lowers the diffusion barrier. Since the canonical Markov walk and damped trajectory calculations are thermodynamically based, we cannot determine the time scale for vacant site mobility from the present calculations. Consequently, it is not possible for us to quantitatively determine the effect of such mobility on the hydrogen-atom diffusion rates in imperfect xenon crystals. For this reason, the diffusion coefficients listed in Tables XIII and XIV should be regarded as lower limits for a system whose potential is described by Eq.(V.1).

Figure 25 shows a semilog plot of the calculated hydrogen-atom diffusion coefficients in a xenon matrix as a function of the percentage of vacant sites in

the lattice. The excellent linearity of this plot indicates that the dependence is well described as exponential. A least squares fit to the data yields

$$D \times 10^{15} = 0.1449 \exp[1.381p] \text{ cm}^2/\text{s} \quad (\text{V.19})$$

where D and p are the diffusion coefficient and the percent vacancies, respectively.

LaBrake and Weitz¹¹ have measured hydrogen-atom diffusion coefficients in vapor deposited xenon matrices at 40 K. They used 193 nm photolysis of HBr to produce hydrogen atoms whose concentration was monitored using laser induced emission from xenon-hydrogen exciplexes. When a xenon matrix vapor deposited at 10 K, denoted Xe(10K), was maintained at 10 K, the hydrogen-atom concentration remained unchanged over a five day period. Thus, the diffusion coefficient at 10 K in Xe(10K) is effectively zero. When the temperature of the Xe(10K) matrix is increased to 40 K, hydrogen diffusion is observed with an estimated diffusion coefficient of $2.6 \times 10^{-13} \text{ cm}^2/\text{s}$. In contrast, when a Xe(28K) matrix is warmed to 40 K, a diffusion coefficient of $5.0 \times 10^{-14} \text{ cm}^2/\text{s}$ is obtained.¹¹ LaBrake and Weitz¹¹ suggested that this difference is due to the presence of a larger number of imperfections in the lattice deposited at 10 K which are not later annealed at 40 K. This view implicitly assumes that the larger number of vacancies present in the Xe(10K) lattice will lead to a larger hydrogen-atom diffusion coefficient.

The data given in Tables XIII and XIV and in Figure 25 support the interpretation advanced by LaBrake and Weitz.¹¹ Eq. (V.19) shows that the diffusion coefficient will indeed increase rapidly with an increase in the number of vacant lattice sites. The horizontal lines shown in Figure 25 are the measured diffusion coefficients¹¹ in Xe(10K) and Xe(28K) lattices. The intersection of

these lines with the calculated curve indicates that there are 1.76% and 1.15% vacancies in Xe(10K) and Xe(28K) matrices, respectively. Since the calculated values of D are lower limits for the reasons discussed above, these percentages are upper limits for the potential surface used in the present calculations.

Summary

Using a two-body Xe/H interaction potential obtained from the results of MP4(SDTQ) calculations, thermal diffusion rates of hydrogen atoms in an imperfect face-centered cubic xenon lattice containing n vacancies have been computed using Monte Carlo variational phase-space theory. Convergence of the required integrals is achieved by combining importance sampling and a damped trajectory procedure with the standard Markov walk. The variational flux through spherical dividing surfaces is minimized as a function of radius of the dividing surfaces.

The minimum-energy diffusion paths have been determined by recording the minimum system potential observed upon hydrogen-atom crossing on each of the dividing surfaces during the damped trajectory/Markov walk. Typical results show that the presence of 1.1% vacant lattice sites lowers the diffusion barrier by about 0.006 eV relative to the perfect fcc crystal system.

The calculations show that the lattice vacancies are mobile. This translation of site vacancies can significantly affect the hydrogen-atom diffusion rate since the process alters the potential barrier to diffusion. Our studies show that the propensity for vacant site mobility increases as the total number of lattice vacancies increases. Although it is clear that vacant site mobility will

increase the hydrogen-atom diffusion rate through the lattice since the process lowers the diffusion barrier, the present calculations do not permit the magnitude of this increase to be determined. This is a consequence of the fact that the canonical Markov walk and damped trajectory calculations are thermodynamically based. Therefore, we cannot determine the time scale for vacant site mobility from the present calculations. For this reason, the diffusion coefficients reported here are lower limits for a system whose potential is described by Eq. (V.1).

The computed values of the hydrogen-atom diffusion coefficient at 40 K indicate that over the range of vacancies considered, the diffusion coefficients increase exponentially with the percentage of lattice vacancies. Comparison of the predicted diffusion rates with the experimental values reported by LaBrake and Weitz¹¹ in vapor deposited xenon matrices suggests that the Xe lattices deposited at 10 K and 28 K have about 1.8% and 1.2% vacant sites, respectively. Since the calculated values of D are lower limits, these percentages are upper limits for the potential surface used in the present calculations.

REFERENCES

1. R. H., Hauge; S. Gransden; J., Wang; J. L. Margrave, *J. Am. Chem. Soc.* **101**, 6950 (1979).
2. H., Frei; L. Fredin; G. C. Pimentel, *J. Chem, Phys.* **74**, 397(1981).
3. A. K. Knudsen; G. C. Pimentel, *J. Chem. Phys.* **78**, 6780(1983).
4. H., Frei; G. C. Pimentel, *J. Chem, Phys.* **78**, 3698 (1983).
5. H., Frei, *J. Chem, Phys.* **79**, 748 (1983).

6. L. M. Raff, *J. Chem. Phys.* **97**, 7459(1992).
7. J. Feld; H. Kunttu; V. A. Apkarian, *J. Chem. Phys.* **93**, 1009(1990).
8. W. G. Lawrence; V. A. Apkarian, *J. Chem. Phys.* **97**, 6199(1992).
9. M. B. Beth Ford; A. D. Foxworthy; G. J. Mains; and L. M. Raff, *J. Phys. Chem.* **97**, 12134 (1993).
10. H. Krueger; E. Weitz, *J. Chem. Phys.* **96**, 2846(1992).
11. D. LaBrake; E. Weiz, *Chem. Phys. Lett.* **211**, 430(1993).
12. M. D. Perry; G. J. Mains; L. M. Raff, *J. Phys. Chem.* **98**, 13766 (1994).
13. L. M. Raff, *J. Chem. Phys.* **93**, 3160 (1990).
14. M. E. Riley; M. E. Coltrin; D. J. Diestler, *J. Chem. Phys.* **88**, 5934(1988).
15. R. J. Leroy, *J. Chem. Phys.* **57**, 573 (1972).
16. J. A. Barker; R. O. Watts; J. K. Lee; T. P. Schafer; Y. T. Lee, *J. Chem. Phys.* **61**, 3081 (1974).
17. P. J. Wadt and W. R. Hay, *J. Chem. Phys.* **82**, 270(1985).
18. B. M. Rice; L. M. Raff; D. L. Thompson, *Surf. Sci.* **198**, 360(1988).
19. P. M. Agrawal; D. L. Thompson; L. M. Raff, *J. Chem. Phys.* **91**, 6463(1989).

Table XII

Hydrogen/Lattice pairwise potential parameters

Parameter	Value
Xe-Xe^a	
D	0.02421405(eV)
α	1.4676000(\AA^{-1})
r_0	4.36230(\AA)
R_{cut}	7.000(\AA)
Xe-H^b	
D	0.000188(eV)
R_{eq}	4.5903(\AA)
R_{cut}	7.000(\AA)

a: taken from reference 9

b: taken from reference 12

Table XIII

**Classical diffusion rates for hydrogen atoms
in perfect fcc xenon matrix and in an imperfect
fcc xenon matrix with vacancy number =5**

T(K)	Ma	E _b (eV)	D _C (cm ² /s)
d 40	75,000	0.1210	2.15x10 ⁻¹⁵
e 40	75,000	0.1153	5.71x10 ⁻¹⁴

- (a) Number of moves in the Moakov/damped trajectory walk
(b) Potential barrier height
(c) Classical diffusion rates
(d) For perfect fcc xenon matrix
(e) For imperfect fcc xenon matrix with defect number=5

Table XIV

**Classical diffusion rates for hydrogen atoms
in an imperfect fcc xenon matrix with
vacancy number =15**

T(K)	M ^a	D ^b (cm ² /s)
12	75,000	3.06x10 ⁻¹²
40	50,000	1.45x10 ⁻¹⁰
80	40,000	3.97x10 ⁻⁴

**(a) Number of moves in the Moakov/damped trajectory walk
(b) Classical diffusion rates**

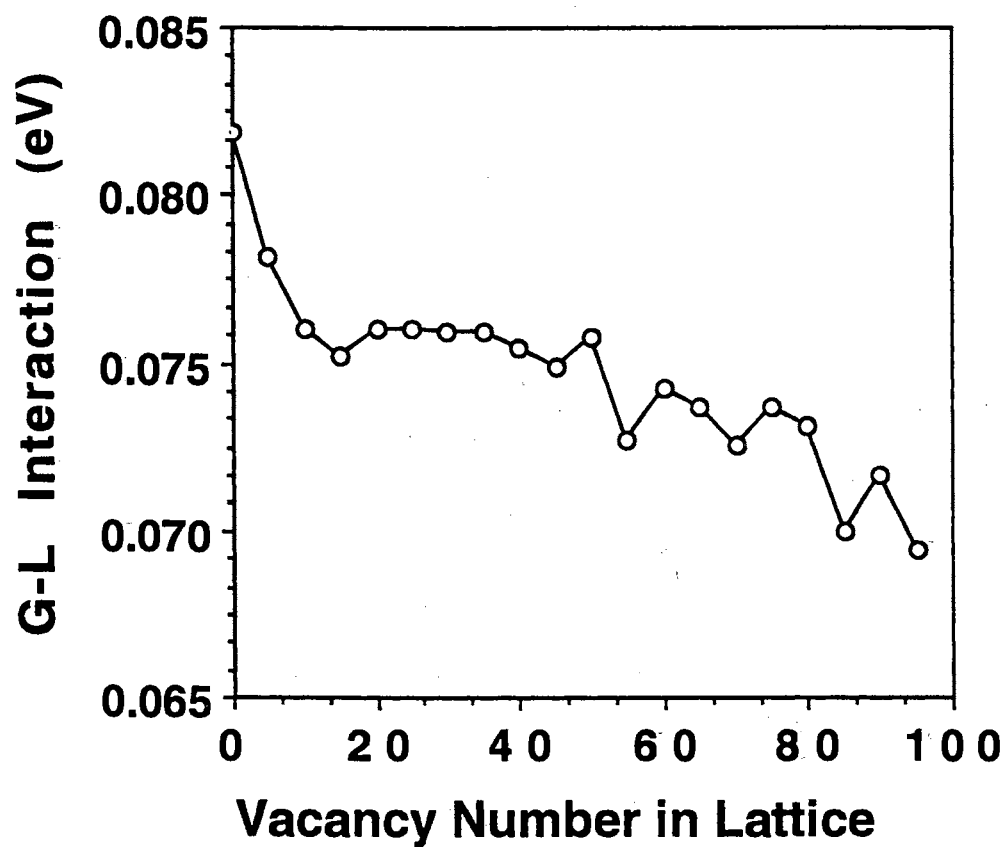


Figure 18. Variation of the Hydrogen-Lattice interaction potential with vacancy number in the crystal.

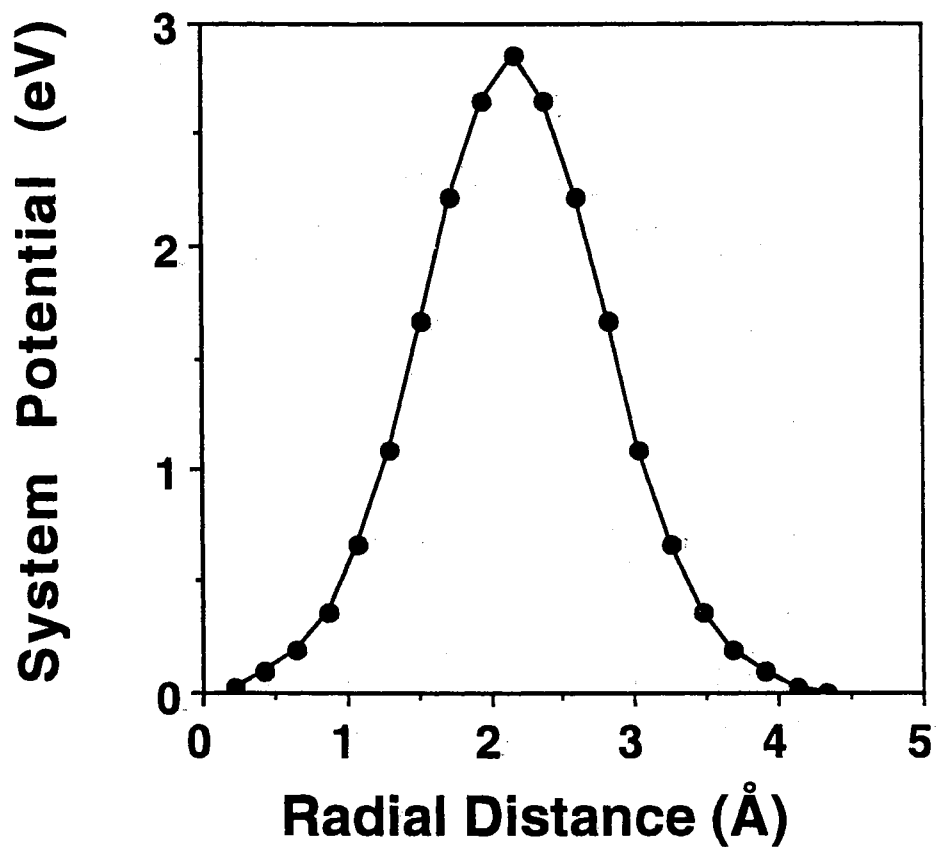


Figure 19. Variation of system potential energy for hydrogen atom movement along a straight line connecting the two adsorption sites in a frozen lattice atoms. The system has 15 vacancies. The abscissa gives the radial diffusion distance covered.

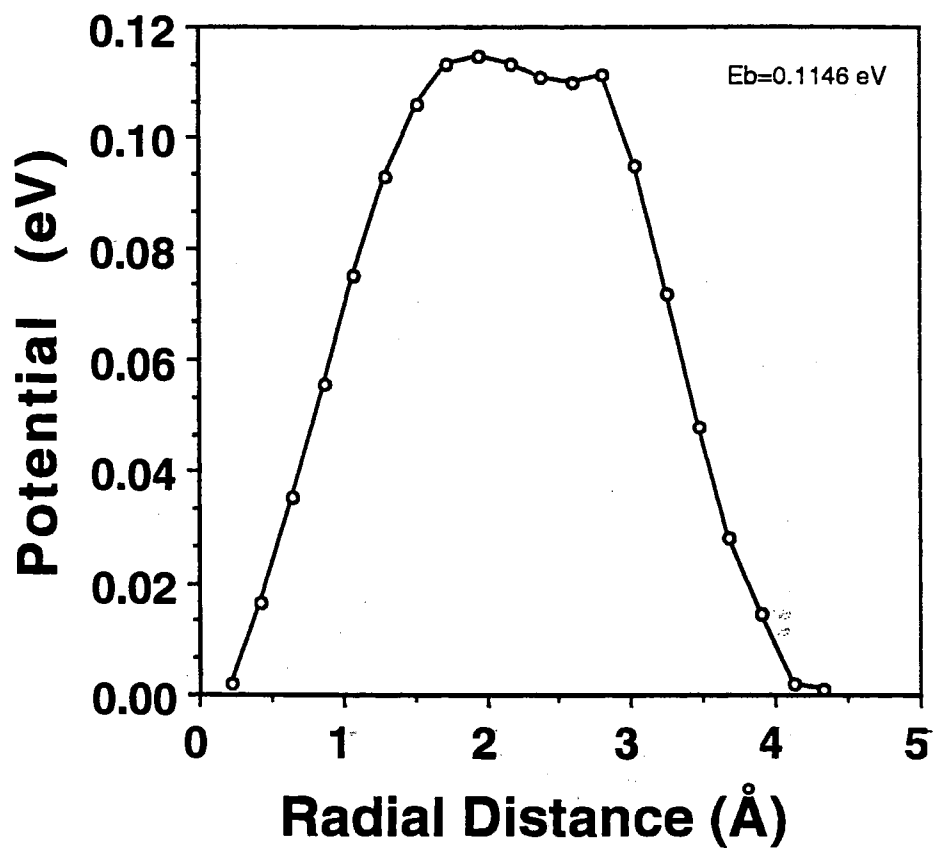


Figure 20. Minimum-energy profile for hydrogen-atom diffusion in a xenon matrix with 5 vacancies. The plotted points are the minimum crossing potentials obtained in the Markov/damped trajectory walk of 75,000 moves. The abscissa gives the radial diffusion distance covered.

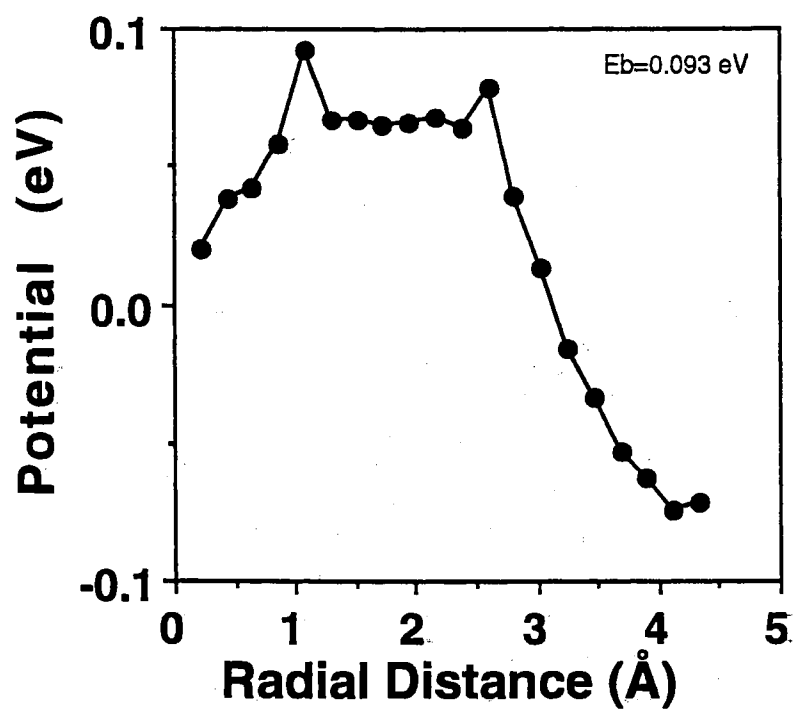


Figure 21. Minimum-energy profile for hydrogen-atom diffusion in a xenon matrix with 15 vacancies. The plotted points are the minimum crossing potentials obtained in the Markov/damped trajectory walk of 50,000 moves. The abscissa gives the radial diffusion distance covered.

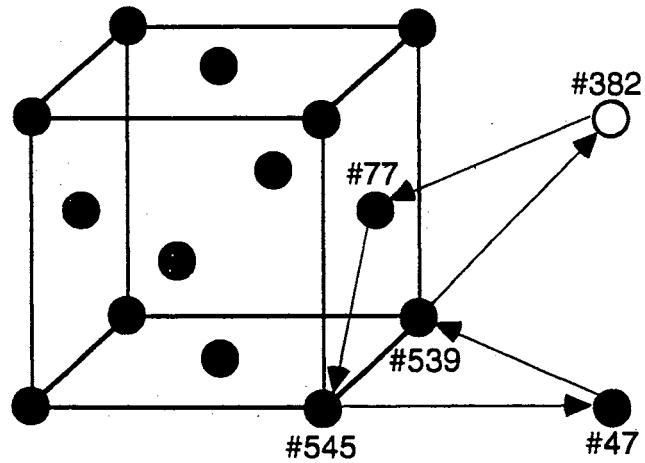


Figure 22: Typical lattice atom motion occurring during the first 200,000 Markov steps in the Monte Carlo calculation. At time $t=0$, site 382 is vacant. The diffusion of the lattice atom as shown by the solid arrows produces a vacancy at site 77 so that the overall result is an apparent diffusion of the vacancy from site 382 \rightarrow site 539 \rightarrow site 47 \rightarrow site 545 \rightarrow site 77.

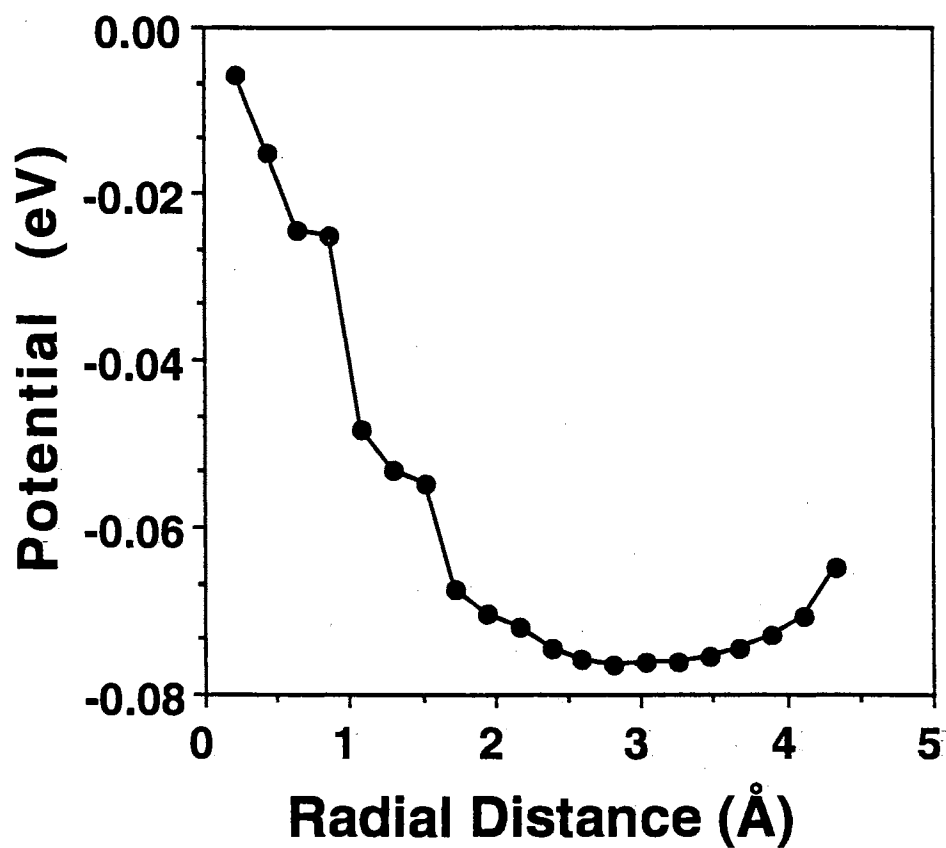


Figure 23. Minimum-energy profile for hydrogen-atom diffusion in a xenon matrix with 5 vacancies. The plotted points are the minimum crossing potentials obtained in the Markov/damped trajectory walk of 200,000 moves. The abscissa gives the radial diffusion distance covered.

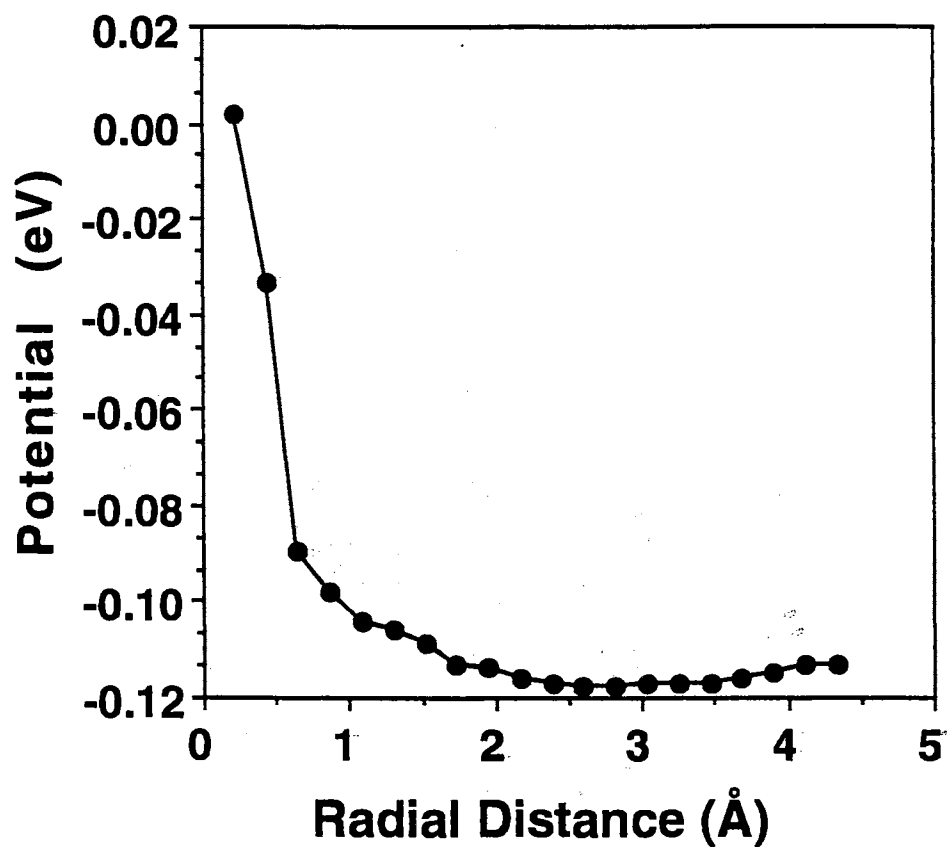


Figure 24. Minimum-energy profile for hydrogen-atom diffusion in a xenon matrix with 15 vacancies. The plotted points are the minimum crossing potentials obtained in the Markov/damped trajectory walk 100,000 moves. The abscissa gives the radial diffusion distance covered.

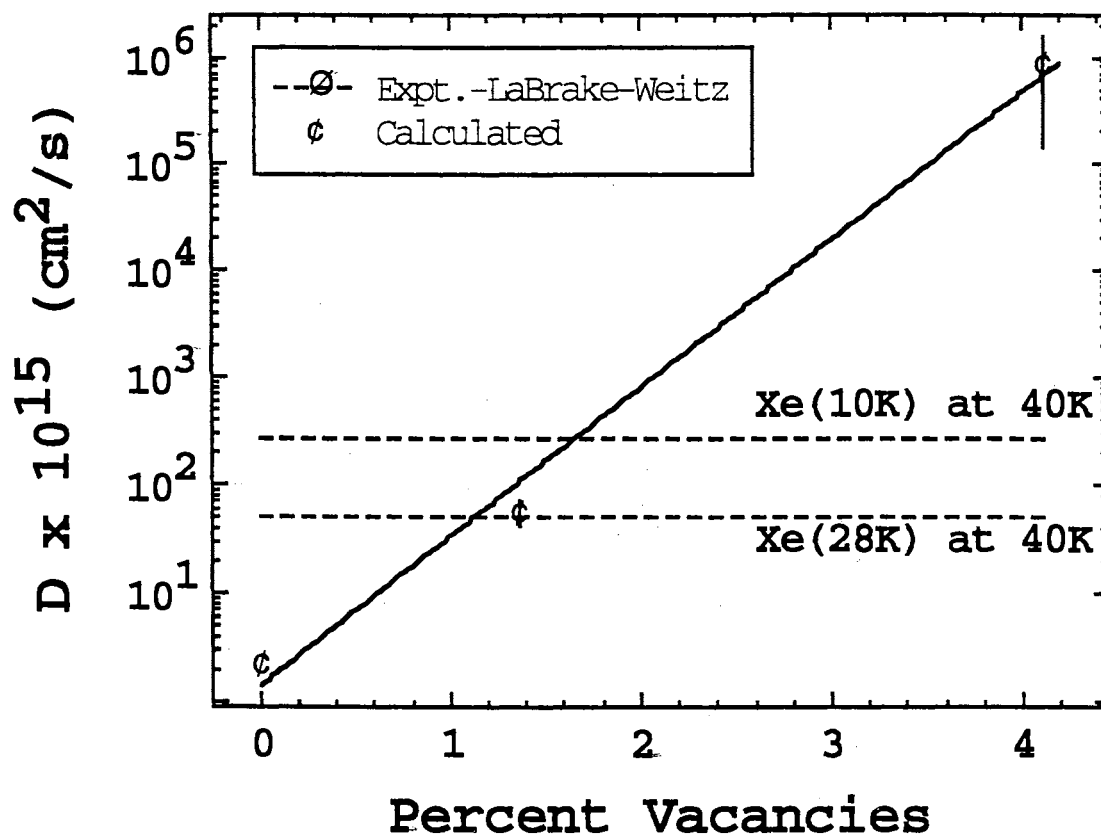


Figure 25. Variation of the computed hydrogen-atom diffusion coefficient with percentage of vacant xenon lattice sites at 40 K. The horizontal dashed lines are the experimental values reported by LaBrake and Weitz (Reference 11) for the matrices indicated in the figure.

2

VITA

Ran Pan

Candidate for the Degree of

Doctor of Philosophy

**Thesis: THEORETICAL STUDIES OF MOLECULAR DYNAMICAL
PROCESSES IN RARE GAS MATRICES AND IN THE GAS
PHASE**

Major Field: Chemistry

Biographical:

Personal Data: Born in Guangshan County, Henan Province, China, On September 22, 1962, the son of Youfu Pan and Dingxiu Chen.

Education: Graduated from Nanxiangdian High School, Guangshan County, Henan Province, China in July 1979; Received Bachelor of Science in Chemistry from Xinyang Teacher's College, Xinyang, Henan Province, China in July, 1983; Received Master of Science in Chemistry from Jilin University, Changchun, China in July 1989; Completed requirements for Doctor of Philosophy Degree at Oklahoma State University in July, 1996.

Professional Experience: Lecturer, Department of Chemistry, Xinyang Teacher's College, July 1983 to August 1986; Research Assistant, Jilin University, September 1986 to July 1989; Chemistry engineer, Tianjin Synthetic Material Institute, July 1989 to December 1992; Teaching Assistant and Graduate Research Assistant, Oklahoma State University, January 1993 to June 1996.

Professional Memberships: American Chemical Society
Phi Lambda Upsilon